Space Programs Summary No. 37-15, Volume VI

for the period March 1, 1962 to June 1, 1962

Space Exploration Programs and Space Sciences

NMF

jpl

JET PROPULSION LABORATORY
CALIFORNIA INSTITUTE OF TECHNOLOGY
PASADENA, CALIFORNIA

June 30, 1962

NATIONAL AERONAUTICS AND SPACE ADMINISTRATION
CONTRACT NO. NAS 7-100

Space Programs Summary No. 37-15, Volume VI

for the period March 1, 1962 to June 1, 1962

Space Exploration Programs and Space Sciences

JET PROPULSION LABORATORY
CALIFORNIA INSTITUTE OF TECHNOLOGY
PASADENA, CALIFORNIA

June 30, 1962

Preface

The *Space Programs Summary* is a bimonthly publication designed to report on JPL space exploration programs and related supporting research and advanced development projects conducted under the sponsorship of the National Aeronautics and Space Administration.

Beginning with this issue the *Space Programs Summary* is divided into six volumes. All information formerly documented in the JPL *Research Summary,* together with reports on advanced development projects, will in the future be reported in Volumes IV and V of the *Space Programs Summary*. The subtitles of all volumes of the reorganized *Space Programs Summary* are:

Vol. I, The Lunar Program (Confidential)
Vol. II, The Planetary-Interplanetary Program (Confidential)
Vol. III, The Deep Space Instrumentation Facility (Unclassified)
Vol. IV, Supporting Research and Advanced Development (Unclassified)
Vol. V, Supporting Research and Advanced Development (Confidential)
Vol. VI, Space Exploration Programs and Space Sciences (Unclassified)

The new *Space Programs Summary,* Volume VI is an unclassified digest of appropriate material from Volumes I through V, plus the reports of the JPL Space Sciences Division.

W. H. Pickering, *Director*
Jet Propulsion Laboratory

Space Programs Summary No. 37-15
Volume VI

Contents

THE LUNAR PROGRAM

I. Introduction 1

II. *Ranger* Project 3

A. *Ranger* 1 and 2 Flight Operations 3
B. The *Ranger* 3, 4 and 5 Spacecraft 4
C. *Ranger* 3 and 4 Flight Operations 7
D. Assembly and Test Operations 10
E. Lunar Capsule Development 12
F. *Ranger* TV Subsystem 14

III. *Surveyor* Project 15

A. Objectives 15
B. Mission and Scientific Operations 16
C. Spacecraft System 17

THE PLANETARY–INTERPLANETARY PROGRAM

IV. Introduction 19

V. *Mariner* Project 21

A. Missions 21
B. Status 21
C. Spacecraft Description 22
D. Scientific Experiments 22
E. Development and Fabrication 27
F. Assembly and Test Operations 28
G. Ground Support Equipment 30

VI. *Voyager* Project 33

THE DSIF PROGRAM

VII. Introduction 35

VIII. Current Activities 40

A. Tracking Operations 40
B. Facilities and Capabilities 40
C. Research and Development 41

SPACE SCIENCES

IX. Introduction 43

X. Lunar Studies 47

A. X-Ray Diffractometer 47
B. Petrographic Microscope 48
C. Seismograph System 50
D. Rocket Radar Experiment 53
E. Toroidal Oscillations of the Moon 57

References 58

Contents (Cont'd)

XI. Planetary Studies 59
A. Television Subsystem 59
B. Ultraviolet Spectrometer 66
C. Scientific Instruments GSE 69
References 71
XII. Solar and Interplanetary Studies 73
A. Sigma Plasma Detector 73
B. Solar Plasma Analyzer 77
C. Particle Flux Detector 79
D. Plasma Probe 81
E. Meteorite Research 83
References 89
XIII. Exobiology 91
A. Soil Studies–Microflora of Desert Regions 91

THE LUNAR PROGRAM

I. Introduction

The JPL Lunar Program consists of two major projects: *Ranger* and *Surveyor*. The *Ranger* Project has entered the flight stage; *Surveyor* is in hardware development.

The objective of the *Ranger* Project is to exploit present technology in support of the U.S. manned lunar flight program. Nine *Ranger* launchings, using *Atlas–Agena* B rockets, are now planned. Four of these flights have been made; the next is scheduled for this year.

Rangers 1 and 2 were engineering evaluation flights to test the basic system to be employed in later lunar and planetary vehicles. Several scientific experiments were carried, but on a noninterference basis. The *Ranger* 3, 4, and 5 spacecraft carries a gamma-ray instrument, a radar reflection experiment, a TV camera, and a rough-landing seismometer capsule. The 1963 flights (beginning with *Ranger* 6) will carry a high-resolution TV package and additional radiation experiments.

The objective of the *Surveyor* Project is to take the next step in advancing lunar technology, by making reconnaissance surveys from lunar orbit, and controlled soft landings on the Moon. Seven flights using *Centaur* launch vehicles are now planned. *Surveyor* spacecraft, being designed and built by the Hughes Aircraft Company under JPL subcontract, will carry a variety of instruments including TV cameras, radiation environment monitors, and geophysical equipment for determining characteristics of the lunar surface.

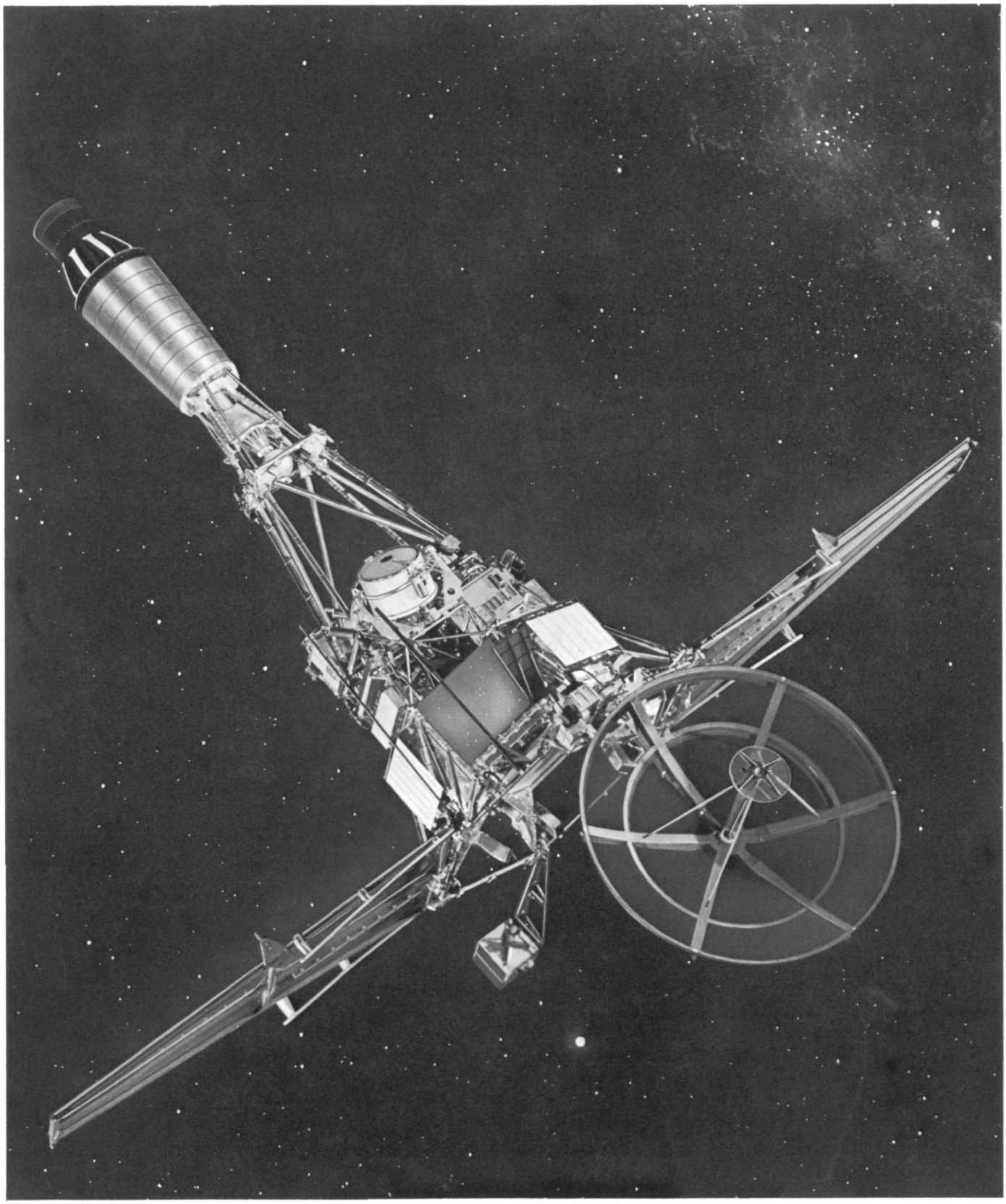

Fig. 1. *Ranger* 1 and 2 flight configuration

II. *RANGER* PROJECT

A. *Ranger* 1 and 2 Flight Operations

1. Ranger *1*

On August 23, at 100410 GMT *Ranger* 1 (Fig. 1) was launched from the Atlantic Missile Range (AMR). Vehicle performance through the parking orbit phase was normal. However, a malfunction in the *Agena* B propulsion system prevented the *Agena* second burn from occurring, thus leaving the second stage and spacecraft in a slightly modified parking orbit, instead of the planned highly elliptical orbit (Fig. 2).

The resulting low satellite orbit precluded the attainment of certain of the original mission objectives. The over-all performance of the *Ranger* 1 spacecraft was successful considering the nature of the orbit. No malfunctions were detected that would warrant making any design or hardware changes in *Ranger* 2.

Telemetry records indicate that all spacecraft controller programmed events took place (Table 1). It was impossible to determine the exact time of any of the programmed commands, since nearly all the commands occurred during periods when the spacecraft was not in view of any tracking station. In each case, however, subsequent telemetry indicated that each commanded function did occur within the proper time interval.

Probably the most serious effect of the satellite trajectory was the fact that the spacecraft was in the Earth's shadow about 45% of the time during each orbit. When the spacecraft returned to the sunlight, the attitude control system would begin its acquisition procedure with a consequent heavy drain on the supply of nitrogen gas used for activation. This gas supply was exhausted within 19 hr after injection.

The friction-lubrication experiment was designed to measure coefficients of friction in the near-total vacuum of space. Although the value of the data obtained was greatly reduced, the experiment apparently performed normally under the circumstances.

Table 1. *Ranger* 1 command sequence

Number	Command
1	Increase transmitter power
2	Turn on scientific instruments high-voltage
3	Extend particle analyzer boom and solar panels
4	Start Sun acquisition
5	Start Earth acquisition
6	Change data encoder rate gyro scale
7	Open semiconductor detector aperture
8	Switch transponder transmitter to high-gain antenna
9	Reduce modulation on beacon transmitter
10	Turn on friction-lubrication experiment

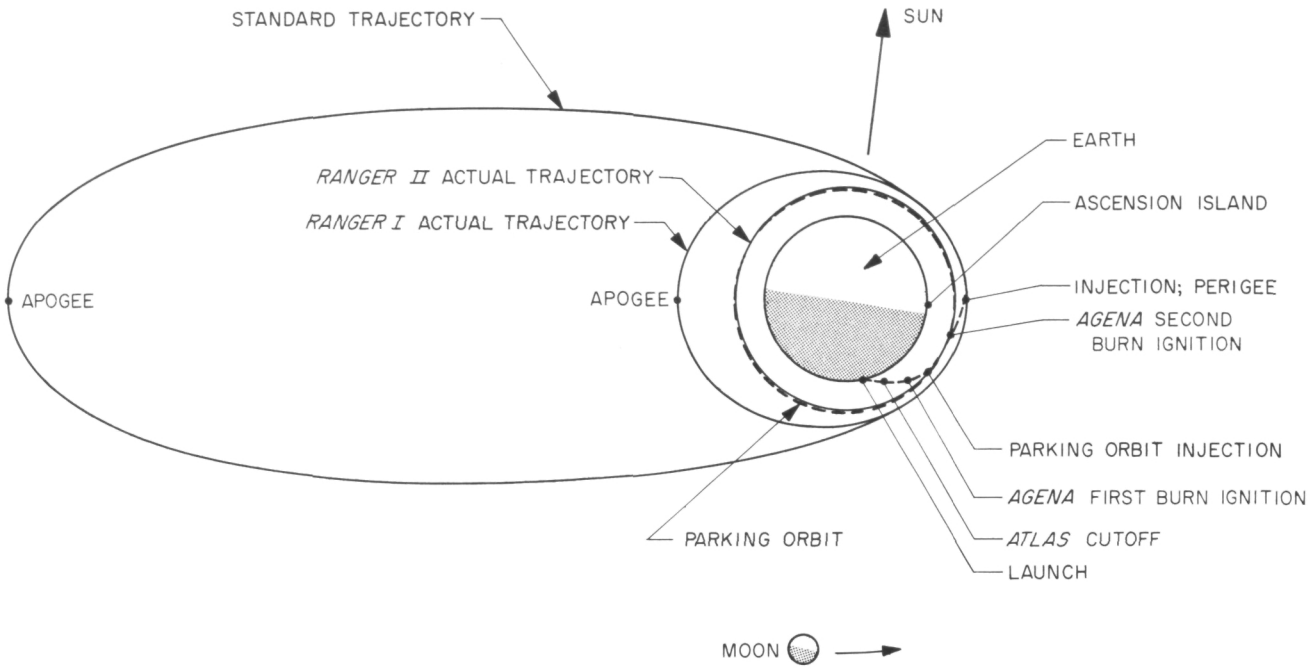

Fig. 2. Orbits of *Rangers* 1 and 2

The value of most of the scientific experiments was seriously reduced because of proximity to the Earth and lack of attitude stabilization. The scientific instruments, in general, performed as expected.

2. Ranger 2

Ranger 2 was launched on November 18 at 0812 GMT, after a countdown that was unusually smooth; the only delays were for correction of minor difficulties in the *Agena* umbilicals and in the *Atlas* LOX tanking measurement.

The *Atlas* performance was completely satisfactory, despite a minor error in staging time, and the *Agena* first burn (to acquire parking-orbit speed) took place on schedule. The second burn did not occur. As in the case of *Ranger* 1, the spacecraft was left in a low Earth orbit, instead of the desired near-escape trajectory (Fig. 2). *Agena* telemetry records show that the cause of the *Ranger* 2 failure was entirely different from that of *Ranger* 1. On *Ranger* 2 the *Agena* roll gyro was inoperative throughout the flight. With no roll control, the *Agena* depleted its attitude-control gas supply shortly after the first burn, and was tumbling at the time of second burn. The second burn start sequence began on schedule, and the engine ignited but immediately shut down, probably because of gas ingestion due to the tumbling motion.

Data was received from *Ranger* 2 at all Deep Space Instrumentation Facility stations during its brief flight, which terminated after approximately six orbits. As in the case of *Ranger* 1, all spacecraft subsystems were determined to be operating, but the scientific results of the flight were slight. The ground operations portion of the system operated better than in *Ranger* 1 in that real-time data operations were achieved both before and after injection. All functions (e.g., spacecraft separation, solar panel extensions, etc.) other than *Agena* second burn took place as planned.

B. The *Ranger* 3, 4 and 5 Spacecraft

The *Ranger* 3, 4 and 5 spacecraft (Fig. 3) consists of two basic units: a JPL-produced bus and a lunar capsule assembly (Fig. 4), produced by Aeronutronic Division of Ford Motor Company under JPL contract. The purpose of the capsule assembly is to emplace a sensitive seismometer on the lunar surface; data from the seismometer is to be relayed back to Earth receiving stations for an extensive period of time after landing.

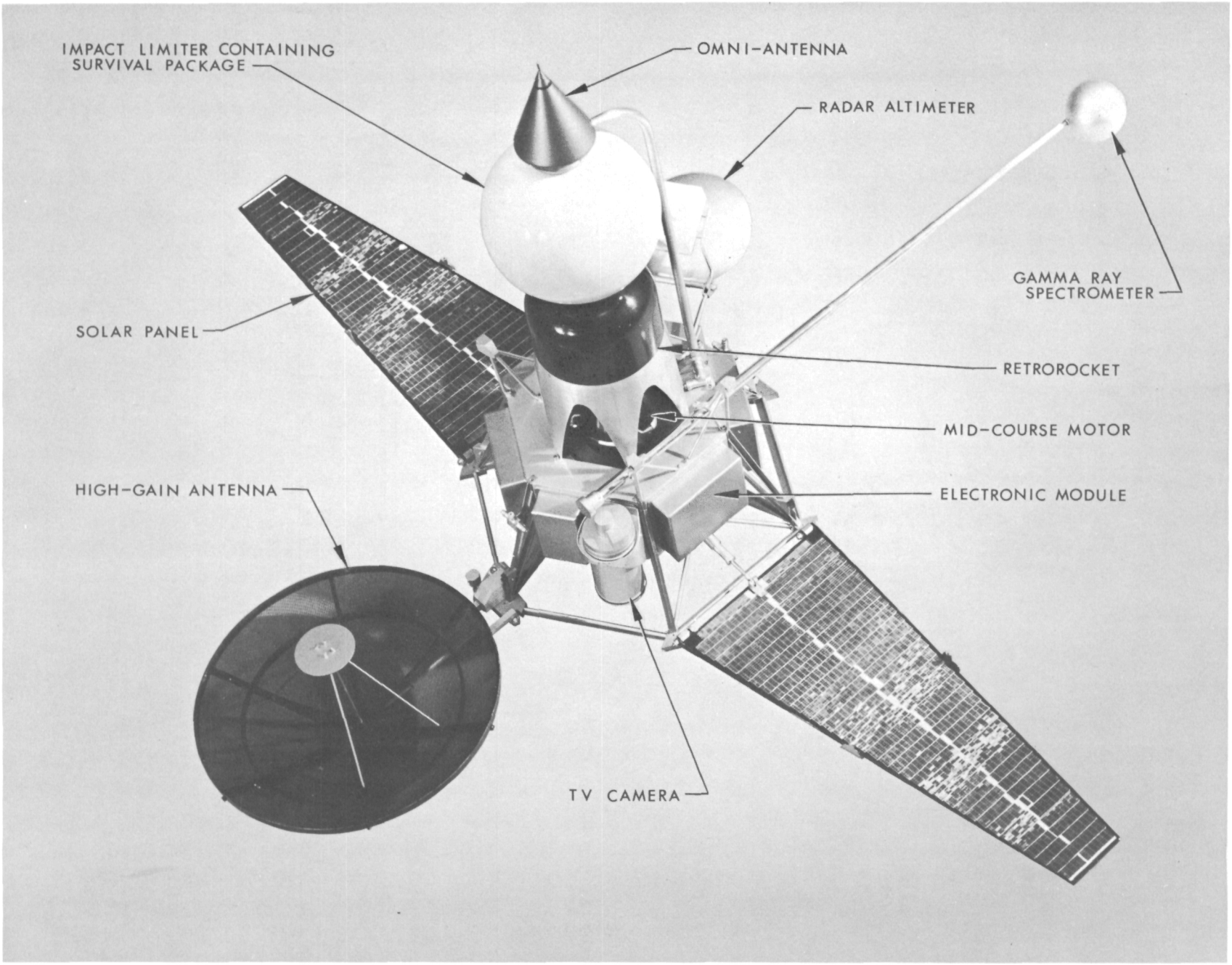

Fig. 3. *Ranger* 3, 4 and 5 spacecraft

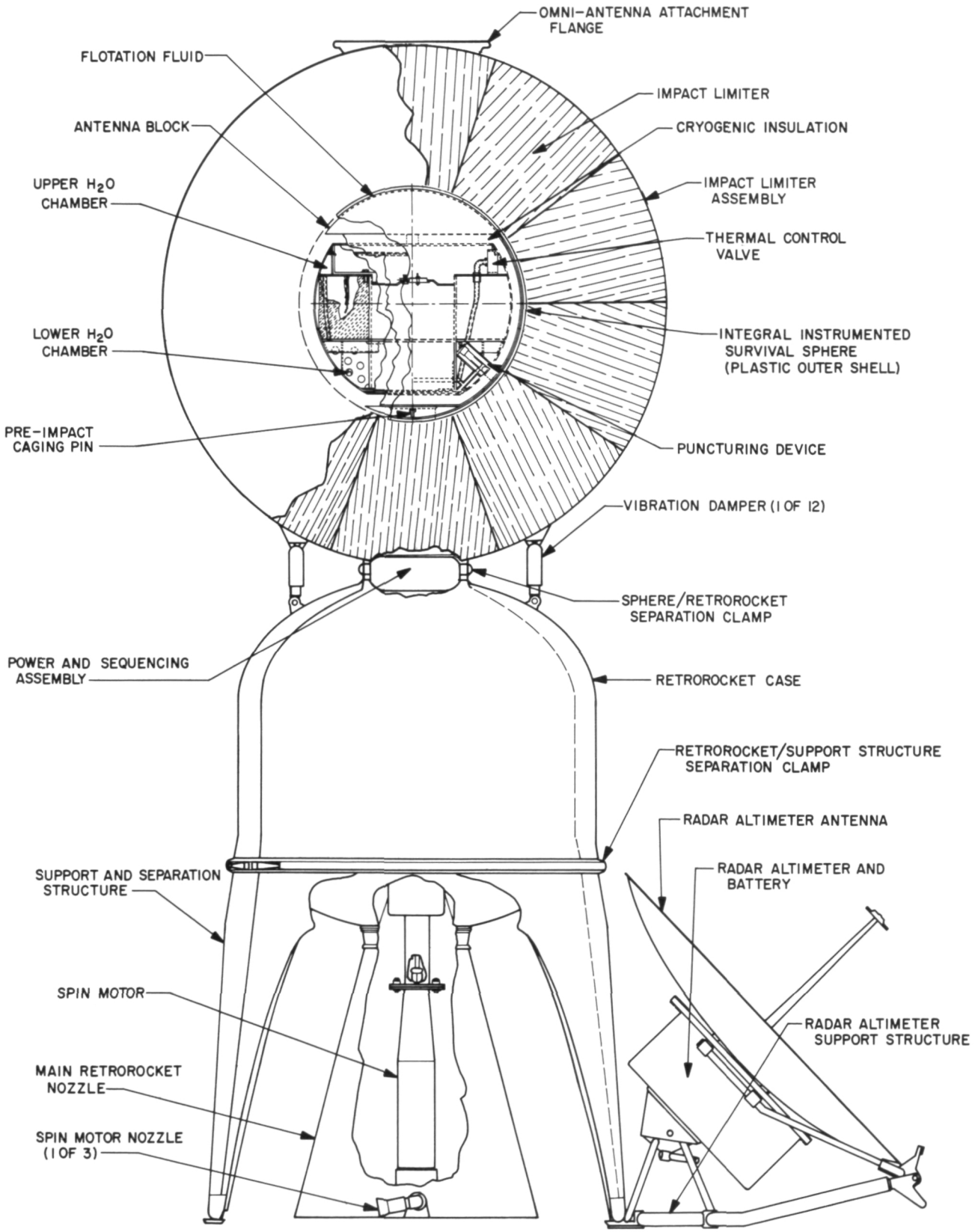

Fig. 4. Lunar capsule assembly

The basic unit of the *Ranger* 4 bus is a 5-ft diameter hexagonal frame. To this frame are mounted the six electronic modules, two solar panels, mid-course motor, high-gain and omni-antennas, attitude control gas system, and scientific instruments.

The capsule assembly, which extends forward of the bus as a superstructure, includes the following components: a support and separation structure; a radar altimeter for sensing the proper instant that the capsule is to be separated from the spacecraft bus; a retrorocket; a spin rocket motor to provide stabilization during the retrorocket braking; a crushable impact limiter to absorb residual energies; and the survival package containing the seismometer. The survival package is a sphere which is fluid floated inside the hollow, spherical impact limiter to distribute the structural loads of impact and to allow erection by Moon gravity to the local vertical after the sphere comes to rest.

The spacecraft is attached to the *Agena* stage by a special adapter and is confined within an aerodynamic shroud. For the launch phase the solar panels are folded in toward the spacecraft roll axis and held in place by pyrotechnic latches, and the 4-ft diameter parabolic high-gain antenna is nested aft of the bus.

Following the first stage sustainer burnout, the shroud is ejected. At the conclusion of the first *Agena* burn, the spacecraft is in a coasting or parking orbit. A second ignition and burn of the *Agena*, resulting in spacecraft injection, precede the separation of the spacecraft from the *Agena*.

After separation, the spacecraft goes into an acquisition operation. The solar panels are erected and the high-gain antenna is rotated to a preset hinge angle. The attitude control system is activated and the solar sensors point the roll axis of the spacecraft toward the Sun, thus placing the solar power system in operation. The spacecraft then turns about the roll axis until the antenna beam points toward the Earth. Upon Earth acquisition by optical sensors (which move with the antenna), the high-gain communication link is established. The spacecraft then continues to coast with its roll axis pointed toward the Sun and its high-gain antenna pointed toward the Earth.

After a suitable tracking period, the required trajectory corrections are computed and the corrective maneuver commands are transmitted to the spacecraft. The resulting mid-course maneuver turns the spacecraft to the prescribed angle in space, effects a correction in the trajectory by an application of thrust, and then returns it to its Sun and Earth orientation as before.

As the spacecraft approaches the lunar surface, a commanded terminal maneuver is performed to aline the vidicon camera for high-resolution pictures of the Moon, and to orient the lunar capsule for its subsequent separation and retrorocket-controlled descent. The omni-antenna and boom are moved away from the capsule, and upon receipt of a signal from the altimeter, the spin rocket motors activate and the capsule is separated from the spacecraft prior to retrorocket firing. The spacecraft will plunge separately onto the lunar surface and be destroyed by the impact. A timer will initiate the sphere/retrorocket separation squibs which will allow the survival sphere to fall free to the Moon's surface.

The primary objectives of the *Ranger* 3, 4, and 5 Project are to:

(1) Collect gamma-ray data in flight and in the vicinity of the Moon.

(2) Relay to Earth, by television, photos of the lunar surface.

(3) Place an instrumented transmitting capsule on the lunar surface to relay lunar seismic data to Earth.

(4) Develop spacecraft and space flight technology (e.g., the performance of both a mid-course trajectory correction and a terminal phase attitude control maneuver when commanded).

In addition, the radar altimeter is to provide a telemetering signal proportional to its received echo strength. This data will have significant scientific value in attempting to describe the lunar surface and also will improve engineering knowledge for altimetry on future lunar landing missions.

C. *Ranger* 3 and 4 Flight Operations

1. Ranger 3

The objective of the *Ranger* 3 flight was to hit the Moon during a period of a few days around third-quarter phase in January 1962 when lunar lighting would have been good for photography and a near-vertical impact trajectory could have been achieved.

Preflight activities continued on schedule until January 19, when during *Atlas* fueling, problems developed with the fuel tank insulation bulkhead. At first it appeared that the mission would have to be abandoned until the February launch opportunity. But *Atlas* personnel, work-

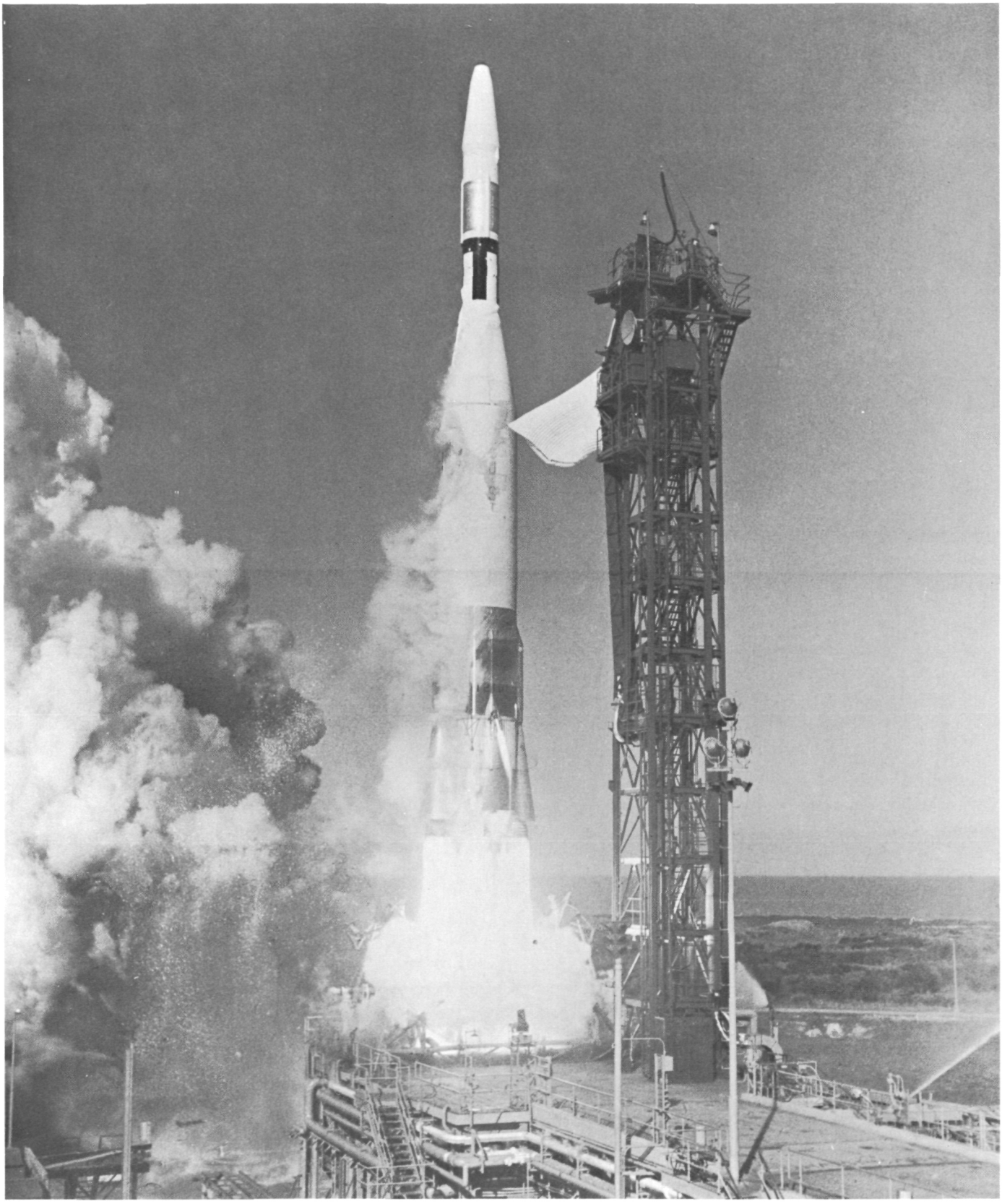

Fig. 5. *Ranger* 3 launch

ing around the clock, made an ingenious and unprecedented repair without removing the vehicle from the pad.

Ranger 3 was launched on January 26, 1962, 203011 GMT (Fig. 5). A failure in the *Atlas* ground guidance system resulted in a late booster cutoff with no control over the sustainer cutoff time to compensate for the excess velocity accumulated. Two programmed *Agena* burning periods followed and the spacecraft was injected into an orbit with too high an energy for it to intercept the Moon. The excess injection energy was considerably greater than that which the mid-course propulsion system was designed to correct, so that the possibility of a successful lunar impact mission was ruled out early in the flight.

The over-all flight performance of the *Ranger* 3 spacecraft was quite successful, but there were a few failures which have resulted in some modifications to the *Ranger* 4 spacecraft and supporting operations. The stations of the DSIF provided tracking and telemetry coverage continuously for 5 days except for periods when the RF signal was too weak to recover. The spacecraft signal was essentially lost at 1854 GMT on January 31, shortly after the supply of gas used for attitude stabilization was exhausted.

About 12 hr after injection, during the first Goldstone pass, the mid-course maneuver commands were sent to the spacecraft. The spacecraft turned through the desired angles in roll and pitch, the mid-course rocket fired at the proper time, and the attitude control system reacquired the Sun and the Earth. However, post-maneuver tracking showed that the desired trajectory had not been achieved. It was soon evident that the commands had been reversed in sign. The sign error was later confirmed as due to a long-standing difference in sign convention between the maneuver code used in the IBM 7090 computer and the maneuver code in the spacecraft. Preflight tests did not reveal the sign reversal because the maneuver digits went through the entire system correctly; only their meaning was changed in the process. Because of the initial large trajectory errors, the reversal of the mid-course maneuver had negligible effects on the remainder of the mission.

On January 28, the execute command for the terminal maneuver was sent from Goldstone. The spacecraft performed its first turn (pitch) properly. An extraneous pitch turn command occurred a few seconds after the first commanded turn ended and continued until the commanded yaw turn ended. The high-gain antenna tracked the Earth as the spacecraft continued pitching until the Earth sensor lost the Earth's light. A roll search was then started, and the RF signal from the high-gain antenna was lost. During the commanded yaw turn, while the spacecraft was still pitching and rolling, the antenna apparently locked on the Moon. Low signal strength from the omni-antenna prevented recovery of any TV pictures.

Intermittent signals continued to be received until February 2, when the spacecraft was at a range of more than 500,000 mi.

2. Ranger 4

Ranger 4 lifted off from Complex 12, AMR, at 205015 GMT on April 23, 1962. The spacecraft impacted the Moon 63 hr and 59 min later. Launch vehicle performance was flawless and all range operations went according to plan. The spacecraft, which was functioning normally from launch through injection, failed sometime before South African (Mobile Tracking Station, DSIF 1) acquisition and from that time on did not execute any programmed functions or respond to any commands. The DSIF tracked the spacecraft transponder until battery depletion 10½ hr after liftoff, and the capsule transmitter from that point to the Moon.

The launch countdown proceeded normally, with holds called at:

(1) $T - 40$ min (duration 88 min) to correct difficulties with the *Atlas* umbilical plugs.

(2) $T - 40$ min (duration 7 min) to rerun the GE guidance loop data.

(3) $T - 15$ min (duration 8½ min) to complete LOX tanking in the *Atlas*.

(4) $T - 5$ min (duration 6 min) to set guidance parameters.

(5) $T - 2$ min 27 sec (duration 9 min) to solve a GE guidance problem; count recycled to $T - 5$ and guidance parameters reset.

At the time of *Ranger* 4 launch, all space flight operations communications were in, although both AMR and DSIF 1 and 5 had been experiencing RF transmission problems. DSIF voice communications with the overseas sites were out at times during the operation, but no critical data was lost by lack of communications. Both IBM 7090 computers were in operation during the critical time. The spacecraft was injected into a nearly standard trajectory at 210414 GMT. During the period when the JPL launch station was tracking the spacecraft, no abnormalities were observed and telemetering data appeared normal. The launch station lost the signal when the spacecraft went below the horizon at liftoff (L) + 7½ min.

The Central Computing Facility backup computations of injection conditions and initial orbit were completed using tracking data from Ascension Island and DSIF 1. There were essentially seven orbits computed during the *Ranger* 4 space flight operations. A preliminary orbit was used only to obtain early pointing information for the DSIF. The first orbit of sufficient accuracy to predict target parameters indicated a lunar impact for the spacecraft.

Spacecraft data telemetered through the *Agena* telemetry showed normal spacecraft performance through both *Agena* burning periods and after injection, up to the time when the record ended at electrical separation of the spacecraft at $L + 16$ min 33 sec. Since none of the AMR down-range receivers are equipped to track the 960-mc spacecraft frequency, there existed a 6-min, 17-sec gap in the signal recovery until DSIF 1 acquired at $L + 22$ min 50 sec. As soon as successful lock was established, it became apparent that a spacecraft failure had occurred. Except for Channel 1 (the spacecraft frequency reference channel) all telemetry channels were in lock but no telemetry commutation was occurring.

All the available evidence indicates that the solar panels were never opened, and the attitude control power for Sun and Earth acquisition was never turned on. The spacecraft continued to tumble throughout the period data was recovered. Power consumption under those conditions and the lifetime of the battery are consistent with that conclusion. The dc power to the transponder and the data encoder apparently was normal. The data encoder VCO frequencies were quite stable until the battery started to fail.

A number of commands were transmitted to the spacecraft for trouble-shooting purposes with no success. Attempts were made to advance the spacecraft telemetry mode, to switch the transponder signal from the omni-antenna to the high-gain antenna, to change the high-gain antenna hinge angle and to over-ride the spacecraft roll control system. It appears that none of the central computer and sequencer (CC&S) commands were given with the possible exception of the transmitter power-up command which is given before DSIF acquisition. The condition of the spacecraft from the time of DSIF 1 acquisition until the transponder signal was lost due to battery depletion, remained essentially unchanged. No event blips or any other evidence of programmed commands were observed. The apparent absence of all enabling signals to the data encoder and command system, combined with the lack of CC&S commands, indicates that the CC&S was not operating.

D. Assembly and Test Operations

1. Buildup of Ranger 5

Assembly of *Ranger* 5 at the JPL Spacecraft Assembly Facility started during the latter part of February 1962 with the fitting of the attitude control gas system to the spacecraft structure (bus). Further spacecraft buildup continued without encountering any major difficulties.

Spacecraft ground integrity checks and initial power turn-on were successfully accomplished and subsystem testing was initiated. Subsystem tests have proceeded on schedule. Some appropriate changes are being made based on *Ranger* 4 experience.

2. System Test Complexes

Since *Ranger* 6 will be the first high-resolution TV mission, a new test equipment utilization schedule has been prepared. Three system test complexes used for *Rangers* 3, 4, and 5 will be updated and used to support the *Ranger* 6, 7, 8, and 9 spacecraft. The Aeronutronic lunar capsule and scientific experiment test equipment will be replaced by the RCA TV subsystem and new science equipment; the operating condition of the equipment will be verified before it is integrated into the system test complex in the Spacecraft Assembly Facility.

The system test complex for *Ranger* 5 field operations will be modified to a *Ranger* 6, 7, 8, and 9 configuration at AMR. All new *Ranger* 6, 7, 8, and 9 test equipment will first be used and verified at JPL.

3. Omnidirectional Antenna Patterns

a. **Ranger 5.** There is excessive RF coupling between the transmitting antenna in the capsule and the spacecraft omni-antenna; to decrease the coupling, several means of providing RF shielding between the two antennas have been devised. In order to evaluate the effect of these shields on the omni-antenna radiation pattern, a *Ranger* 5 mockup is being assembled on the Mesa Antenna Range facility, JPL, Pasadena.

b. **Rangers 6, 7, 8, and 9.** Radiation patterns of the *Ranger* 6, 7, 8, and 9 omnidirectional antenna mounted on a full scale mockup have been completed. Typical radiation patterns are shown in Fig. 6. The spacecraft attitude is shown by the figures drawn on the pattern; e.g., 0 deg is a nose-on view of the spacecraft, and 180 deg is a tail-on view. The patterns indicate that program requirements for omni-antenna coverage have been met.

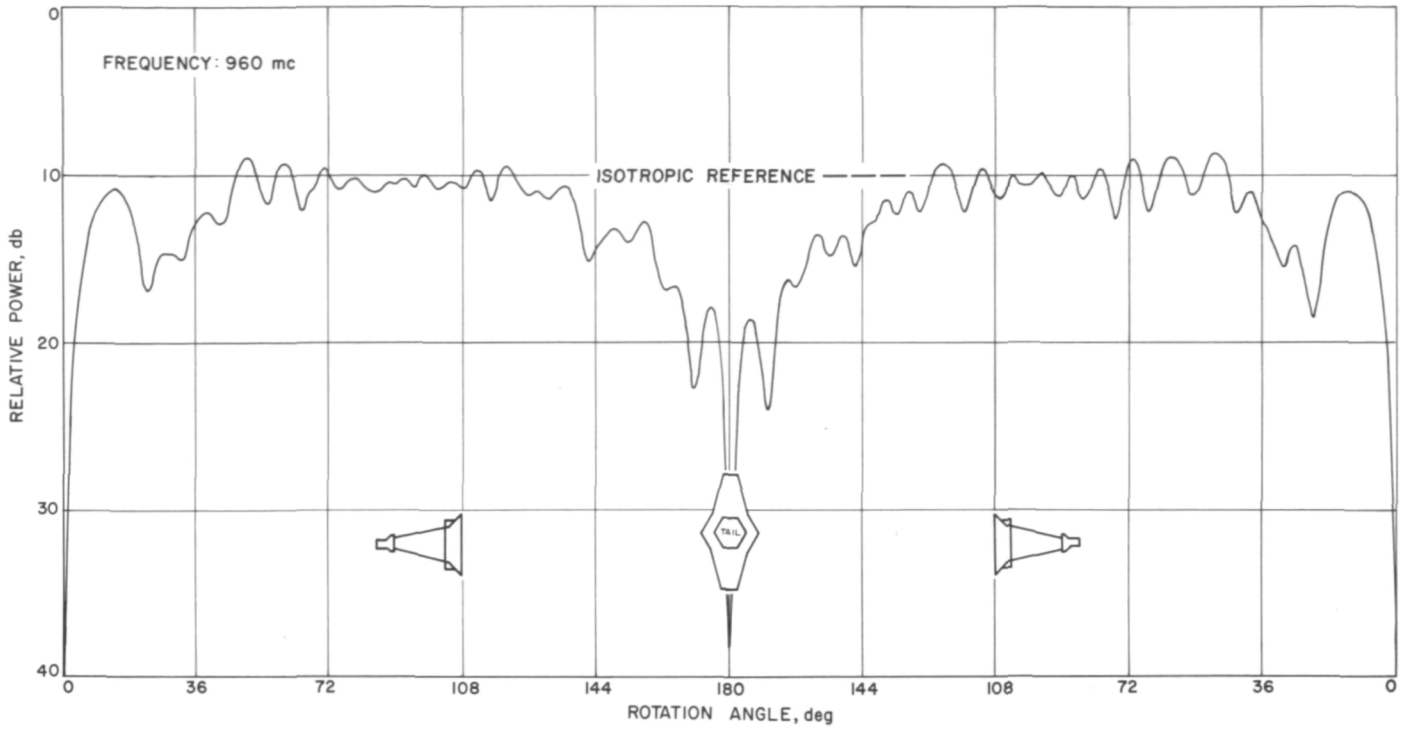

Fig. 6. Typical omni-antenna radiation patterns for *Rangers* 6, 7, 8, and 9

4. *Mid-Course Propulsion System*

The lunar impact mission of *Ranger* 5 and the high-resolution television investigation of the lunar surface on *Rangers* 6, 7, 8, and 9 will require that the spacecraft make a single mid-course propulsion maneuver to remove or reduce *Agena* injection dispersion errors. This maneuver will be accomplished through the use of a small, monopropellant-hydrazine-fueled propulsion system capable of delivering a variable total impulse in conjunction with an integrating accelerometer system.

During this reporting period, flight acceptance testing and assembly of the *Ranger* 5 and *Ranger* 5 spare mid-course propulsion systems were completed, and the propulsion system installed in the spacecraft. Flight acceptance testing and assembly of the *Ranger* 6 and *Ranger* 6 spare mid-course propulsion systems have started.

Prelaunch preparation of the *Ranger* 4 mid-course propulsion system consisted of two phases. Just prior to the final system test, the propulsion system was removed from the spacecraft for a complete visual inspection and a leak check of the tankage and plumbing. After the successful completion of the leak checks, the propulsion system was returned to the spacecraft for the final system test. Immediately after the final system test, the propulsion system was returned for final preparation, fueling, and pressurization. Propellant filling and pressurization of the propulsion system were completed without incident.

During the countdown, the flight-readiness of the system was verified by monitoring the pressures and temperatures of the nitrogen and fuel tanks. In-flight telemetry data, which was received at AMR until the spacecraft passed over the horizon, indicated no degradation in the pressure levels in the tanks. It is of interest to note that the propulsion system had been fueled and pressurized for 15 days prior to launch.

An early failure in the *Ranger* 4 spacecraft prevented the spacecraft from performing commands; thus, no mid-course maneuver was performed.

5. *Vibration Testing*

The *Ranger* 6, 7, 8, and 9 mechanical test model was type approval vibration tested during March 1962. During dynamic testing, a system (spacecraft–fixture combined) torsional mode was observed. In an effort to control this mode a new technique was utilized. Two accelerometers, located diametrically opposite on the circular shake fixture, were used as controllers. The voltage outputs of the accelerometers were used to control the vibration level during the test. With large structures (such as spacecraft shake fixtures) which have bending

and translation resonances in the test frequency range, multiple accelerometer control systems are necessary to control vibration test levels and to prevent possible damage to the spacecraft.

E. Lunar Capsule Development

1. Introduction

Aeronutronic Division of Ford Motor Company, under a JPL subcontract, has developed a complete lunar capsule subsystem for *Rangers* 3, 4, and 5. Capsules have been supplied for *Rangers* 3 and 4 on schedule and with no significant deviations from specifications.

During this reporting period a number of improvements to the *Ranger* 3 capsule configuration were designed, tested, and delivered for use on *Ranger* 4. Notable among these were changes to the retrorocket, spin rocket, and the altimeter deployment mechanism. A redesign effort of the payload electronics has been initiated in support of *Ranger* 5 to increase reliability.

The reporting material in the section relating to *Ranger* lunar capsule was abstracted from the Aeronutronic document: *Twelfth Bimonthly Technical Progress Report, Development of a Lunar Capsule Subsystem*, April 1962.

2. Flight Results

***a. Ranger* 3.** *Ranger* 3 was launched January 26, 1962. Booster guidance malfunction prevented lunar impact, and thus prevented operation of most of the landing capsule functions. Telemetry records indicated no signal was received confirming deployment of the radar altimeter; it was concluded that the probability of altimeter deployment malfunction existed and warranted product improvement in this area. The deployment mechanism was redesigned and qualified for *Ranger* 4.

During prelaunch checkout of the *Ranger* 3 payload, it was noted that the spacecraft transponder receiver threshold was degraded by spurious radiation from the Capsule 10 transmitter. The spurious signal, at 890 mc, was most prominent in the shroud-on condition. Capsule 12 was placed on the spacecraft as prime flight item. Some degradation of the transponder threshold was noted with this sphere; however, the amount of degradation was not sufficient to jeopardize the prime objective of the mission.

***b. Ranger* 4.** No significant problems were encountered during launch preparation with the exception of RF interference experienced from Capsule 14. Personnel from both JPL and Aeronutronic are currently involved in test work designed to increase understanding of this problem and to alleviate its effects.

3. Payload Electronics

A design review for *Ranger* 5 has been made of all electronic equipment in the payload. The objectives were to increase reliability, improve fabrication techniques, and improve and expand tests.

In support of the redesign effort for *Ranger* 5, the space flight payload from *Ranger* 3 was evaluated under simulated launch, lunar impact, and post-lunar impact. The effect of environmental testing and incident radiation at 960 mc on the transmitter RF spectrum was determined.

a. RF tests. RF tests were performed in a quiet box to measure the combined carrier power, sideband power and index of modulation, and to provide a spectrum analysis. These tests were repeated after flight vibration and lunar impact simulation. The transmitter operation was unaffected by these environments.

b. Vibration test. The sphere was vibrated to proof test levels in three axes with both sine and noise inputs. No failures or malfunctions occurred during this test. X-ray examination before and after vibration showed no motion of the inner sphere relative to the impact limiter.

c. Impact test. A simulated lunar impact test was conducted on the Hyge machine. The timer did not start as a result of the pre-impact acceleration, and none of the timed sequences occurred. It was concluded that the 25-*g* switch did not close for a sufficient duration during the 50-msec acceleration phase to actuate the squib switches. The caging pin was not withdrawn prior to impact and was broken due to high shear forces.

d. Vacuum–thermal tests. Subsequent to impact testing, the capsule was instrumented for external activation and monitoring of post-impact events in a vacuum–thermal environment. The closure of the 25-*g* switch was simulated by activation of the squib switches which initiated the timer. All events were normal.

The transmitter was removed and replaced with a resistive thermal load. The sphere was then reinstrumented for a thermal test. The thermal test proceeded

with a hot (200°F) and a cold (−320°F) cycle for 3 days. The transmitter was then started and the test was concluded 10 days later. The battery voltage fell rapidly at −30°F, after operating 760 hr.

4. Propulsion and Ordnance Devices

a. Retrorocket. A retrorocket nozzle modification program was initiated to provide an external reinforcement to the expansion cone for the *Ranger* 4 flight. The reinforcement consisted of perforated stainless steel cone of 0.010-in. shim stock bonded to the exterior of the nozzle. The cone extended 8.6 in. forward of the aft face of the nozzle.

Since Aeronutronic and Hercules were unable to obtain test time in the Arnold Engineering Development Center facility to support this program, an altitude chamber with a diffuser evacuation system was provided at the Hercules Bacchus facility (Fig. 7). The system (procured from Inca Engineering Corporation) maintained test chamber pressure at about 1 psia until thrust tail-off. Camera coverage of all tests was good and indicated successful operation of the nozzles. Figure 8 shows the retrorocket nozzle after firing. Nozzle damage shown occurred as a result of gas blow-back and the CO_2 quench system.

Hercules personnel, under the supervision of Aeronutronic, installed the modification on the four flight motors at AMR. The modification is not expected to influence axial (thrust) performance of the motor to a significant degree, but will reduce the estimated cross velocity dispersion contribution due to the tip-off torque caused by nozzle deterioration.

b. Spin motor. The spin motor improvement program has been completed. The following design changes were incorporated as a result of this program:

(1) Removal of the Mylar diaphragm over the grain.

(2) Removal of the epoxy spacing washer at the grain end.

(3) Modification of the igniter installation to eliminate potential leakage.

(4) Fabrication of a special tool to size the exhaust nozzles.

The spin motor qualification program was divided into two phases: (1) igniter qualification and grain qualification, and (2) motor assembly qualification.

Igniter and grain assemblies were exposed to a number of environments. All motors and igniters fired successfully with no indications of other than random variations in performance. There appears to be no correlation of performance variations with the various environmental exposures.

Of the 12 motor assembly qualification firings, eight were on the torque fixture and four on the gas dynamic fixture (Fig. 9). All test firings were successful, with no indications of leakage or incipient failure.

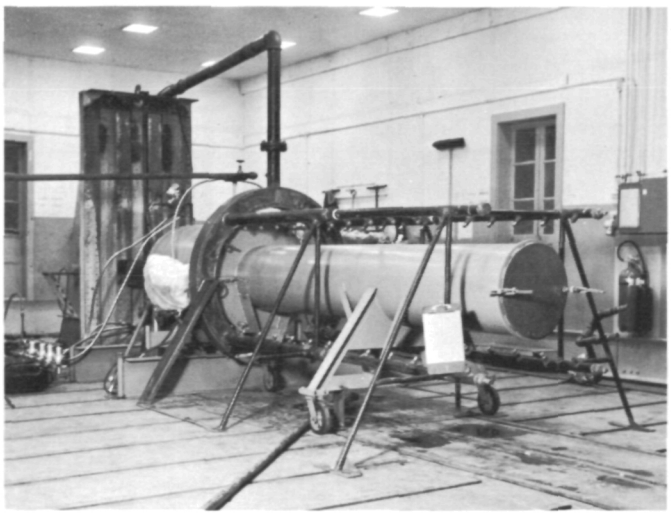

Fig. 7. Altitude test chamber and diffuser installation

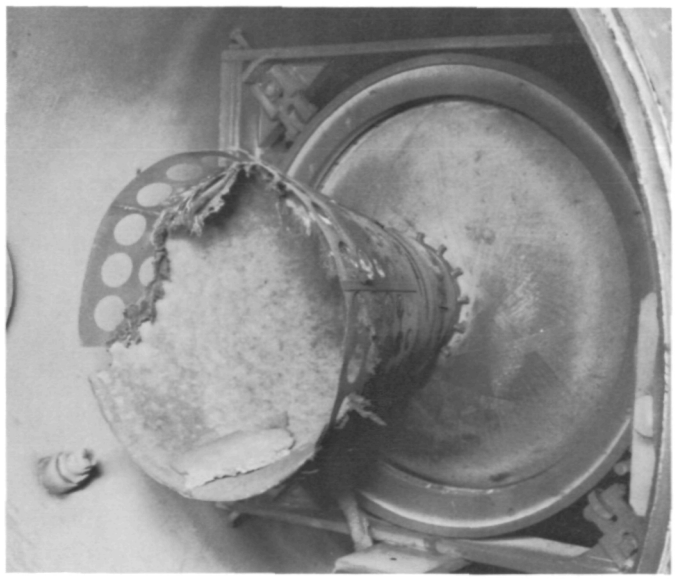

Fig. 8. Retrorocket nozzle with modification, after firing

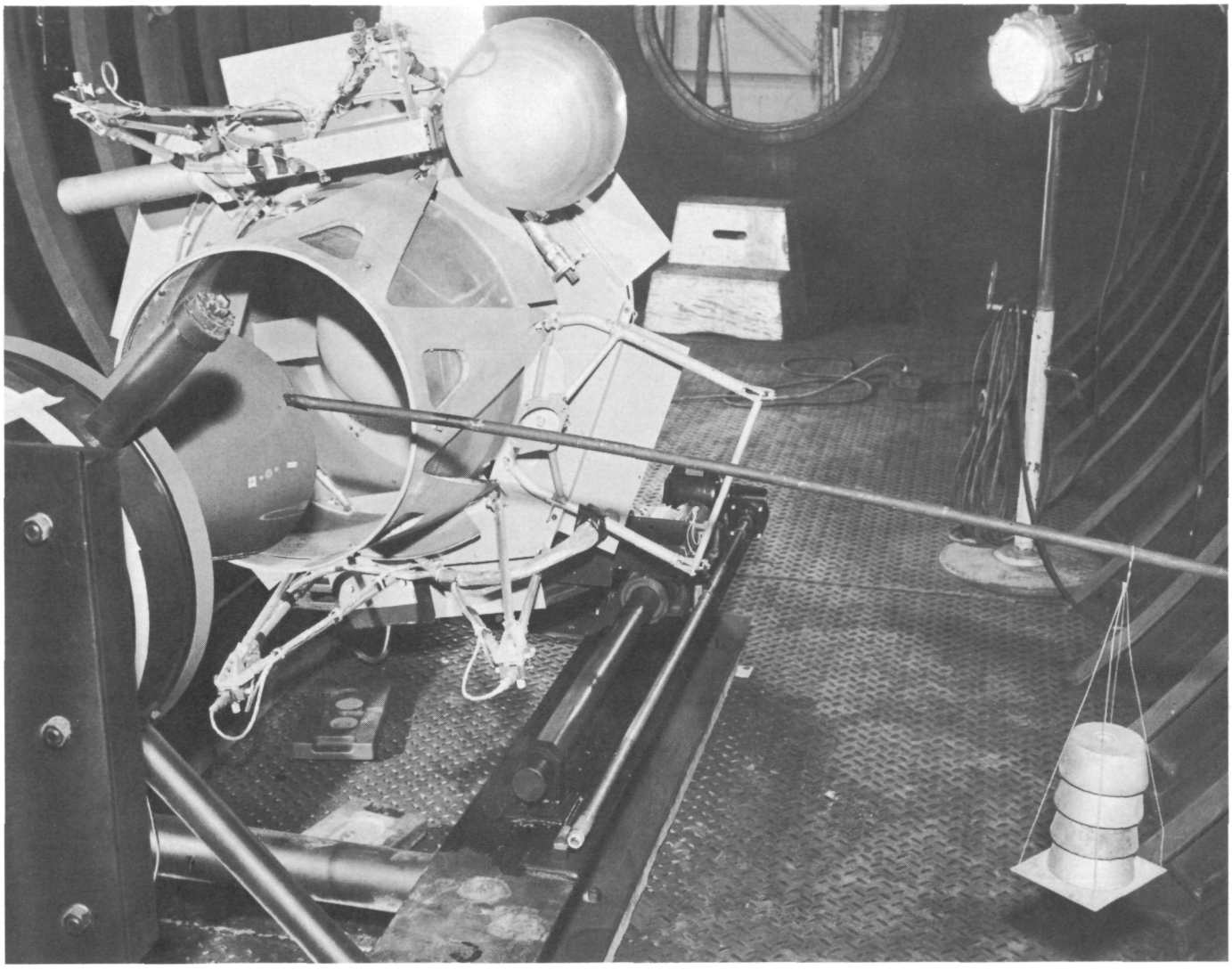

Fig. 9. Gas dynamics test fixture

F. *Ranger* TV Subsystem

A TV subsystem is being developed for *Rangers* 6, 7, 8, and 9 by RCA under contract to JPL. The primary objective of *Rangers* 6, 7, 8, and 9 will be to produce high-resolution TV pictures of the lunar surface. TV coverage will be terminated by lunar impact.

The *Ranger* 6, 7, 8, and 9 spacecraft is composed of two basic units: the RCA TV subsystem and the JPL-produced bus. The TV subsystem will mate with the bus as does the lunar capsule of the *Ranger* 3, 4, and 5 series. Two significant differences are that the subsystem structure will not separate from the bus, and there will be no retrorocket to reduce the impact velocity, which will be approximately 6500 mph.

The *Ranger* TV subsystem structure consists of three major assemblies: (1) the central box which houses the main electronic components, (2) the camera subassembly with associated bracketry and equipment, and (3) the thermal shield. Camera view apertures are provided in the thermal shield.

Vacuum–thermal testing of the thermal test model in the space simulation facilities at RCA Astro-Electronics Division has been completed. Vibration testing of the mechanical test model has continued at JPL, with satisfactory performance of the TV subsystem structure. The camera alinement is being modified to provide additional redundancy of coverage, with initial effort being concentrated on the redesign of the camera bracket and the field-of-view holes in the thermal shield.

III. *SURVEYOR* PROJECT

Surveyor is an unmanned lunar exploration project managed by the Jet Propulsion Laboratory for the National Aeronautics and Space Administration. The project is supported from within NASA by the Marshall Space Flight Center and the newly formed Launch Operations Center. Within JPL, the participation of the Deep Space Instrumentation Facility (DSIF) and the establishment of a Space Flight Operations Facility (SFOF) are involved. Hughes Aircraft Company is under contract to JPL to develop and operate the spacecraft. Scientists from various universities and government agencies, and the JPL Division of the Space Sciences are participating in the *Surveyor* scientific effort.

A. Objectives

The primary objectives of *Surveyor* are to successfully accomplish the soft landing of a number of scientific instrument payloads on the lunar surface (seven missions, 1963, 1964, and 1965); to provide for a minimum of 30 days (90 days desired) of scientific observations and measurements on the lunar surface with a modest quantity of reliable and sensitive scientific instruments; and to telemeter the scientific and engineering data to Earth for retrieval, reduction, and timely dissemination.

The scientific objectives of *Surveyor* are to measure the physical properties of the Moon, and to analyze the composition of the lunar surface and subsurface in various selected maria regions visible from Earth. The scientific measurements are intended to aid in establishing a better understanding of the internal structure and composition of the Moon and its local atmosphere, and to obtain additional data that may assist the scientific community in determining the origin of the Moon and understanding the physical phenomena associated with the origin of the solar system.

Additional objectives are to demonstrate the engineering feasibility of lunar exploration with automated remotely controlled soft-landing spacecraft systems, to evaluate the performance of the subsystems in the cislunar environment and during the landing phase, and to contribute to the technology required for the successful accomplishment of eventual manned lunar landings and operations.

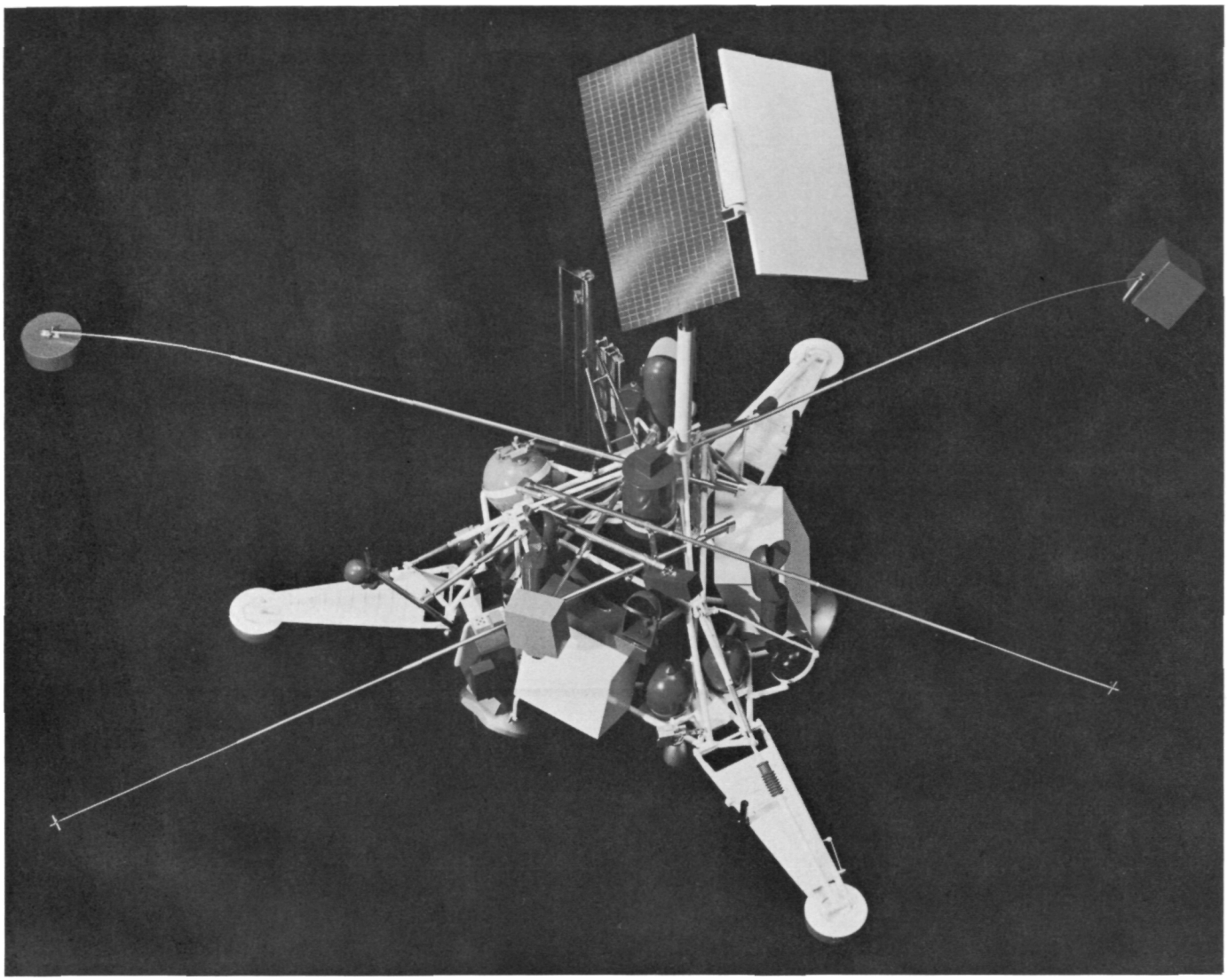

Fig. 1. The *Surveyor* post-landing configuration

B. Mission and Scientific Operations

The *Surveyor* spacecraft will be boosted to injection by an *Atlas–Centaur* launch vehicle. Launch and pre-injection tracking are to be provided through the facilities of the Atlantic Missile Range.

During transit, the DSIF will be used for spacecraft orbit determination and for transmitting the necessary commands to effect a mid-course maneuver to minimize the lunar landing dispersion. The DSIF will also be used to receive engineering and scientific data telemetered from the spacecraft during transit and operations on the lunar surface.

After spacecraft injection, all mission operations will be controlled from the JPL SFOF. Accumulation of engineering and scientific data, and the processing and partial reduction of the scientific data, will be accomplished at this facility. The SFOF will be the focus of continuing operations associated with the conduct of experiments during the 30- to 90-day life of the *Surveyor* on the lunar surface.

Surveyor scientific experiments and associated instruments or measurements are given in Table 1.

Table 1. *Surveyor* scientific experiments

Experiment	Instruments or measurements
Surface chemical analysis	X-ray fluorescence spectrometer X-ray diffractometer Gas chromatography (detection of volatile constituents)
Surface physical analysis	Densitometer (ray scattering) Thermal and electrical conductivity measurements Acoustic-velocity measurements Vidicon with variety of magnifications
Local subsurface properties (drill to 4 or 5 ft)	*X-ray spectrometer* Vertical temperature-gradient measurements Thermal and electrical conductivity measurements Densitometer
Structure	Three-axis seismometer
Fields, particles, and atmosphere	Radiation detector Magnetometer Plasma probe Atmospheric-pressure gage

C. Spacecraft System

The spacecraft is being developed in two configurations, sharing the same basic bus, in order to utilize fully the anticipated progressive increase in launch-vehicle capability. The first configuration, the A-21, has a nominal separated spacecraft weight of 2100 lb; the second, the A-25 (Fig. 1), has a weight of 2500 lb. They differ primarily in scientific instrument payload and retromotor propellant loading.

The full-scale A-21 mockup is currently nearing completion, and thermal-test models of spacecraft quadrants are being constructed for high-vacuum and solar-simulator test. A prototype command and data-handling console (the prime *Surveyor*-peculiar ground equipment to be installed in each DSIF station) is ready for preliminary testing.

THE PLANETARY–INTERPLANETARY PROGRAM

IV. Introduction

The Planetary–Interplanetary Program at present consists of the *Mariner* Projects using the *Atlas–Agena* B for early missions and the *Atlas–Centaur* vehicle for more advanced missions, and eventually the *Voyager* using the *Saturn* vehicle. The missions planned for these projects are subject to change because of such influences as new scientific discoveries or unexpected developments in booster vehicle availabilities.

The primary long-range objective of the NASA Planetary–Interplanetary Program is the development of automatic, unmanned, interplanetary spacecraft technology and the use of this technology in the form of space probes to gather fundamental scientific knowledge concerning the planetary and interplanetary environments, the planets themselves, and solar phenomena, both out of and within the plane of the ecliptic. High on the list of priorities is the search for life forms (if any) on the nearby planets.

It is planned by 1970 to have rather completely demonstrated and, to some reasonable extent, exploited (in terms of acquired scientific data) spacecraft capable of (1) being put into orbit around and (2) landing on the surface of Mars and Venus. During this decade there is also planned an initial effort toward extending the above capability toward the planets Mercury and Jupiter and space shots out-of-the-plane-of-the-ecliptic and in toward the Sun.

The secondary long-range objective of the program is the development of technology and the collection of scientific data which will contribute to the successful eventual manned exploration of the planets and interplanetary space.

The immediate objective of the program is the initial probing of Venus and Mars.

V. *Mariner* Project

A. Missions

The intent of the first *Mariner* flights is to perform flyby missions to Venus in 1962 using the *Atlas–Agena* B vehicle.

The objectives of these early missions are to: (1) develop and launch two spacecraft to the near vicinity of the planet Venus, (2) receive communications from the spacecraft while in the vicinity of Venus, and (3) perform a Venus-oriented scientific experiment, and as many other experiments as possible oriented toward interplanetary space and the near vicinity of the planet. This mission will provide the first opportunity to make scientific measurements from the close proximity of a planet other than Earth.

Later *Mariner* missions will be performed with the primary purpose of making scientific investigations of the planets Venus and Mars during their periods of availability in 1964 through 1967.

A more advanced *Mariner* spacecraft will be developed with the additional purposes of: (1) making interplanetary scientific investigations in the regions between Earth and Mars, (2) developing experience in the design of a spacecraft that has considerable flexibility with regard to the specific missions it is basically capable of covering, and (3) providing experience and knowledge which will permit a quality and efficient design of the later *Voyager* spacecraft. To these ends, the spacecraft will be designed for a precision flyby mission and will incorporate the capability of either carrying or not carrying a small landing capsule. In between periods of Mars and Venus availability, the spacecraft will be utilized as an interplanetary probe.

B. Status

Two completely assembled flight spacecraft for the 1962 *Mariner* missions were subjected to system tests and environmental tests during March and April. Incompatibilities between subsystems were uncovered and corrective actions were taken during, and subsequent to, these tests. The environmental tests include a space simulation test series, and a composite shake test series involving the *Agena* spacecraft adapter and the spacecraft.

The preliminary design phase of the more advanced *Mariner* has been completed. Mission objectives, design characteristics and restraints, and functional specifications are currently being finalized and readied for publication. Detail layout and hardware drawings are now in process. Some prototype hardware fabrication is underway and the mockup is being updated as the design progresses.

C. Spacecraft Description

The *Mariner* Venus (1962) spacecraft (Figs. 1 and 2) has a conical configuration that bears a strong genetic resemblance to the *Ranger* series. The spacecraft is approximately 10 ft long, 5 ft in diameter at the base, and weighs approximately 450 lb. A hexagonal frame at the base of the spacecraft mounts the electronics cases, mid-course motor, erectable solar panels, movable high-gain communications antenna, and superstructure.

The spacecraft electronics cases house the central computer and sequencer, attitude control electronics, communications equipment data encoder, command subsystem, scientific equipment, battery, and power supplies. Within the annulus formed by the cases is the mid-course motor. During launch, the solar panels and the high-gain antenna are retracted and held in place by pyrotechnic latches.

The superstructure extends approximately 6 ft above the base and supports the omnidirectional antenna; it serves as an attachment point for the scientific instruments and sensors. The scientific instrumentation payload is integrated around the radiometer experiment, which is located to obtain the required antenna-scan amplitude.

D. Scientific Experiments

The scientific experiments for the *Mariner* Venus (1962) mission are classified into three categories:

(1) Planet-oriented—performed in the close vicinity of Venus to obtain information about the planet and its atmosphere; the instrumentation includes microwave and infrared radiometers.

(2) Vicinity of planet—performed in the vicinity of

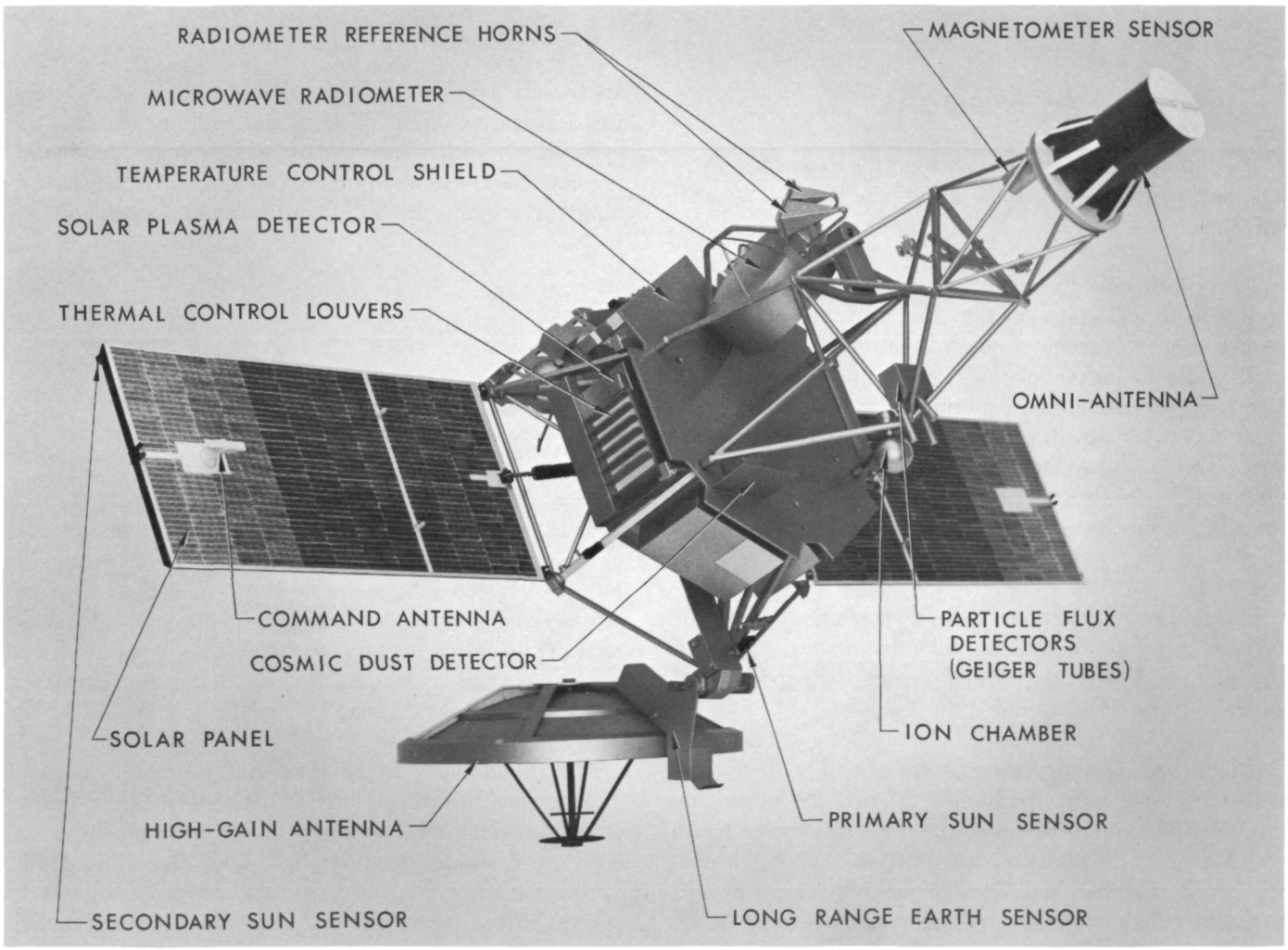

Fig. 1. *Mariner* Venus (1962) spacecraft

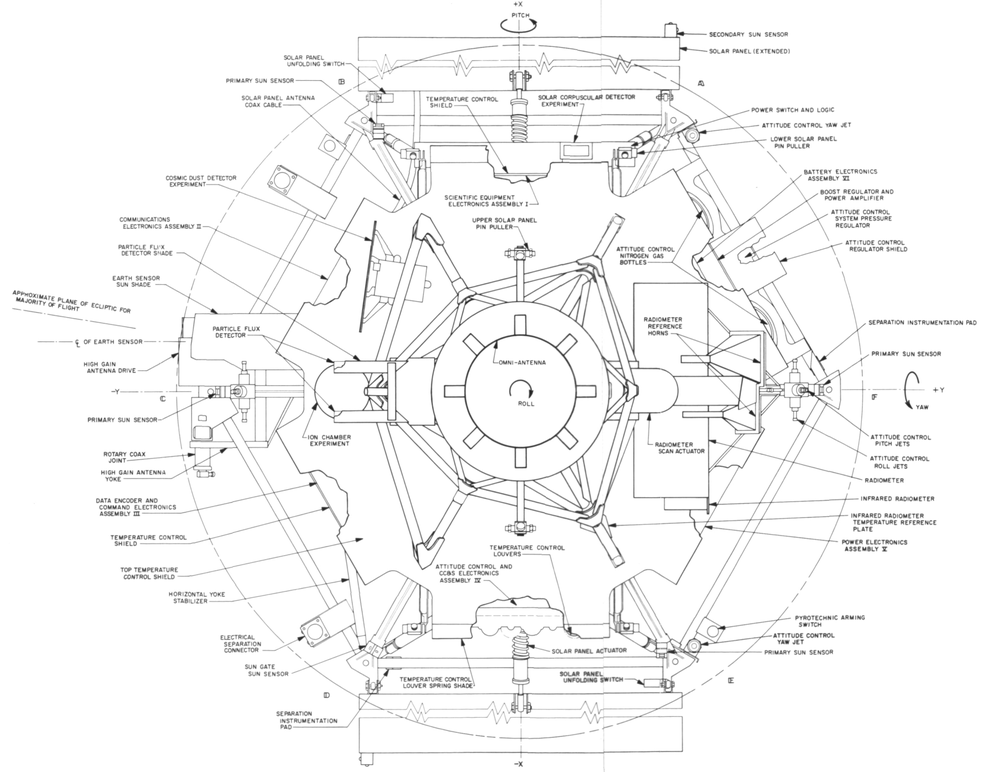

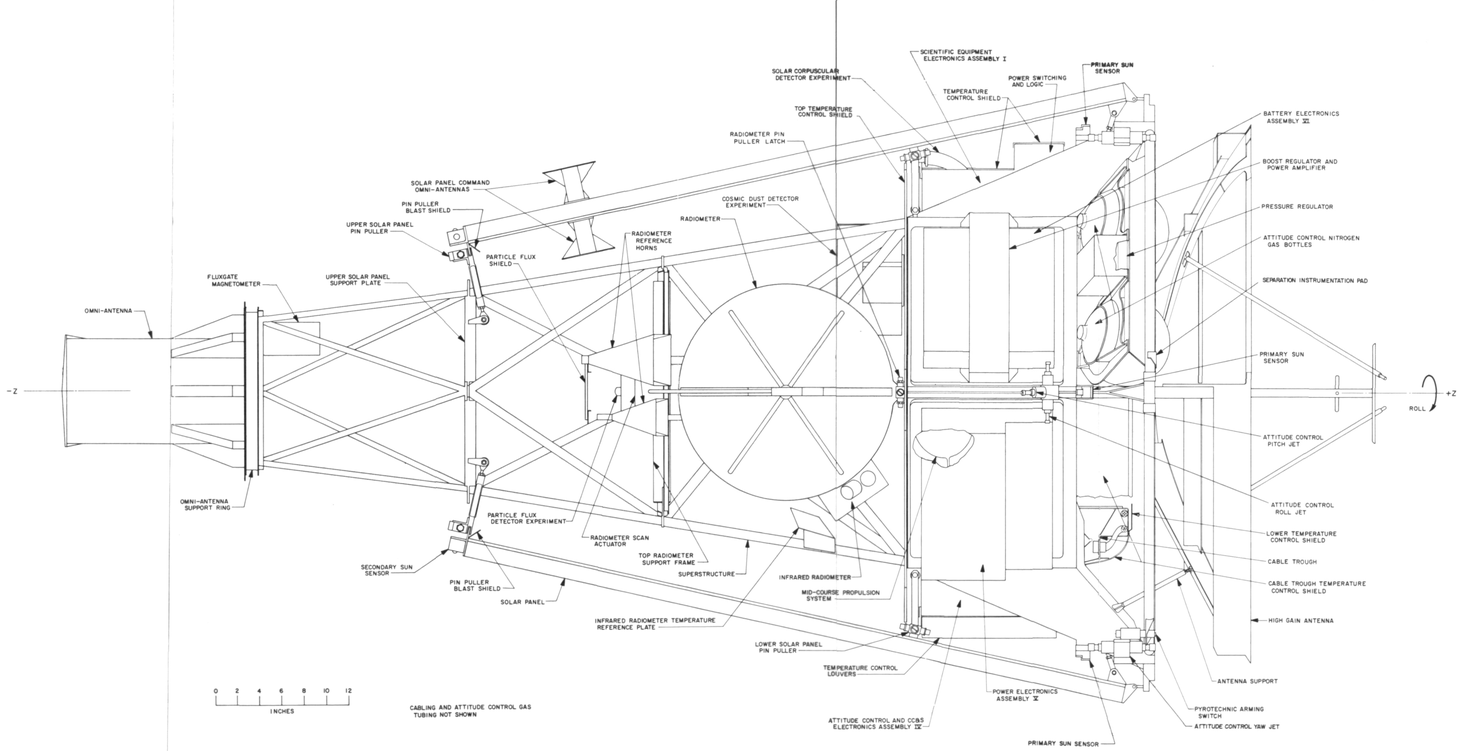

Fig. 2. Spacecraft configuration for *Mariner* Venus (1962)

"Page missing from available version"

VI. *Voyager* Project

Voyager missions are envisioned to evolve to sophisticated orbiters and landing experiments beginning in 1966 or 1967 using *Saturn* vehicles. Planetary orbiters are a necessary part of the evolution and are a logical step in the development of spacecraft technology. Orbiters are probably required to permit sufficient observation of the planet to know how to proceed with landing missions. Furthermore, orbiters may well constitute an important step in the actual landing experiments. The emphasis on planetary orbiters, therefore, will be to contribute to the successful accomplishment of the landing objective.

The primary programming efforts conducted during this reporting period consisted of working with Marshall Space Flight Center (MSFC) in determining the feasibility, schedule, funding requirements, and mission suitability of a three-stage C-1 *Saturn* for use in the *Voyager* project. A vehicle concept has been generated by MSFC which could provide approximately 5500 lb of payload injected into Mars or Venus trajectories beginning in 1965 or 1966.

Specific efforts directed to accomplishment of the *Voyager* Project were initiated at the start of FY 62. A brief synopsis of these efforts is as follows:

The Systems Division is participating with the technical divisions and the Marshall Space Flight Center in the generation of mission objectives and the preparation of preliminary systems design specifications for interplanetary spacecraft to be used as planetary orbiters and landers and out-of-the-plane-of-the-ecliptic probes using the *Saturn* vehicle as the booster.

The Space Science Division is conducting *Voyager* scientific feasibility studies, establishing the feasibility of meteorological, biological, and certain adaptions of geological experiments for the *Voyager*, as well as refining knowledge of the Mars and Venus environments as they affect experiments and spacecraft for these flights.

The Guidance and Control Division is continuing its studies of guidance and control requirements, methods, and techniques for advanced planetary missions, both those currently planned and those that become necessary or desirable as a result of discoveries on early planetary exploration missions that require further exploratory operations. The methods to be used include study of possible mission requirements to deduce the general requirements for guidance and control subsystem performance, evolution of subsystem configurations to accomplish the required tasks, and parametric and error analyses of typical missions and operating situations to determine the ranges or parameters and tolerances required.

The Engineering Mechanics Division is performing *Voyager* spacecraft studies, including analytical investigations of configuration, thermal control, entry and landing dynamics, post-landing and roving techniques, booster compatibility, multiple mission or universal design concepts and compromises, and structural design problems.

Page intentionally left blank

Page intentionally left blank

THE DSIF PROGRAM

VII. Introduction

An integral requirement in the conduct of scientific investigations of outer space is the establishment of a precision tracking and communications network capable of communicating with space vehicles and determining their positional location in space. The Deep Space Instrumentation Facility (DSIF) has been established to satisfy this requirement in lunar and planetary programs. Although the DSIF is primarily designed for use with spacecraft in deep space exploration, it may be used with other spacecraft where its capabilities can be used to advantage. The design philosophy of the DSIF is to provide a precision radio tracking system which will measure two angles, radial velocity, and range, and then to utilize this tracking system to send radio commands and to receive radio telemetry in an efficient and reliable manner.

The DSIF is comprised of three permanent deep space stations and one mobile station (Table 1). The three permanent stations are located approximately 120 deg apart on the Earth to provide continuous coverage of a deep space probe (Fig. 1). Their locations are near Goldstone, California (Figs. 2, 3, and 4); Woomera, Australia (Fig. 5); and Johannesburg, South Africa (Fig. 6). The Mobile Tracking Station (MTS, Fig. 7) is presently located near the permanent station in South Africa.

The permanent stations are equipped with 85-ft diameter parabolic reflector antennas with maximum angular tracking rates of 1 deg/sec; the MTS has a 10-ft diameter parabolic reflector antenna with a maximum angular tracking rate of 20 deg/sec. The MTS is used mainly for early acquisition, and tracking and communications with spacecraft from its injection into orbit until it reaches about 10,000-mi altitude.

Because of operational loading requirements, it is planned to install a total of six 85-ft antennas and three

210-ft antennas. Although three 85-ft antennas will be used primarily on lunar missions, and the other antennas on planetary missions, all of them will be capable of being used on any mission as scheduling demands. It is also planned to have a transportable station available for use either with a transportable 30- to 40-ft antenna or for connection to an existing antenna belonging to another facility.

The DSIF will be improved and modernized consistent with the state of the art and project requirements. A basic design requirement of the DSIF is that it be possible to incorporate these improvements quickly, easily, and economically. The research and development activities and the development engineering of new equipment for the DSIF are performed at the Goldstone Station. In most cases new equipment is installed and tested at Goldstone before it is integrated into the system. Once the new equipment has been accepted for general use within the DSIF, it is classed as Goldstone Duplicate Standard (GSDS) equipment, which standardizes the design and formalizes the documentation of like items throughout the net. An 85- and a 30-ft Az-El antenna are installed at Goldstone for primary use in research and development.

The Jet Propulsion Laboratory is directly responsible for the research, development, construction, maintenance, and operation of the DSIF under a contract between the

Table 1. DSIF station identification

Mobile Tracking Station (MTS)	DSIF 1
Pioneer Station (Goldstone)	DSIF 2
Echo Station (Goldstone)	DSIF 3
Woomera Tracking Station	DSIF 4
Johannesburg Tracking Station	DSIF 5

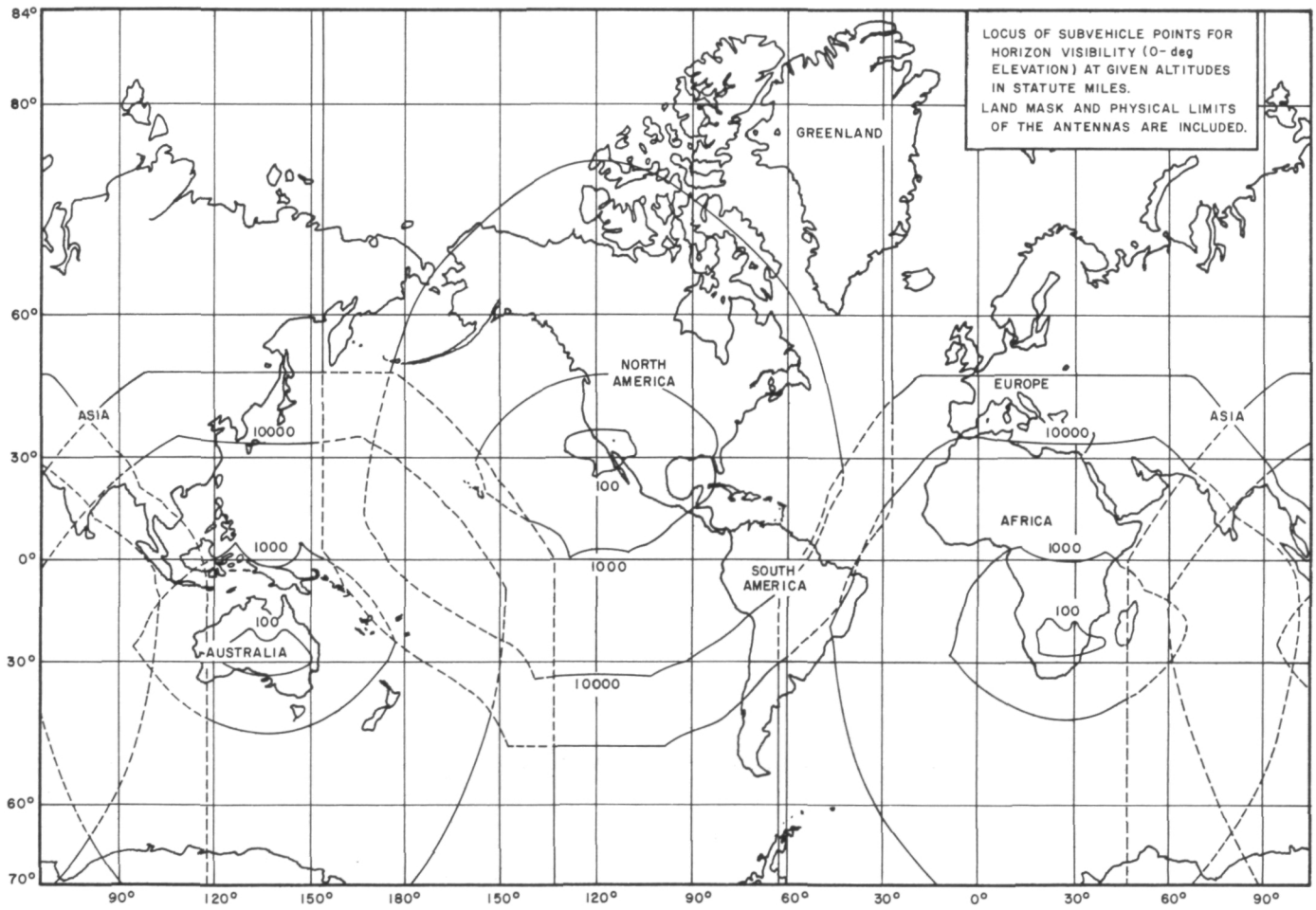

Fig. 1. DSIF station coverage for 85-ft diameter polar mount antennas

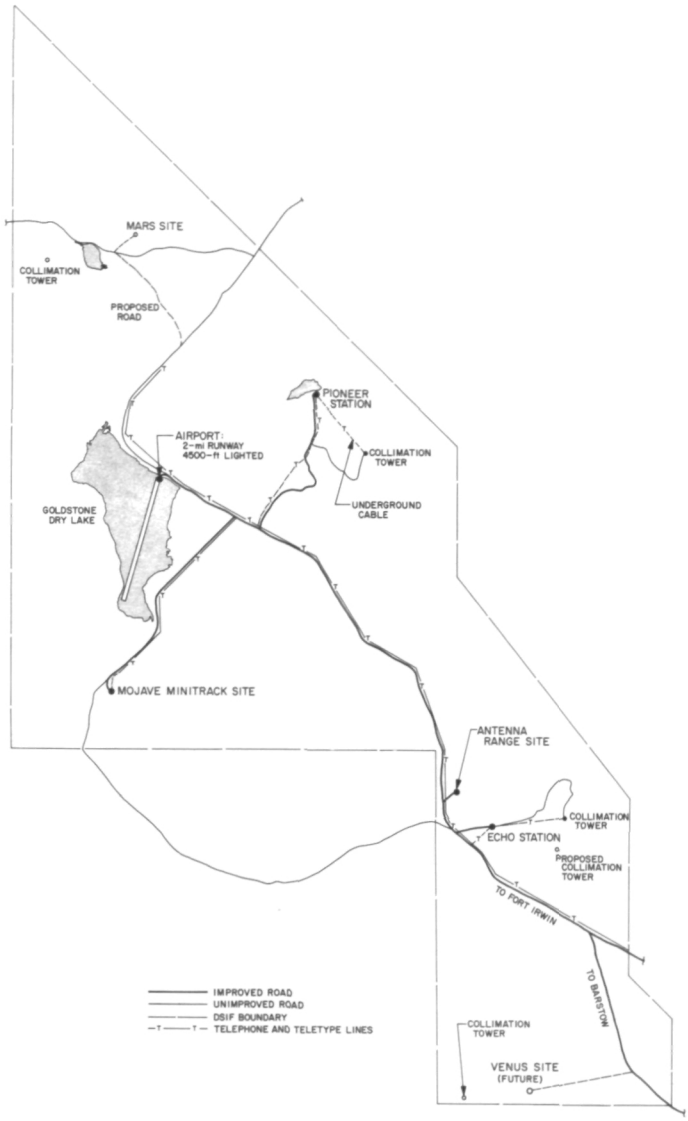

Fig. 2. Goldstone Station Complex

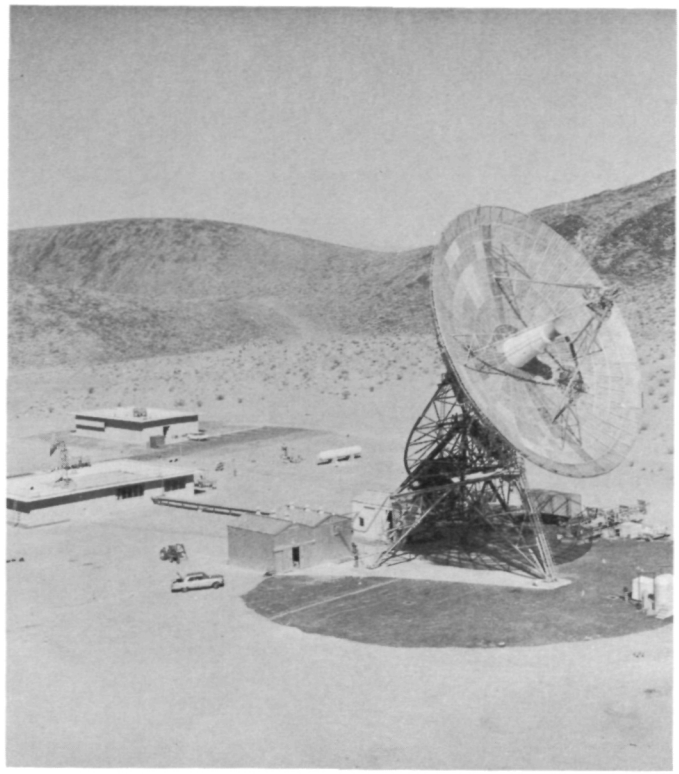

Fig. 3. Pioneer Station Goldstone

California Institute of Technology and the National Aeronautics and Space Administration. The permanent overseas stations are operated and maintained by cooperating agencies of their respective countries, while the Goldstone and mobile stations are operated and maintained by United States personnel under contract to JPL. A JPL technical liaison and coordination engineer is resident at each overseas station.

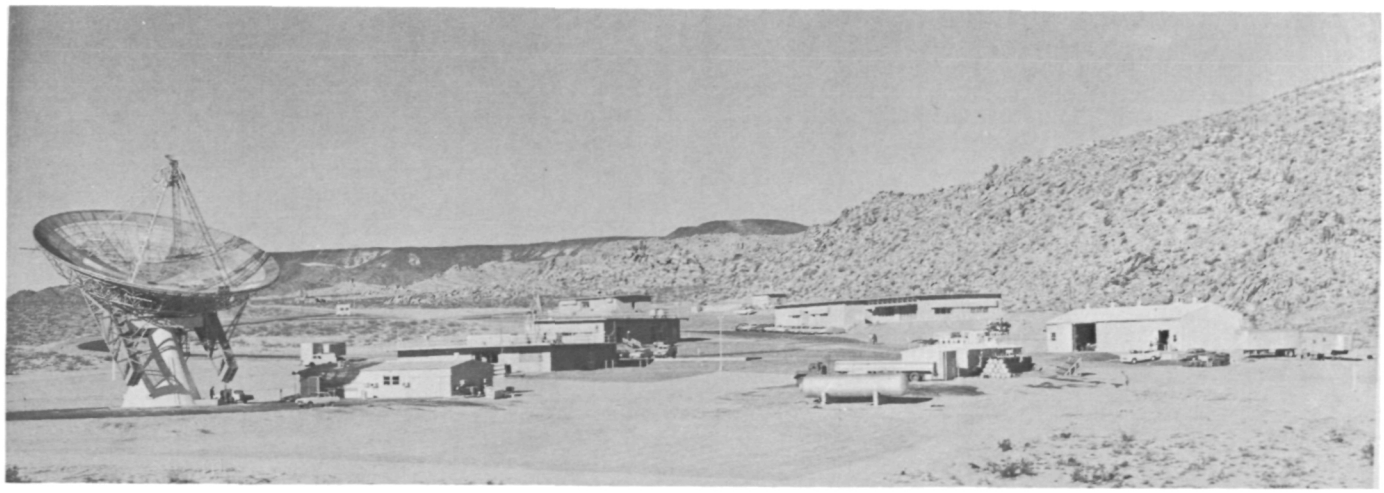

Fig. 4. Echo Station, Goldstone

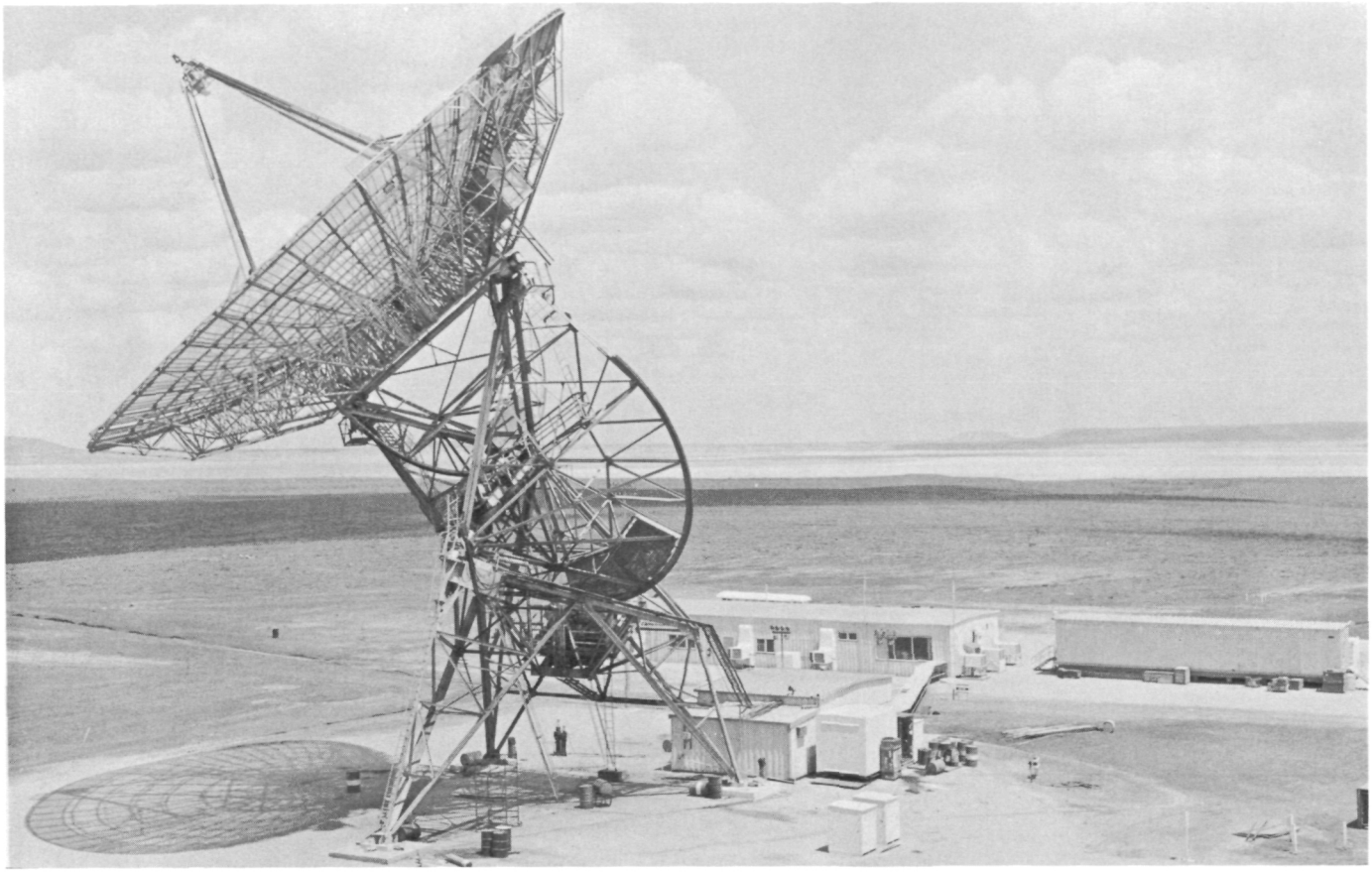

Fig. 5. Woomera Station, Australia

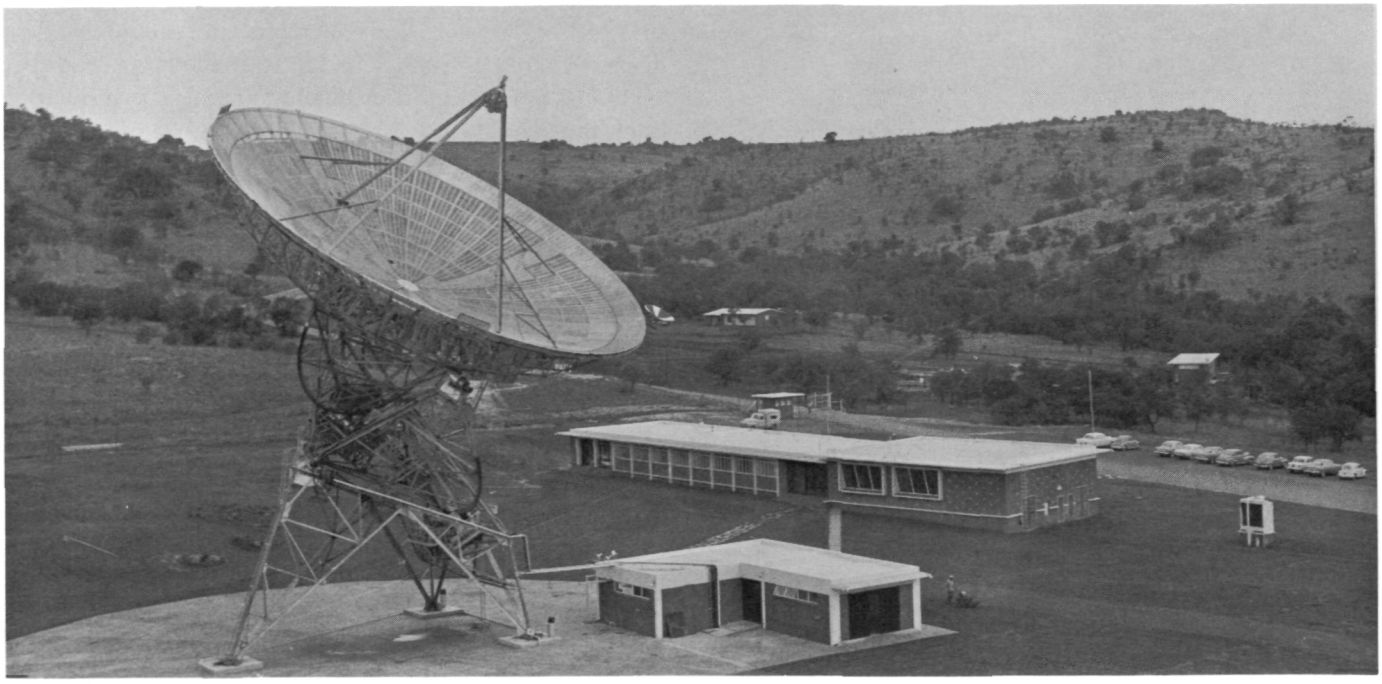

Fig. 6. Johannesburg Station, South Africa

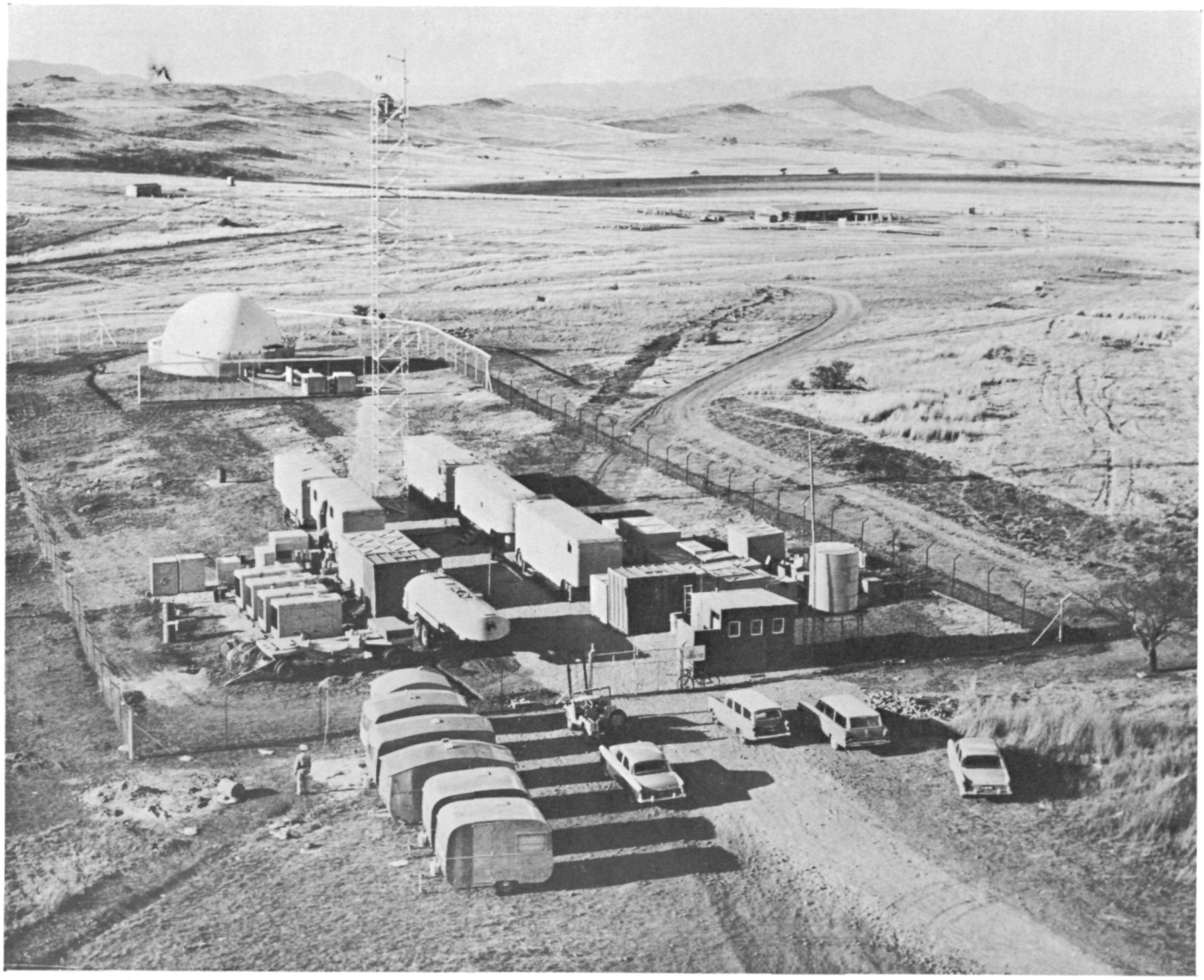

Fig. 7. Mobile Tracking Station, South Africa

VIII. Current Activities

A. Tracking Operations

All stations successfully tracked *Ranger* 4 following its launch until it impacted on the Moon. Both the MTS and Johannesburg Station were able to obtain two-way lock until the transponders' batteries were depleted about 10½ hr after launch. This was the first time the newly installed transmitter at Johannesburg had been used to track a spacecraft. Following depletion of the transponder batteries, the spacecraft was tracked by means of the capsule transmitter signal. A failure in the spacecraft control system prevented the spacecraft from performing any of its planned maneuvers, and precluded the transmission of telemetry. Various attempts to transmit commands to the spacecraft were unsuccessful.

B. Facilities and Capabilities

Improvements in the DSIF facilities and capabilities include the completion of a 10-kw transmitter at the Johannesburg Station, the addition at all stations of stable voltage controlled oscillators for generating the transmitter excitation frequency, and the erection of a new HA-Dec 85-ft antenna at the Goldstone Echo Site. When this antenna installation is complete, the 85-ft Az-El antenna will be moved to the High Power Transmitter Site, approximately 3 mi south.

In preparation for the installation of new equipment, engineering development is proceeding on the design of: a wide beam S-band tracking antenna which can be used as an aid in acquisition; ranging equipment which will be used with prototype S-band transmitting and receiving equipment on *Ranger* 8 and 9 flights; S-band receiving equipment which is planned for installation in the DSIF by January 1964; an interim 50-w transmitter for installation at the Woomera Station for use on *Mariner* launches; and a frequency synthesizer which will be used to generate the transmitter excitation frequency from an atomic oscillator frequency standard for *Mariner* flights. The coordinate converter has been moved to the Goldstone Echo Site and minor modifications made in it to facilitate testing and operation.

Engineering studies and tests are being conducted to determine the feasibility of diplexing 10 kw of transmitter power with low noise receiving systems using maser and parametric amplifiers. It has been determined that no system degradation results with diplexing high powers and standard narrowband phase lock receivers; but low noise amplifiers have not been used in this manner.

C. Research and Development

Recent results of DSIF supporting research and development are primarily in the following areas:

Low noise systems. The recently developed Cassegrain antenna feed system has been used to test a polarization tracking system which will automatically track a received signal in polarization. An S-band Cassegrain system is under development.

Tests on the closed cycle helium refrigeration system at Goldstone show that there is a loss of helium through a relief valve every time the refrigerator is stopped. This would be a problem at the overseas stations, and it is proposed that it be solved by adding auxiliary storage tanks.

Antenna modifications. An analysis of the 85-ft Az-El antenna has been made to determine the modifications which would be required to make the antenna usable at X-band. This analysis shows that extensive changes in the reflector surface and structural support will be required, but that the bearings and other structural parts can withstand the additional weight, provided the antenna is stowed in winds above 50 mph.

An extensive investigation into the effects of hail on the antenna surface and structure and the possibilities of occurrence of hailstorms in South Africa has been made. This investigation shows that large hailstones can severely damage an antenna.

X-band communication components. X-band Cassegrain feed systems are being designed for listening with circular polarization; tracking with circular polarization; listening with linear polarization (rotation remotely controlled); and transmitting at high power with circular polarization. These feeds will be used with an X-band maser, which is now being built, and a system of temperature instrumentation.

An X-band parametric amplifier has been developed with a noise temperature between 300 and 360°K, 20-db gain, and a 10-mc bandwidth.

Ranging system. Equipment has been designed and constructed to demonstrate that extremely accurate range measurements can be made at interplanetary distances by transmitting and receiving a range code which can be synchronized rapidly and reliably. At planetary distances the code and carrier will be regenerated in the spacecraft transponder, while at lunar distances a simple turn-around transponder will be satisfactory. In addition, a system using interrupted continuous wave signals has been developed and tested. In this system both the transmitter and receiver are keyed to minimize interference.

Advanced Antenna System. A preliminary design of a large aperture low noise antenna has been completed. This antenna will be capable of improving the DSIF communication capability by at least six times the capability with the present 85-ft antennas. The design specifies a parabolic reflector 210 ft in diameter and 88 ft in focal length with an Az-El mount and a separate instrumentation tower. Work is now proceeding on design specifications for submission to possible bidders.

Page intentionally left blank

Page intentionally left blank

SPACE SCIENCES

IX. Introduction

The origin of the solar system and the origin of life are two questions that have concerned man throughout recorded history. A planned space program may provide the challenge and opportunity to gather data which will contribute to the solution of these problems.

The scientific objectives of the JPL/NASA space exploration programs are to gather fundamental scientific data concerning the extraterrestrial phenomena of the solar system, and to collect scientific data which will contribute to the successful manned exploration of the Moon, planets and interplanetary space. To implement these objectives, a program of integrated scientific studies has been initiated. These studies are classified into four general areas of investigation: (1) lunar, (2) planetary, (3) solar and interplanetary, and (4) exobiology.

1. Areas of Investigation

The origin of the Moon is unknown and probably related to the origin of the solar system. Some of its known properties are anomalous and the unobservable properties have been the object of much extreme speculation. Its primary surface features have almost certainly been formed by processes of relatively much less importance on Earth, and the phenomena tending to alter and erode these features have been primarily of a different nature than those for the Earth. A record may be found near the surface which pertains directly to the early formative stages of the Earth–Moon system and of the solar system.

Measurements to be made on and in the Moon are also important because of their contribution to the present national goal of manned lunar exploration. The burden rests primarily with the unmanned program for the discovery of structural properties vital to the safety of manned exploration, and for the determination of chemical properties necessary for exploitation and support of the expeditions.

The planets may, as a result of presently planned ventures of space exploration, gain considerable prominence as sources of understanding of a number of important questions. The properties of the planets must be related to the origin of the solar system in a critical way.

Venus and Mars are the immediate targets for exploration by deep space probes; these and several of the other planets are also being studied by more conventional Earth-bound techniques to supplement the scientific data acquisition of the space probes.

So little is known about Venus that much conjecturing has been possible. The surface is probably invisible from

the Earth at all but the longest wavelengths, those in the microwave region. None of the properties of the atmosphere, which must be understood for the design of efficient surface exploration vehicles, is truly known.

While the surface of Mars is visible at many wavelengths, its very visibility has only been the start of extreme extrapolation. Although a number of atmospheric phenomena are interesting and little understood, it is the structure of the surface and the existence of life there which transcends all other questions in interest and importance.

The extension of the atmosphere of the Sun through which the deep space probes pass represents a region in which many relatively little understood phenomena occur. The measurement of the properties and composition of the charged and uncharged particles to be found there, and their interaction with each other and existing fields, may yield results directly relating to the properties of the Sun (which is the only star that can be explored in this manner), solar–terrestrial interactions and relationships, and the origin of cosmic rays and interplanetary dust and their interactions with the Sun.

The hazards to manned space flight to be encountered in interplanetary space are not yet sufficiently understood, and their further investigation is an important facet of the deep space exploration program.

The search for extraterrestrial life, the study of exobiology, may well be the most stimulating intellectual venture of the present decade. It is likely that the discovery of extraterrestrial life or of certain key biotic substances may provide vital clues to the understanding of the origin of life on Earth. The recent findings on Mars of the probable existence of substances containing carbon–hydrogen bonds in the dark regions, and of the seasonal variation in tonal contrast of these regions, suggests that space probes containing biologically oriented experiments to Mars may well be able to perform positive experiments. The discovery and study of prebiotic substances on the Moon, coupled with pertinent Earth-based studies, offers the opportunity to expand our present understanding of questions relating to the problem of the origin of life.

2. *Instrumentation*

Instrumentation for the measurement of the lunar surface texture will involve a combination of optical systems sensors and detectors including refracting, reflecting, and fiber optics; vidicon emission orthicons, photographic film, and electrostatic film; magnetic tape, magnetic cores, and thermoplastic tape. Radar systems to several frequencies can be used to examine texture and reflectivity properties.

Measurement of physical properties will involve the use of bevemeters, penetrometers, drills, infrared radiometers, gamma-gamma density detectors, magnetic susceptibility coils, contact thermoprobes, etc.

Instruments for the determination of petrological properties may include X-ray spectrographs, X-ray diffractometers, gamma-ray spectrographs, mass spectrometers, absorption and emission spectrometers, Rutherford scattering instruments, neutron activation and inelastic scattering instruments, gas chromatographs and wet chemical analysis instruments, etc. For the examination of noncrystalline phases and examination of external and internal features of grains, a petrographic microscope system will be used. Measurements of lunar body properties will utilize seismometers and gravimeters.

Measurements of the lunar particles and field environment will use instruments similar to those used in interplanetary space. Lunar atmosphere measurements may use modified Redhead gages, ion mass spectrometers, etc.

In addition to various kinds of photographic systems, planetary flyby missions will examine the surface and atmosphere with ultraviolet, infrared, and microwave radiometers and spectrometers. Radar systems at several frequencies can be used to examine texture and refractivity properties. During atmospheric descent, pressure, temperature, density and speed-of-sound probes will be used. Atmospheric composition can be measured by means of optical, ultraviolet and infrared spectrometers, gas chromatographs, mass spectrometers, and instruments using special chemical and nuclear properties. Measurements of surface properties will utilize instruments similar to those used on the Moon with the addition of applicable meteorological instrumentation.

Instruments to be used for measurement in interplanetary space include gas filled and solid state ionization chambers, geiger counters, proportional counters, several types of solid state detectors, scintillation counters, Cerenkov counters, and combinations of these instruments into particle spectrometers. In addition, electrostatic analyzers, Faraday cups, and magnetic spectrometers will be used. Instruments for the measurement of magnetic fields include search coil, spin coil, fluxgate, proton precession, alkali vapor, and metastable helium magnetometers. Instruments for the measurement of micrometeoroid flux

and properties include devices relying on momentum transfer, electromagnetic and electrostatic interaction, foil penetration, and foil ionization.

The instruments for the detection of prebiotic and biotic material will include the measurement of special chemical properties using standard biochemical analytical techniques. Growth and metabolism will be observed by fluorometric and radioisotope methods or changes in the turbidity of nutrient solutions. Form and change of form of the possible biotic material will be examined with special microscopes.

Page intentionally left blank

X. Lunar Studies

A. X-Ray Diffractometer

X-ray diffraction will be used for mineralogical analysis of lunar materials. The objectives are to identify the types of minerals of the lunar assemblage, to determine the relative quantities of the mineral types, and to ascertain, as far as possible, the precise compositions of the complex minerals.

A prototype of an X-ray diffractometer intended for use on *Surveyor* has been received at JPL (Fig. 1 and Table 1); the instrument was assembled by Philips Electronics Company of Mt. Vernon, New York.

Table 1. Characteristics of *Surveyor* X-ray diffractometer prototype

Parameter	Value
Scan range, deg	7 to 90
Scan speeds, deg/min	
Slow forward	½
Fast forward	4
Reverse	8
Focus-to-specimen distance, cm	8.5
Divergence slit, deg	3
Receiving slit, in.	0.006
Two Soller slits, deg	4.5
Counter	Proportional with xenon and halogen quench
Tube power (1 ma), kv	25

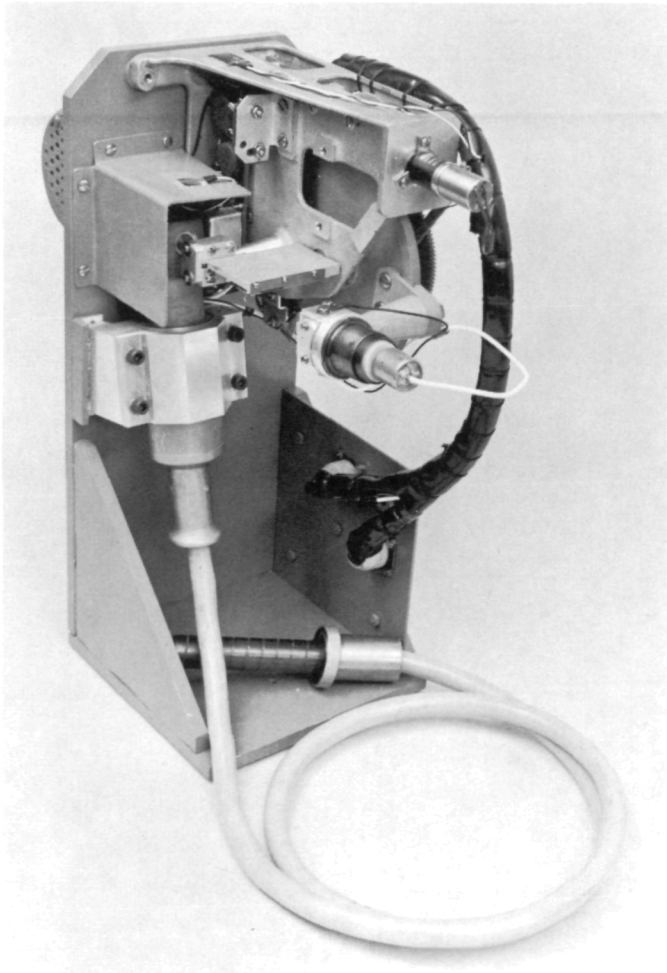

Fig. 1. Prototype of *Surveyor* diffractometer

The diffractometer is similar in configuration to standard commercial diffractometers except that the lunar instrument is inverted and employs a shorter focus-to-specimen distance as shown in Fig. 2. X-rays from the Cu target will pass through the 0.003-in. Be base and will be intercepted by a proportional counter. The counter will employ a discrimination circuit which is capable of reducing background from Fe fluorescence.

Functional specifications for acceptance are given in Fig. 3 and results obtained from the prototype tests are given in Table 2. The specifications were defined experimentally by investigating the quality of diffraction data required to distinguish minerals and mineral compositions in certain prominent three-phase assemblages. Comparison of the two columns (Table 2) shows that the prototype exceeded required specifications in each category.

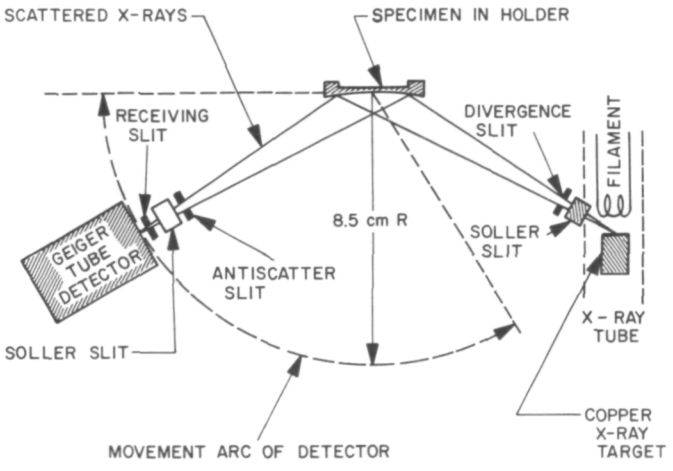

Fig. 2. *Diffractometer circuit*

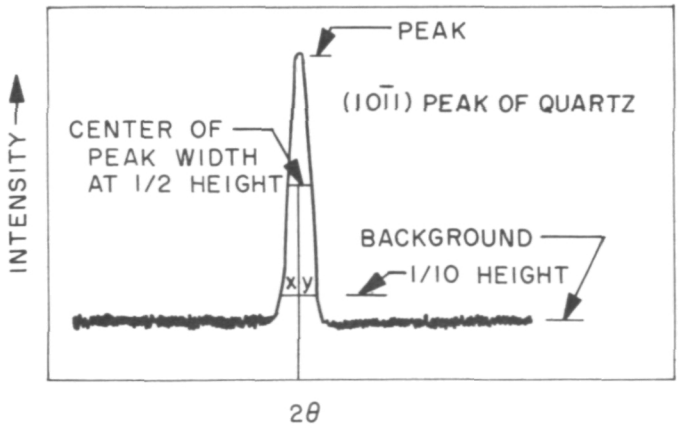

Fig. 3. Functional specifications

Table 2. Results obtained from functional *verification tests*

Parameter	Specification	Test result[a]
Peak width at ½ height, deg (2θ)	≤ 0.22	0.205
Peak width at 1/10 height, deg (2θ)	≤ 0.43	0.357
Asymmetry (x/y)	≤ 1.12	1.09
Peak/background	≥ 27	29.4
Peak intensity, pps	≥ 2300	3290
Reproducibility of peak intensity, %	≤ 3	1

[a] Average of 19 runs.

B. Petrographic Microscope

A petrographic microscope (Fig. 4) will be used on *Surveyor* for remote observation of crushed rock samples in transmitted light. The scientific objectives are:

(1) Identification of rock type and its genesis by means of: identification of rock texture, identification of shapes and relative sizes of different mineral grains, and determination of relative abundances of minerals in sample.

(2) Detection of glass by use of cross-polarized light and estimate of composition of glass by refractive index.

(3) Determination of particle shape and size distribution of possible loose surficial material.

1. Operation

A sample consisting of particles in the size range 75 to 300 μ is delivered to the microscope by the spacecraft and is deposited in the centrifugal hopper. The hopper and its contents are then heated; when the particles reach a temperature of 270 to 280°F, the hopper spins and the particles are thrown against a thermoplastic tape. The first layer embeds itself by local softening of the tape; the particles which do not contact the tape fall away leaving a monoparticle layer.

The tape is threaded through a sprocket mechanism which is driven by a rotary solenoid. After the particles

have been embedded in the tape, the tape is transported with a second tape to an impulse heat sealer where the particles are immersed in a solid sandwich of tape. The particles are moved to the field of view of the objective lens and are viewed in both plane-polarized and cross-polarized light.

The objective lens is initially focused on a plane below the plane containing the tops of the particles. The zone of focus of the lens moves in seven discrete 40-μ steps through the image plane of the particles to a point above the best image plane. A visual image is taken at each step of the focusing sequence. The sequential images ensure that one good image is available for all particles. They also show the direction of movement of Becke lines, enabling an estimate to be made of the refractive indices of individual particles. Figure 5 is a sequence of images from the slow-scan TV monitor showing the Becke lines for crushed glass particles.

Since the capability required is to view 500 particles from each bulk sample, and each field of view contains only 5 to 10 particles, many different fields of view are needed for each sample. The rotary solenoid drives the tape to bring more particles to the objective lens and the imaging sequence is repeated.

2. Testing

A breadboard model of the *Surveyor* petrographic microscope (Fig. 4) has been received at JPL from

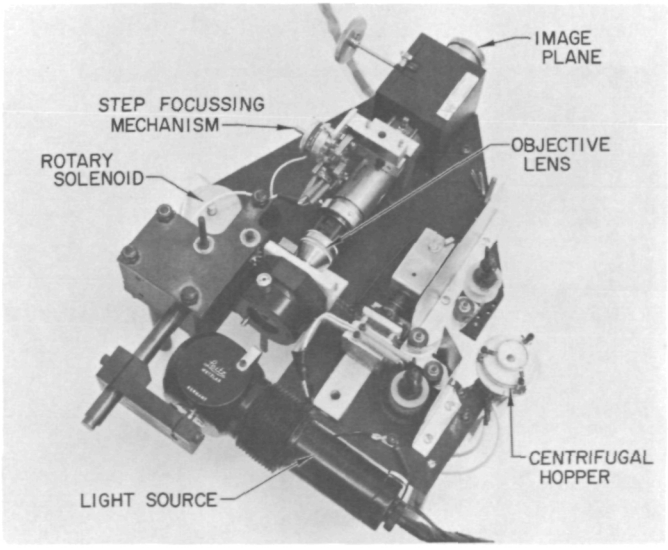

Fig. 4. Petrographic microscope breadboard

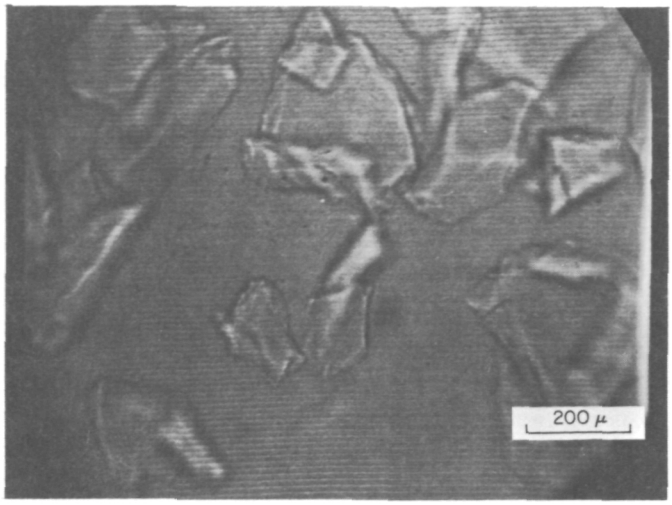

(a) Below plane of focus; Becke lines (concentrations of light) inside glass particles

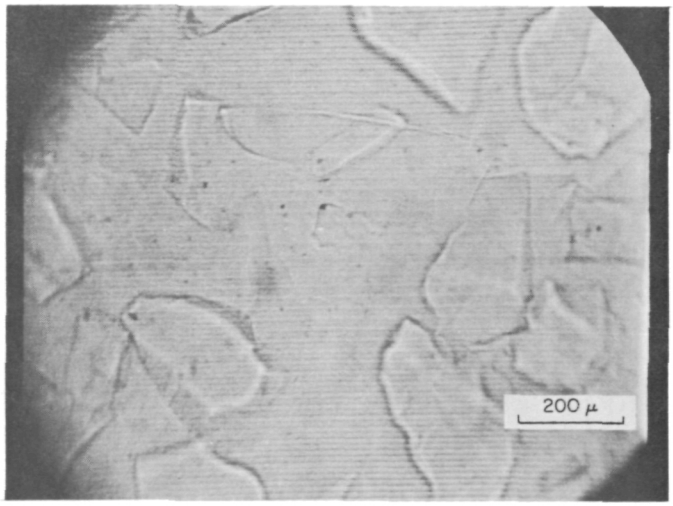

(b) Close to correct focus; Becke lines at edge of particles

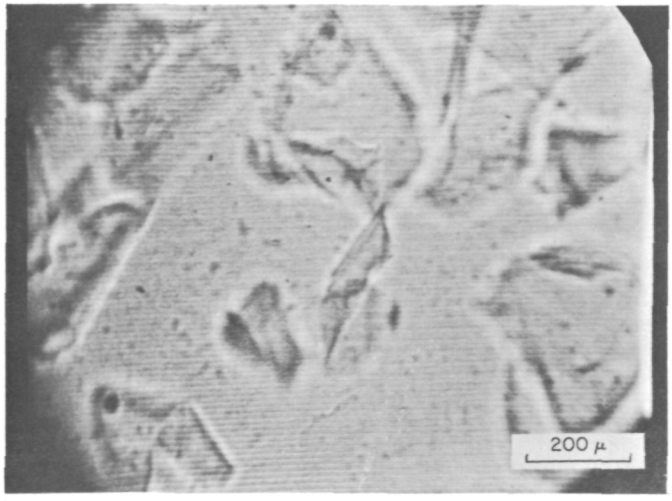

(c) Above correct focus; Becke lines in mounting medium

Fig. 5. Crushed glass particles (n = 1.515) in medium n = 1.54; plane-polarized light

Armour Research Foundation, Chicago. Tests to the end of April 1962 indicate that the over-all design of the optical system is correct. A magnified image of sufficient quality can be transmitted to the faceplate of a vidicon. The resolution of the system is now determined by the diameter of the electron beam in the vidicon, which is about 25 μ. The optical magnification now being used is $\times 16$ which will allow final resolution of shapes of 5- to 10-μ particles. Figure 6 shows crushed basalt particles (phenocrysts are olivine). The white plagioclase laths in the center of the field are 8 to 10 μ wide.

Experiments are underway using narrow bandwidth illumination in order to produce light and dark interference bands in birefringent minerals in cross-polarized light, instead of colored bands which cannot be discriminated by the TV system. Figure 7 shows such light and dark bands in forsterite grains; birefringence $\gamma - \alpha = 0.040$.

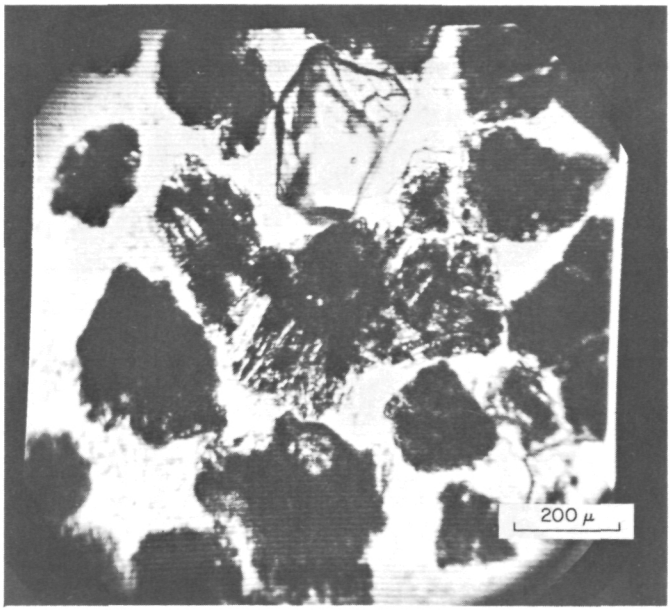

Fig. 6. Crushed basalt particles

Many problems exist, especially with the emplacement of particles on, and suspension in, the thermoplastic tape. The original design was for a gravity-feed of heated particles onto an inclined tape surface. The positive centrifugal system now being tested was designed to ensure complete expulsion of the particles of one sample before the next sample is introduced and to eliminate, as much as possible, a critical operating attitude.

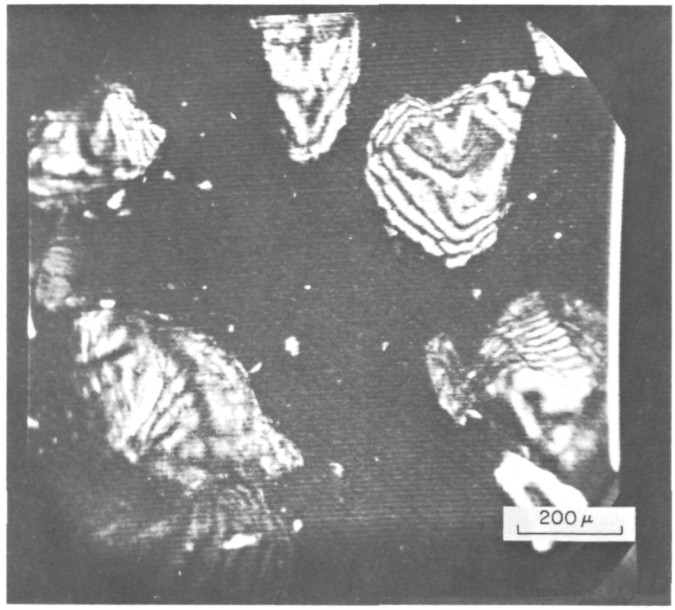

Fig. 7. Crushed forsterite grains in cross-polarized narrow-bandwidth light

C. Seismograph System

The Lamont Geological Observatory of Columbia University, under a JPL contract, is developing a seismograph system for the *Surveyor* project. The basic system consists of a three-component long-period seismometer (Fig. 8),

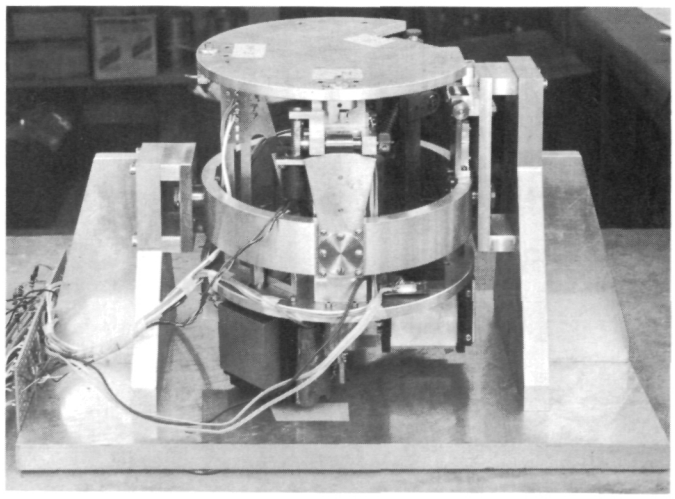

Fig. 8. Three-component long-period seismometer

a short-period vertical seismometer (Fig. 9), feedback control circuitry, a leveling system, and a calibration system.

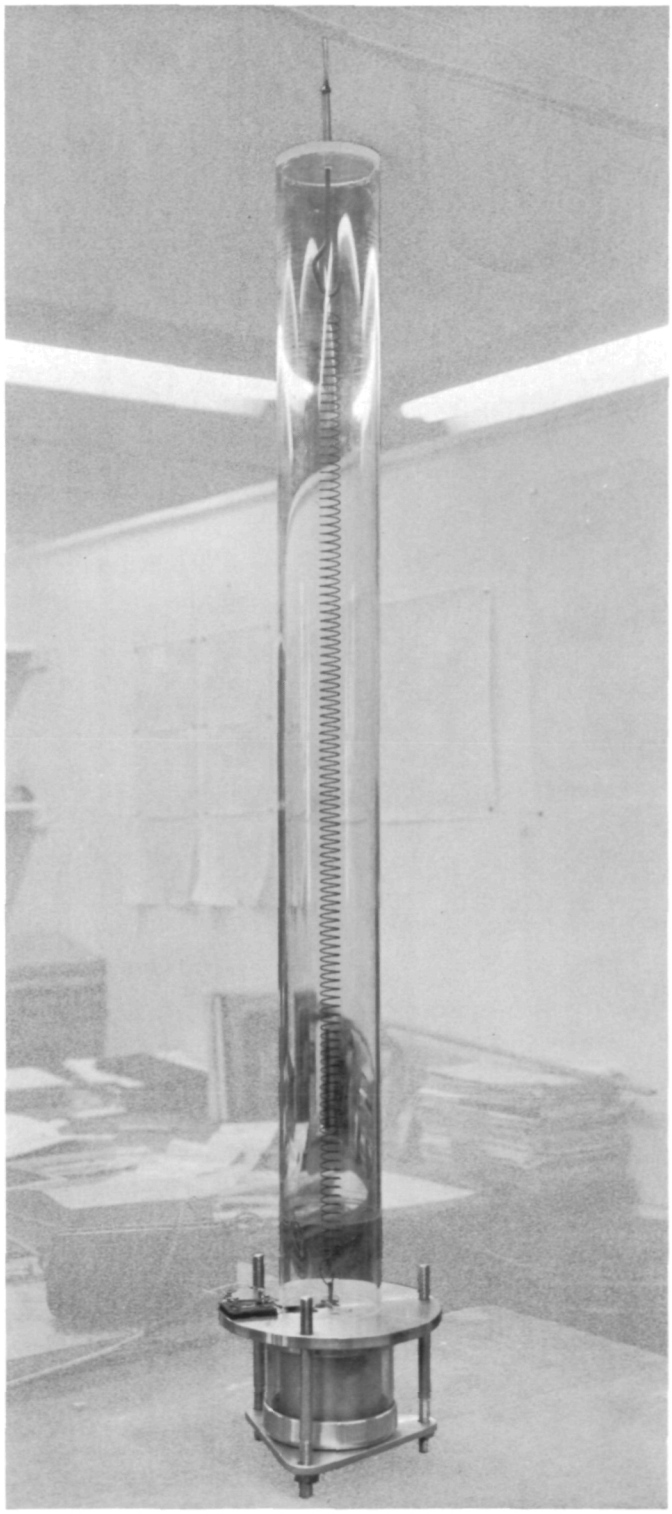

Fig. 9. Short-period vertical seismometer

One of the three long-period seismometers will measure vertical displacement; the two others will measure mutually perpendicular components of ground motion. Each of the long-period seismometers is equipped with displacement transducers of the capacitance type. Each will have a free-resonant period of 15 sec, will be tuned to provide an output of 25 mv/mμ of ground displacement, and will have a magnification of 10^6. The response curve is shown in Fig. 10.

The short-period vertical seismometer is equipped with a moving-coil transducer (velocity transducer) and will have a free-resonant period of 1 sec. This instrument will provide an output of 50 mv/mμ of ground displacement at a frequency of 1 cps. The long helical spring (Fig. 9) is not part of the instrument design but is required as a test fixture to permit operation in the gravitational field of the Earth. The response curve for the short period vertical instrument is shown in Fig. 11.

Caging of all the seismic masses will be accomplished by a single bellows-type compressional system. When the system is compressed (caged) the seismic masses and supports will be lifted and firmly locked so that vibrational or shock effects will not damage the system. After landing on the lunar surface, two squibs will be detonated. Each squib will rupture one of two diaphragms, releasing the contained compression, and thereby uncaging the system.

A servosystem, consisting of a two-axis, motor-driven gimbal and motor-drive circuitry for leveling the seismometers, will begin operation after the spacecraft

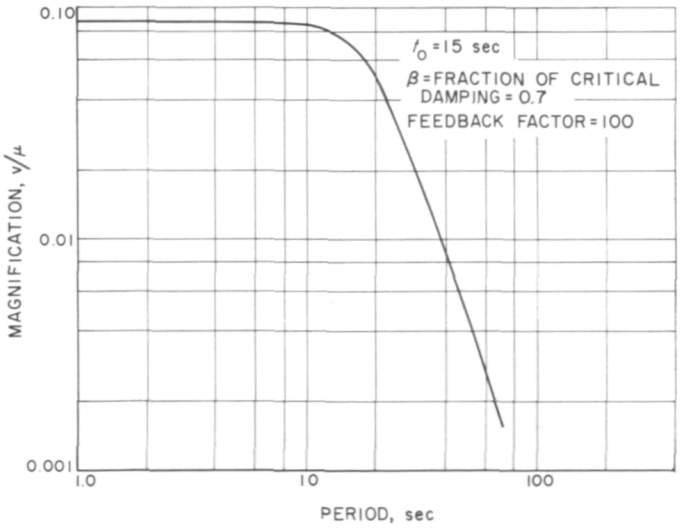

Fig. 10. Response of long-period seismograph

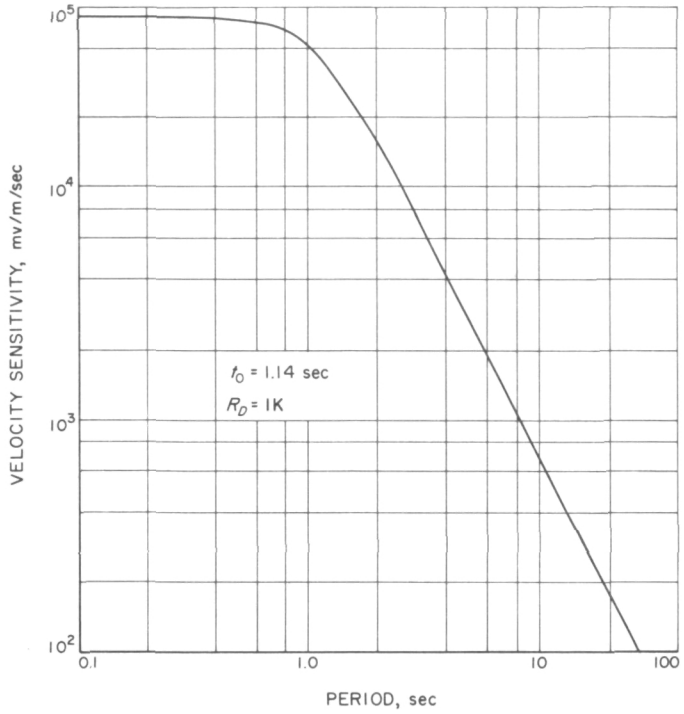

Fig. 11. Response of short-period seismograph

lowering mechanism has placed the instrument package on the lunar surface. The system will be capable of leveling from a tilt of ±15 deg to within 10 sec of arc of the local vertical. Leveling will occur automatically, and also upon command, to compensate for anomalous drifts resulting from thermal and mechanical effects, as well as tilt.

Feedback control circuitry (Fig. 12) is used for maintaining central alinement of each of the three-component, long-period seismometers. A portion of the output signal is fed back, through a low-pass filter, to the coil of the coil-magnet assembly provided for damping the seismograph. Thus, the instrument is held centered to some fraction of its open-loop displacement. By monitoring the feedback signal required for servo-centering, gravity tide and tilt information will be obtained, provided thermal and mechanical drifts can be sorted out on the basis of their essential character and independent temperature information.

Completion of the first prototype model is expected in May 1962. Construction is being performed by the Inter-

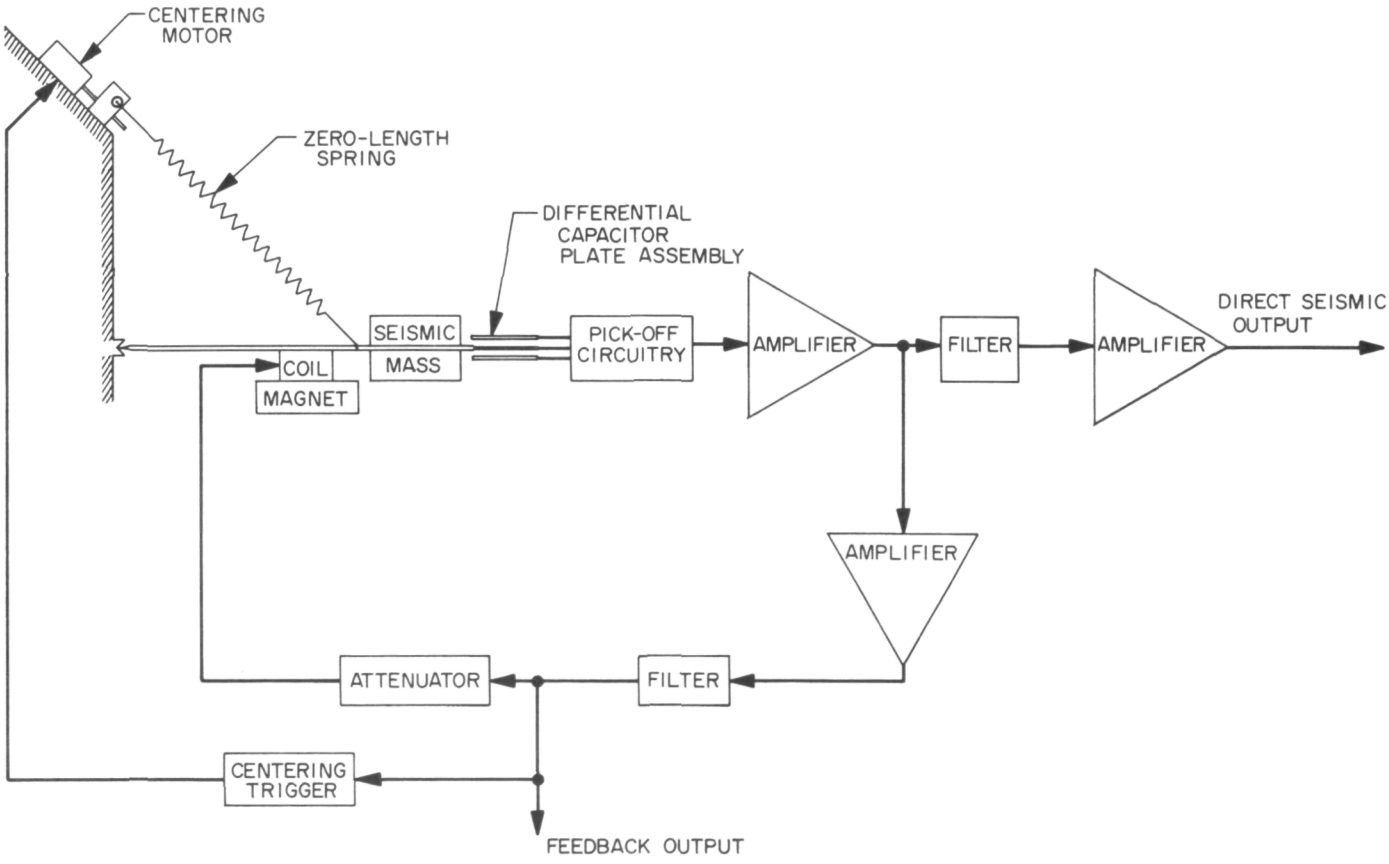

Fig. 12. Circuit of feedback controlled seismograph

national Telephone and Telegraph Company Federal Laboratory at Nutley, New Jersey, under subcontract to the Lamont Geological Observatory.

D. Rocket Radar Experiment

A rocket-borne radar experiment is to be performed for the purpose of obtaining high-altitude radar scattering data from terrains of known roughness and composition. This data will then be compared with the various radar scatter theories to establish their validity (Refs. 1, 2, 3), and to permit conclusions about the nature of unknown terrain surfaces from their radar return characteristics. Lightweight systems and technology developed from the experiment may then be applied to the exploration of lunar and planetary surfaces.

Instrumentation of the experiment requires a radar and telemetry transmitter (Fig. 13) to be installed in the rocket; and telemetry receivers, and calibration and data recording equipment on the ground. A camera (Fig. 14)

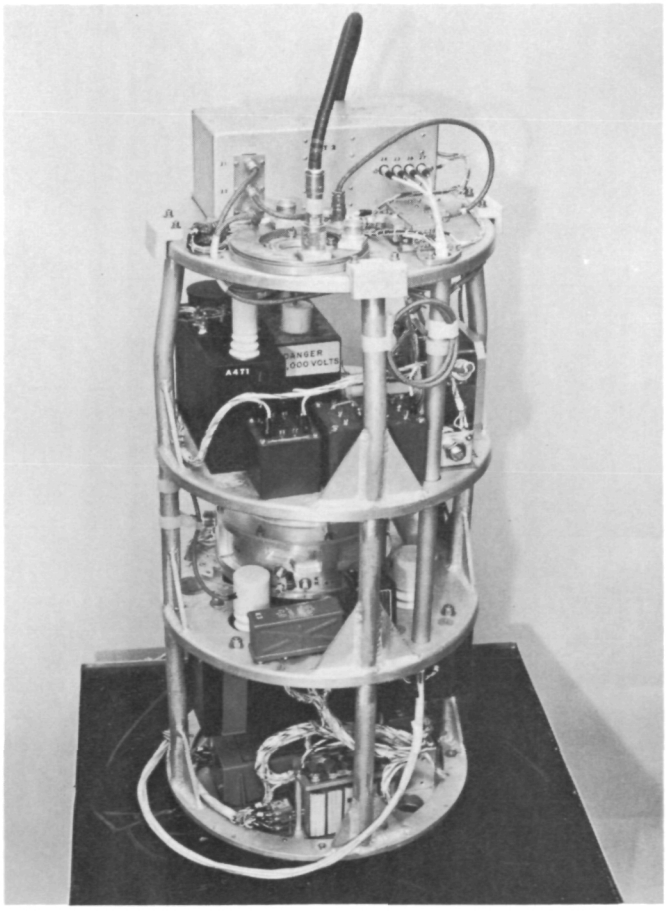

Fig. 13. Rocket radar unit

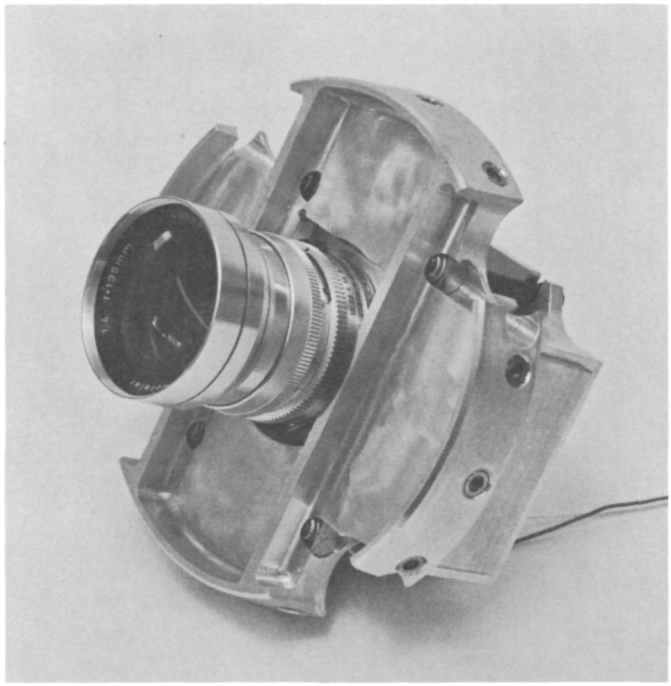

Fig. 14. Nose cone camera and mount

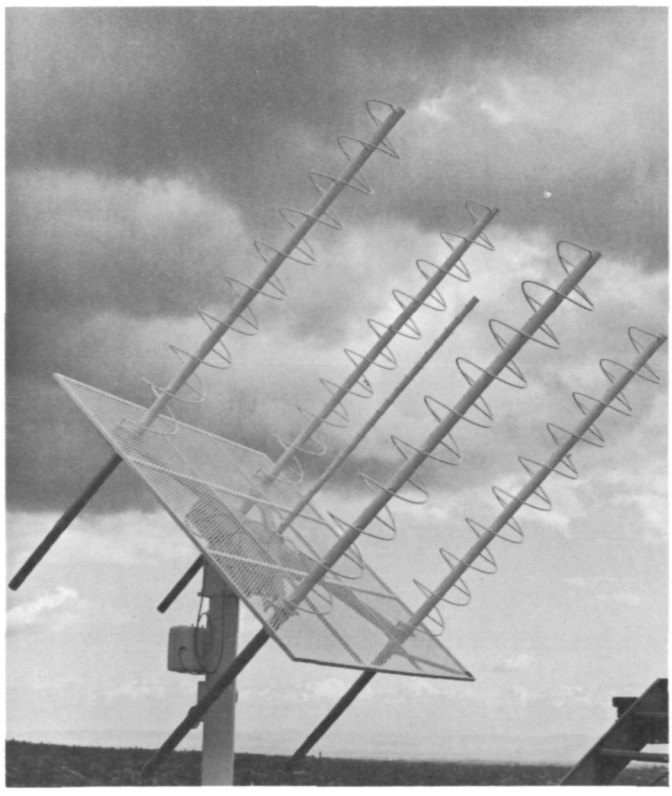

Fig. 15. GSE antennas

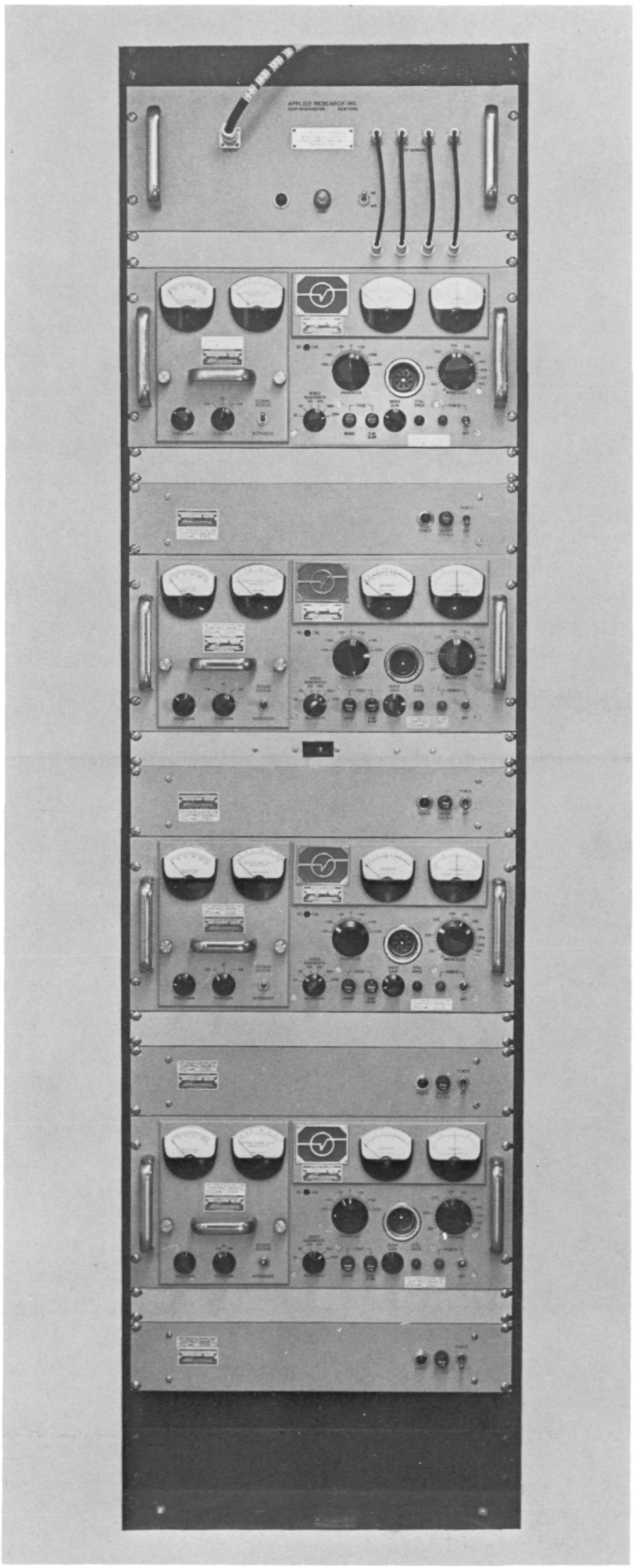

Fig. 16. Telemetry receiver rack

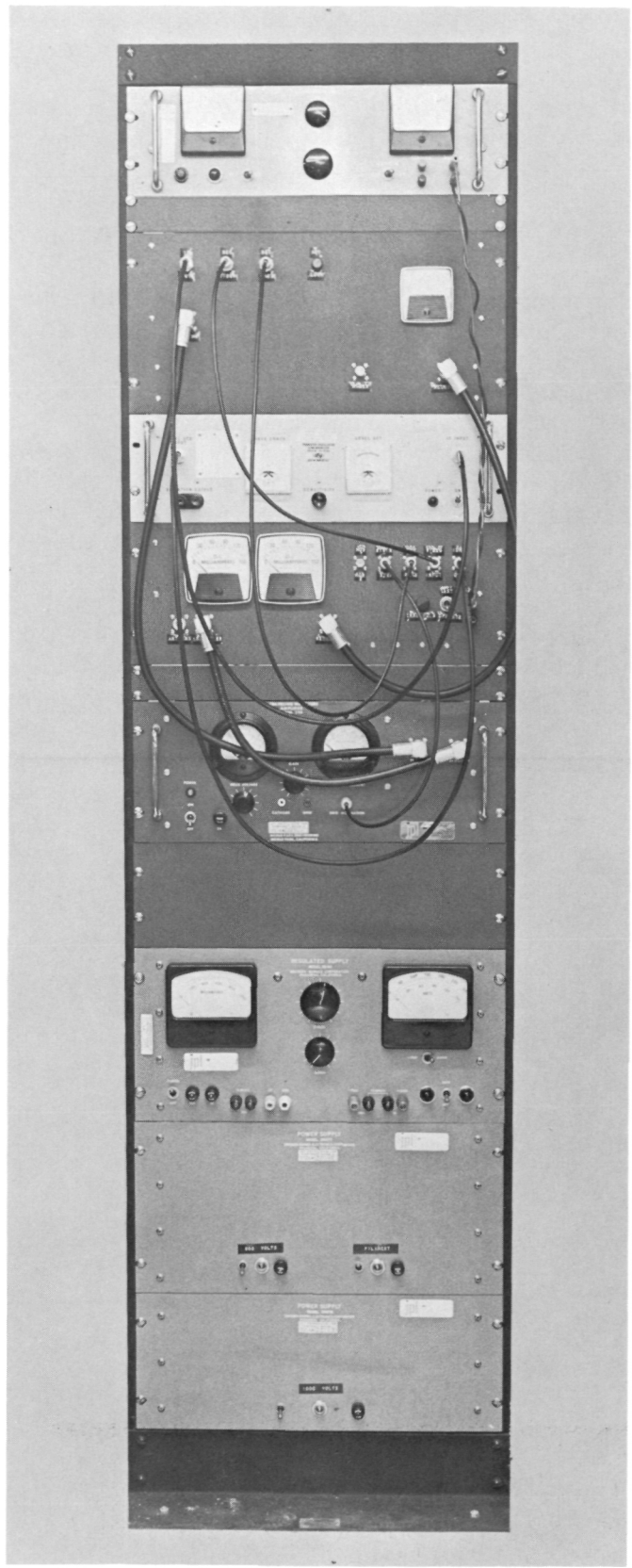

Fig. 17. Calibrator rack

is carried in the rocket nose cone to record the exact location of the radar scattering terrain.

In order to obtain minimum weight, the radar transmitter tube will not be cooled and can therefore be operated only for short periods. For this, and power consumption reasons, the radar will transmit three bursts of 4-sec duration at approximate altitudes of 225, 137, and 84 km. The radar is to operate with a frequency of 1 kmc, a pulse length of 10 μsec, a pulse repetition rate of 300 pps, and a peak power of 50 kw.

The transmitted signal is right-circularly polarized; two separate receivers are used to measure both right and left circular components of the return signal. The receivers have a sensitivity of -100 dbm and a linear dynamic range of at least 40 db; the 40-db linear dynamic range is accomplished by using the output of the last two IF amplifier stages.

Outputs of each radar receiver are used to frequency modulate the four VHF telemetry transmitters. A separate transmitter and center frequency is used for each output in order to obtain sufficient bandwidth to reproduce the pulses.

The telemetry is received by a simultaneous lobing quad-helix array (Fig. 15) which will be used to track the rocket manually. The output of the second IF amplifier of each telemetry receiver is converted from 5 mc to 750 kc center-frequency FM and recorded on magnetic tape. The demodulated output of each receiver is also displayed on an oscilloscope and recorded on high-speed movie film. Figure 16 illustrates the telemetry receiver rack.

Continuous calibration of the experiment during transmissions is accomplished by a ground-based transponder. The amplitude of each transmitted radar pulse is recorded from the output of a calibrated receiver. The received pulse is also used to trigger a 1-kmc calibration transmitter after a delay of 850 μsec. The output of this transmitter is automatically frequency controlled to the received radar frequency, so as to be receivable by the radar receivers. The output is a staircase pulse with 5 steps, each 20 μsec wide, with 6-db power dif-

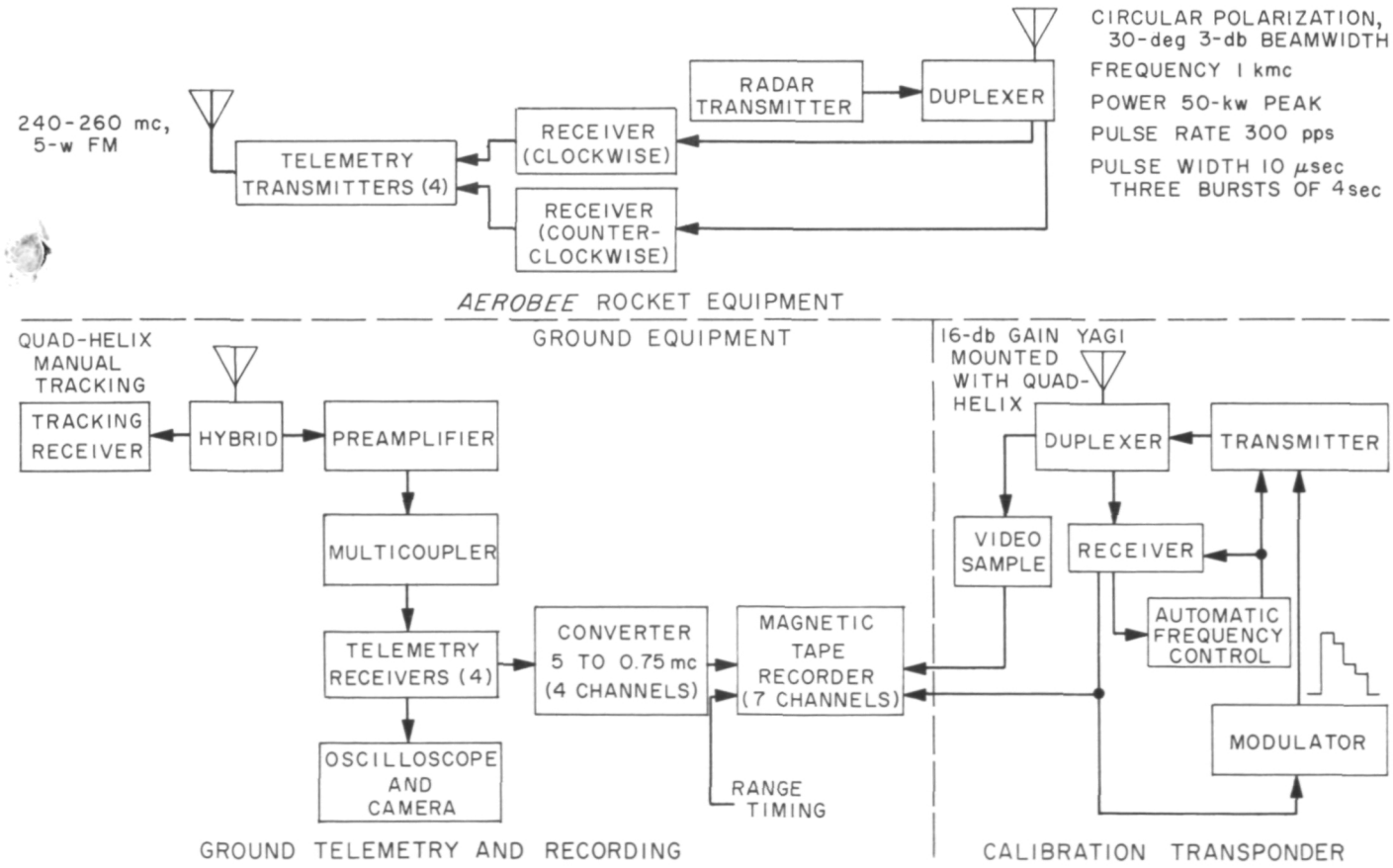

Fig. 18. Rocket radar experiment, over-all block diagram

ference between steps. This pulse calibrates the radar receivers, and the telemetry transmitters and receivers, for sensitivity, linearity, and dynamic range performance over the duration of the experiment. A video sample of the transmitter staircase is also recorded. The calibrator rack is shown in Fig. 17.

The calibrator antenna is a 16-db gain Yagi, and is mounted in the center of the telemetry receiving quadhelix antenna array (Fig. 15).

Figure 18 is a block diagram of the experiment. Figure 19 is a block diagram of the airborne radar system with the transmitting and receiving portions; Fig. 20 shows details of the calibration transponder.

Two radar units are presently in the final testing stages. One unit has a 10-μsec pulse width, the other an optional 3 μsec. Both units will be flown over the White Sands Missile Range, New Mexico, aboard attitude-stabilized *Aerobee*-150 rockets. The first flights were scheduled for this spring; parachute recovery of the payloads will be attempted.

The radar units are built by the Bendix Corporation, York Division, York, Pennsylvania; lightweight modulator designs were investigated by the Massachusetts Institute of Technology Electronic Systems Laboratory (Ref. 4). The Ohio State University Antenna Laboratory is participating in the design and interpretation of the experiment, and has provided the radar antenna design.

The University of New Mexico Engineering Experiment Station is participating in the interpretation of radar scattering by using acoustical models, and the measurement of the surface properties at the White Sands Missile Range. The *Aerobee* rockets, as well as attitude stabilization and parachute recovery packages are being supplied by the Goddard Space Flight Center.

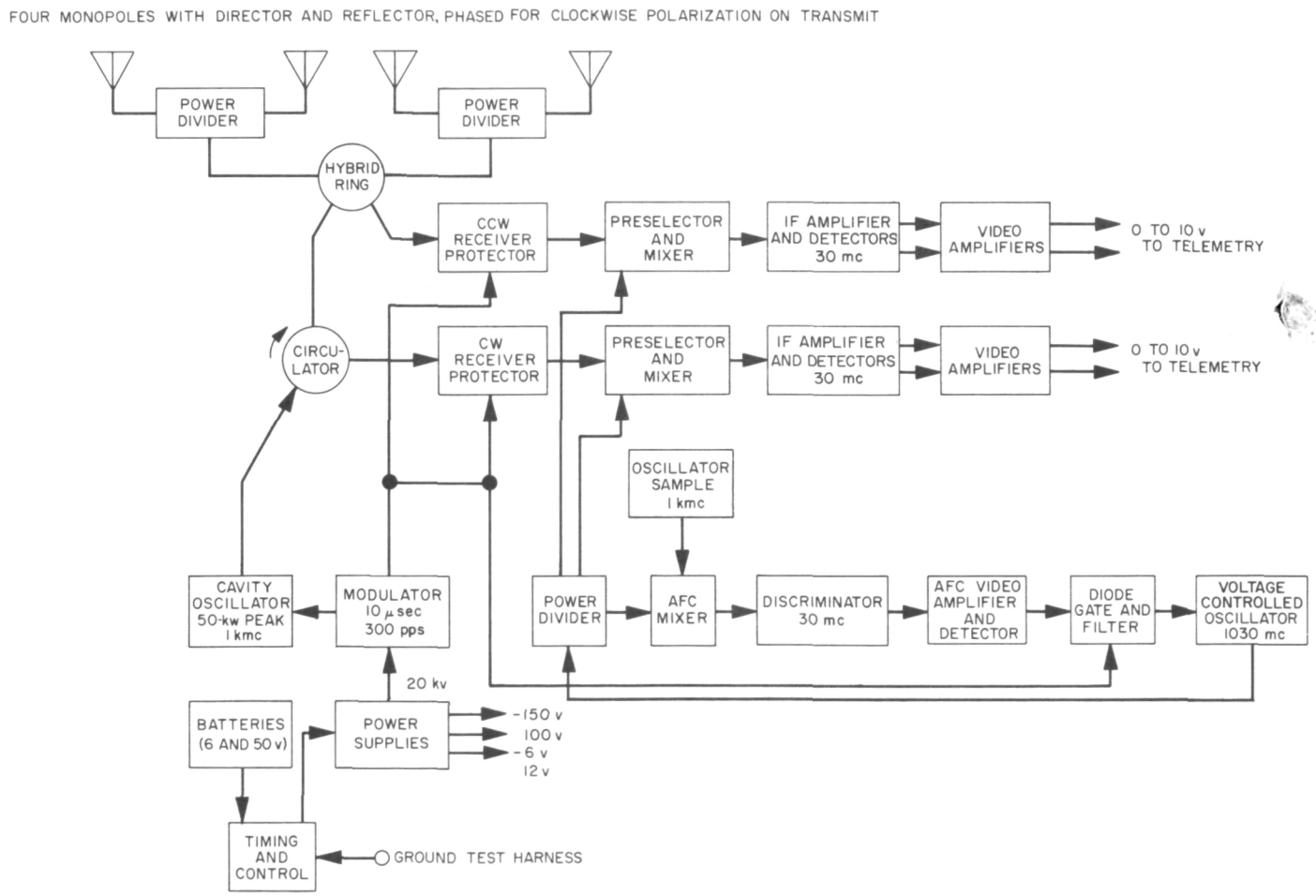

Fig. 19. Airborne radar unit

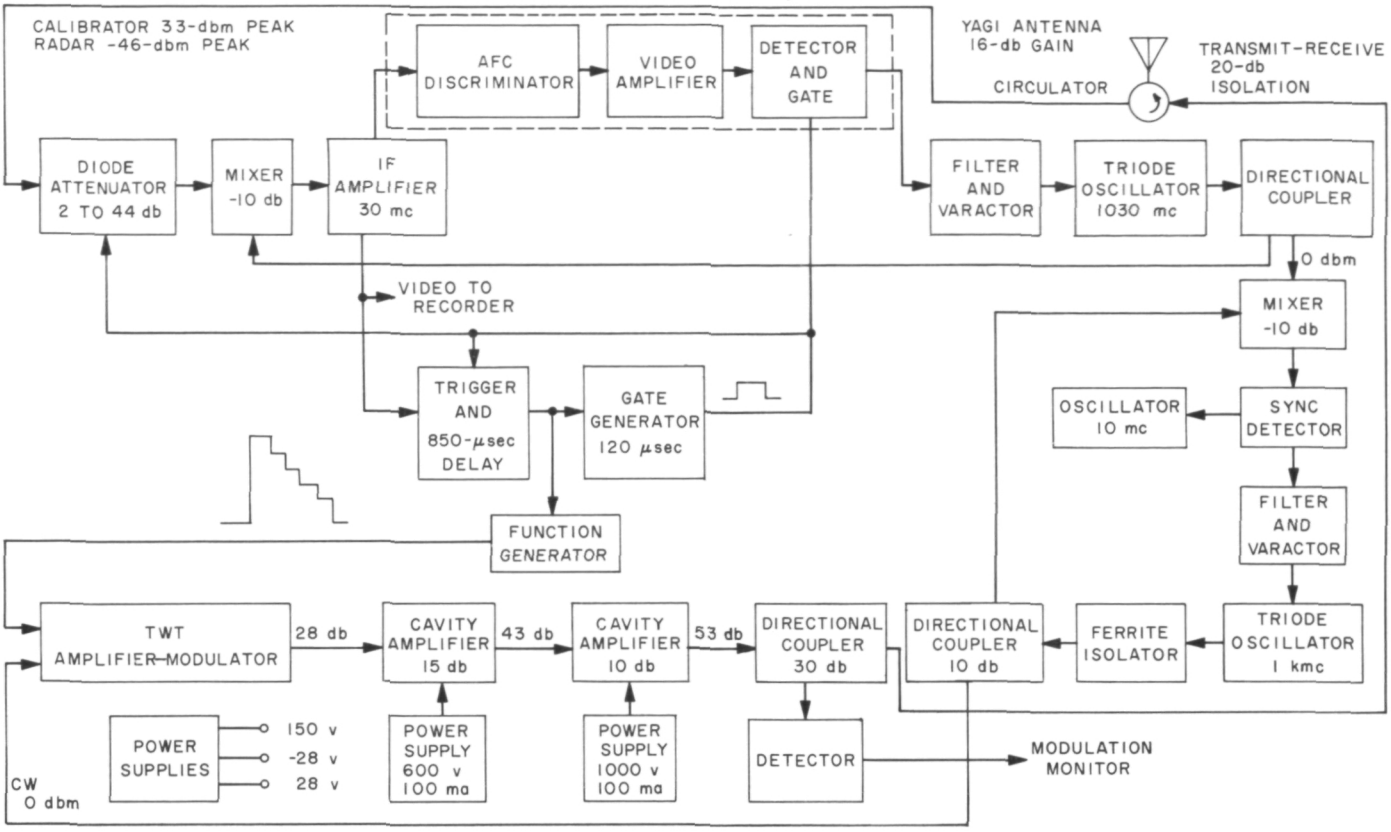

Fig. 20. GSE calibrator

E. Toroidal Oscillations of the Moon

If excited, the free vibrations of the Moon may be recorded by the long-period seismograph system to be placed on the Moon as part of a program of the National Aeronautics and Space Administration. (*See Section: C. Seismograph System.*) The free toroidal periods have been calculated for three models of the Moon originally presented by Bolt (Ref. 5). The toroidal oscillations involve only shear motions, and knowledge of their frequencies of vibration is valuable for studying the variation of shear velocity with depth throughout the interior of a planet.

Moon Model I is a homogeneous sphere of radius $R = 1738$ km, mean density $\rho = 3.33$ gm/cm^3 and mean shear velocity $\beta = 4.7$ km/sec. Models II and III, which agree with the total mass of the Moon, are defined by the Roche laws of density distribution:

$$\text{Model II} \quad \rho = 3.415 - 0.135X^2;\ X = r/R$$

$$\text{Model III} \quad \rho = 4.430 - 1.830X^2$$

Model II is similar to that calculated by Jeffreys (Ref. 6) for the self-compression of a Moon composed of ultrabasic rock with a surface density near 3.29 gm/cm^3. Model III, which was selected to show the effect of a heavy central core, has an extreme density distribution starting at 2.60 gm/cm^3 at the surface and increasing to 4.43 gm/cm^3 at the center of the Moon. The variation of shear velocity with depth was calculated from the empirical velocity–density relation based on Jeffreys' (Ref. 6) shear wave velocity distribution for the Earth, and Bullen's (Ref. 7) density distribution:

$$\beta = -0.60 + 1.52\rho \qquad 2.5 < \rho < 4.5$$

The system of differential equations defining the toroidal oscillations of a planet (Ref. 8) was solved numerically on the IBM 7090 computer using the fourth-order Adams-Moulton predictor–corrector method. The variation of density and rigidity, μ ($\mu = \beta^2\rho$), was specified at 20-km intervals throughout the interior of the Moon. The calculated periods of oscillation are shown in Table 3.

Table 3. Periods of toroidal oscillations, min

n	Mode	Moon Model		
		I	II	III
2	Fundamental	15.48	16.30	16.13
	First overtone	5.43	5.68	5.44
3	Fundamental	10.02	10.57	10.85
	First overtone	4.59	4.800	4.63
4	Fundamental	7.60	8.04	8.47
	First overtone	3.99	4.18	4.07
6	Fundamental	—	5.54	6.06
	First overtone	—	3.34	3.32

For high values of n, the free toroidal oscillation may be regarded as dispersive surface waves (Love waves) and the frequencies of vibration, f, can be used to compute the phase velocity, C, of Love waves on a sphere using the relation, $C = 2\pi Rf/(n + \frac{1}{2})$. It is evident that Models II and III will have greatly different Love wave dispersions because of the wide difference in shear wave velocity structure in the surface layers between the two models. Observations of Love wave trains by the long-period seismograph system will allow a differentiation to be made between the two models.

References

1. Brown, W. E., Jr., "A Lunar and Planetary Echo Theory", *Journal of Geophysical Research,* p. 3087, October 1960.
2. *Surface Electromagnetic Reflection Characteristics,* Report 1179-4, Ohio State University Antenna Laboratory, November 1, 1961.
3. *Scatter Theories and Their Application to Lunar Radar Return,* Semi-Annual Progress Report 33, University of New Mexico Engineering Experiment Station, September 1961.
4. *Investigations of Spacecraft Radar Systems for Exploring the Planet Venus,* Report on Jet Propulsion Laboratory Contract N-28112, MIT Electronics Systems Laboratory, August 15, 1961.
5. Bolt,B., *Nature,* Vol. 188, p. 1176, 1960.
6. Jeffreys, H., *Royal Astronomy Society Monthly Notices, Geophysical Supplement,* Vol. 4, pp. 62 & 548, 1937.
7. Bullen, K. E., *An Introduction to the Theory of Seismology,* p. 218, Cambridge University Press, 1953.
8. Alterman, Z., H. Jarosch, and C. L. Pekeris, *Proceedings of the Royal Society,* London, Vol. 252, p. 80, 1959.

XI. Planetary Studies

A. Television Subsystem

A photogeomorphological survey of the Mars surface is to be made by two TV cameras mounted on the planetary horizontal platform (PHP) of *Mariner:* one for the purpose of obtaining high-resolution photographs of the Martian surface (Camera A), and another having a wider field of view for obtaining colorimetric information from the planet and its atmosphere (Camera B). High-resolution pictures will be taken with a long focal-length objective having a red filter, while overlapping larger areas will be covered by a short focal-length camera. Sequentially operated filters on the second camera will permit heterochromatic analysis for an improved understanding of Martian morphology.

Two views of Mars as observed from *Mariner* for a 1964 planned trajectory approaching to 13,000 km are shown in Fig. 1. These present views of most interest for geomorphological picture studies. Depicted are a subsolar view at −3.34 hr and a Mars terminator view at 0.66 hr from closest approach. Superimposed are the corresponding scanned fields of view for the two TV cameras with objective fields of 0.62 deg (Camera A) and 3.15 deg (Camera B). The more valuable information will be secured in the region of the Mars terminator when the major portion of the 100 pictures to be transmitted to Earth will be taken.

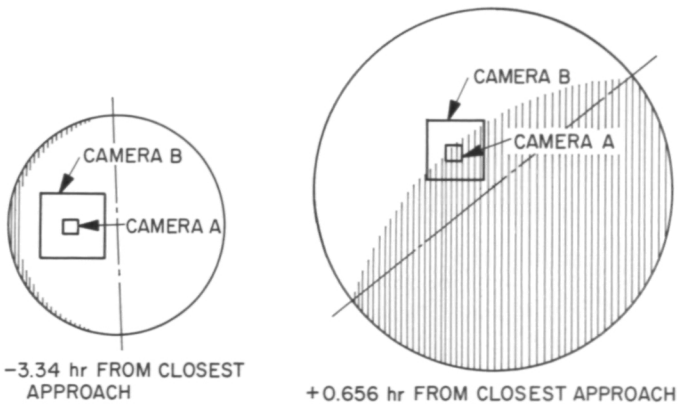

Fig. 1. View of Mars as observed from *Mariner* spacecraft

The relative intensity of Mars luminosity, as observed from Earth (Ref. 1), is shown in Fig. 2. The data is for a phase angle of 39 deg, corresponding to the *Mariner* picture of Fig. 1. Relative intensity was determined by photometric microdensitometry of a photographic negative of the planet taken with a red filter. The maximum variation of intensity over the sub-solar portion of the planet is of the order of 15%. Small areas of the surface that would be covered by the narrow-angle camera have greatly reduced light gradations, approaching 1% of the maximum high-light illumination. Pictures that will be imaged onto the photosensitive surface of the TV camera tubes may thus be categorized into two classes: bright low-contrast pictures and dark pictures of medium-to-high-contrast with an over-all dynamic range of illumination of the order of 100:1.

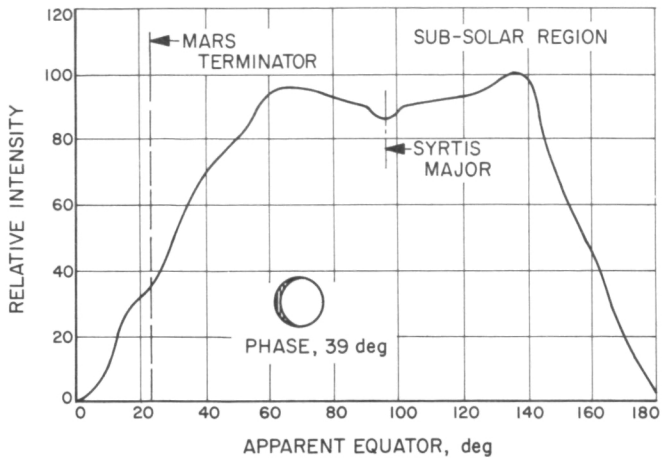

Fig. 2. Relative intensity of Mars 1939 luminosity as observed from Earth

A block diagram of the TV subsystem is shown in Fig. 3. Scanning and control functions for the two cameras will be logically controlled from a master 1-mc clock signal. To simplify control operations, both cameras will take pictures continuously and alternately,

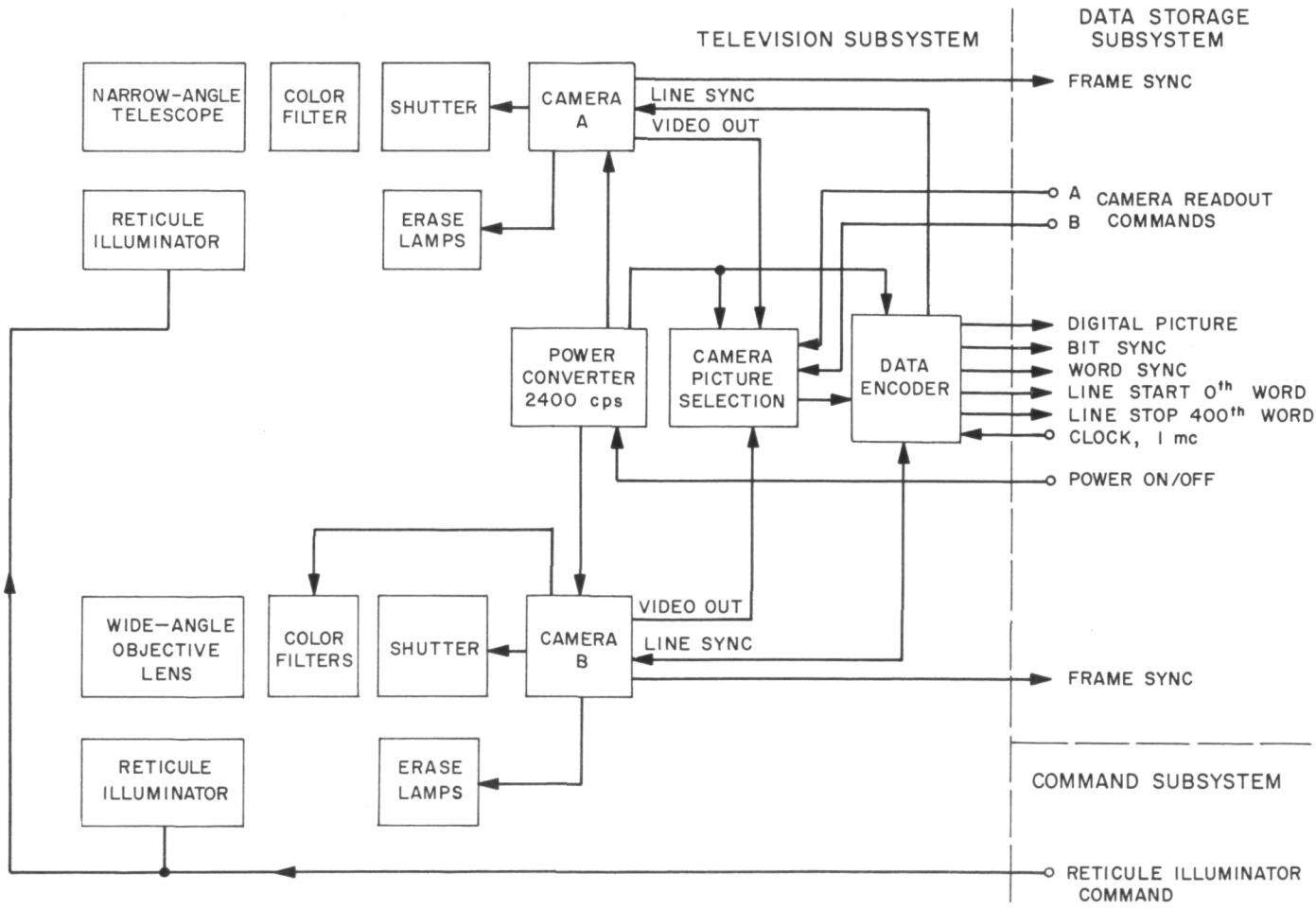

Fig. 3. *Mariner* television subsystem

following planetary acquisition. The stored picture readout time is 14.8 sec, and an equal period is taken to reprocess the photosensitive target. Thus, with interleaved operation, the maximum picture taking rate is 4 pictures/min. Command signals at stated intervals will select pictures for data encoding and subsequent transmission to Earth.

The provisionally selected camera tube for the Mars mission is a 1-in. vidicon using electrostatic deflection and focusing and an antimony sulfide oxysulfide (ASOS) photoconductive target. There are presently no tubes available that completely meet *Mariner* requirements. Although the ASOS electrostatic vidicon is somewhat lacking in sensitivity, it is compact, ruggedized, lightweight, economical of power, has adequate storage time for slow picture readout, and can withstand decontamination temperatures of over 100°C. An electrostatic tube, unlike tubes relying on magnetic fields for beam control, will not cause interference with the magnetometer experiment.

Resolution is expected to exceed the requirements for the 400-line TV scan that will be used for both cameras with an active scanned area of 0.44×0.44 in.

A typical transfer characteristic for an ASOS vidicon (estimated from Fig. II E-8 of Ref. 2) is shown in Fig. 4. Related are the phototarget illumination in ft-candle/sec, and the target high-light current in microamperes. The gamma over the linear range is 0.72. A provisional exposure of 40 msec for the high-resolution camera produces a phototarget illumination of approximately 0.3 ft-candle/sec over the sub-solar region. Thus, with the expected dynamic range of Mars illumination of 100:1 the vidicon sensitivity (i.e., the ability to produce a high-resolution picture clear of noise) should exceed 0.003 ft-candle/sec. The minimum vidicon signal for clear pictures is seen to be in the region of 0.006 ft-candle/sec.

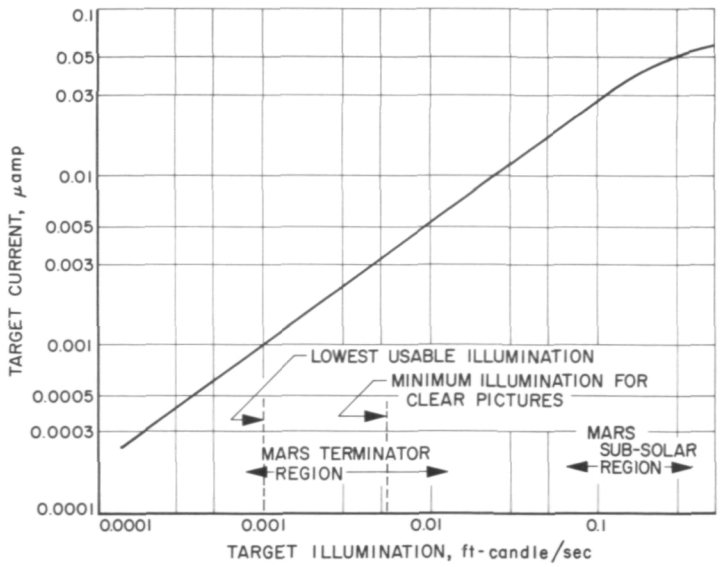

Fig. 4. ASOS vidicon transducer characteristics

The output signal from the vidicon after suitable amplification will be quantitized into 64 levels for digital encoding. To ensure a maximum number of quantitized shades of gray in any one picture, some form of exposure control is desirable. However, the problem of platform stability during exposure has defined a shutter time that has been chosen as a compromise between picture smearing and vidicon sensitivity. An alternative to light exposure control is to change the electronic operating parameters of the vidicon tube to match the target illumination for a particular scene.

A vidicon camera–tube assembly is now being fabricated that will incorporate a modified *Ranger* shutter and the necessary electronic circuitry for logical control. Flight approved components are being used throughout, and the modules are being constructed in a manner that will simplify integration into the final flight packaging. Only essential electronic units such as the video preamplifier, and the vidicon supply distribution box will be contained on the PHP with the cameras. One of the units to be mounted on the PHP is shown in Fig. 5.

The major portion of the electronics, including all vidicon control functions, will be contained in a separate package on the main bus, with a second unit that will include the 2400-cps power converter. Insofar as applicable, proven *Ranger* camera circuitry will be utilized with necessary changes to conform to the *Mariner* control functions.

The immediate objective is to have a complete experimental electronic assembly that will enable vidicon camera–tubes to be evaluated in terms of the Mars mission. This same assembly will permit circuit functions to be checked for correct operation. It is hoped to obtain an improvement in vidicon sensitivity by optimization and refinement of the target control circuitry; more particularly by improving the electromechanical layout surrounding the vidicon target. A solution to the exposure problem is being sought that will permit a simple, reliable intelligence system to be inserted that will evaluate conditions existing at picture taking time in terms of (1) past picture history and (2) light-intensity interpretations made by a strategically placed photocell.

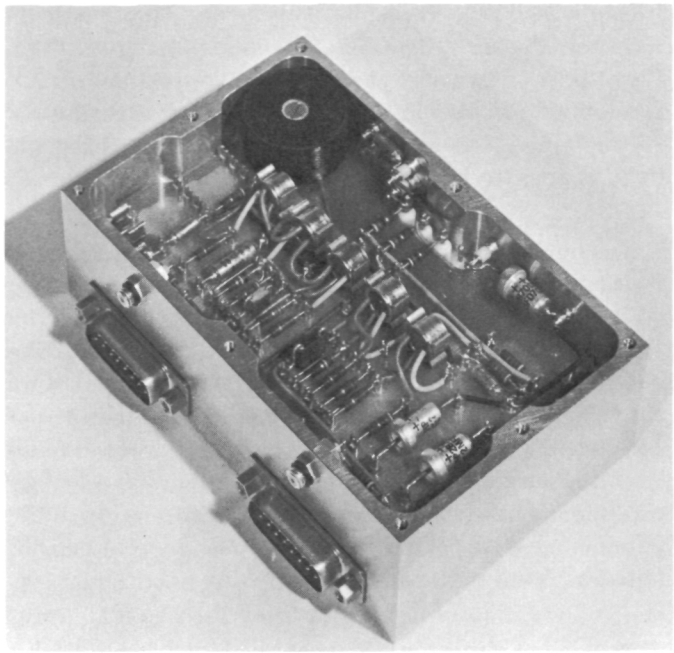

Fig. 5. Vidicon distribution and 125-kc oscillator unit for *Mariner* TV camera

This system will then perform simple electronic control functions as required to adjust camera performance for optimum picture resolution.

1. Electronics

Picture quality for the *Mariner* television experiment will be determined ultimately by the optical–electrical transfer characteristics of the vidicon transducer. The transducer may be evaluated in terms of the ratio of the vidicon output signal to the background noise. Corresponding resolution and sensitivity are then expressed in terms of signal-to-noise ratios. This form of comparison is particularly applicable to space television systems since contamination by noise is a significant problem. Within this frame of reference, a high-quality picture is defined as that produced by a peak-to-peak video signal at least 30 db above an rms noise background. An acceptable picture has a 20-db signal-to-noise ratio.

a. Preamplifiers. Vidicon sensitivity at low levels of target illumination is almost completely determined by the preamplifier performance. Thermal noise at the preamplifier input terminals may be defined by the Nyquist equation, $\overline{e_n^2} = 4KTRB$ v rms, where K = Boltzmann's constant, R = the vidicon signal output resistance, T = temperature, and B = the noise bandwidth of the video amplifier.

The video bandwidth required for the *Mariner* slow-scan system is

$$B = \frac{N}{2t\rho} = \frac{400 \times 400}{2 \times 14.8 \times 0.78} = 7.0 \text{ kc}$$

where N = the number of picture elements, t = time of the vertical scan in seconds, and ρ = the line time utility factor. This bandwidth is sufficiently low to make practical the beam-modulation system utilized in *Rangers* 3, 4, and 5. In this system the scanning beam is chopped at a high frequency and the photoconductive target modulates the beam in accordance with the incident illumination. The resultant output signal takes the form of a modulated RF signal with the video spectrum now transferred from dc to RF and surrounding the carrier as shown in Fig. 6. The *Mariner* beam-chopping oscillator is a 125-kc stabilized free-running oscillator with a simple binary relationship ($\times 8$) to the 1-mc clock frequency. Thus, four samples are provided per picture element of 72 μsec. The carrier frequency of 125 kc is sufficiently low to permit simple RC coupling networks for the transistor amplifiers and yet is high enough to allow adequate post-detection filtering of the carrier.

The advantages of beam modulation for *Mariner* are: (1) Video information is in the form of an RF signal and may be amplified and transmitted as a high-level signal over a coaxial cable with a minimum of interference from the power supply and other noise producing sources (Fig. 6). This reduces weight on the PHP as the camera and preamplifier only need be placed on the PHP with the major portion of the electronics on the bus. (2) Grounding problems are greatly reduced as the vidicon output signal is now at RF, thus eliminating the need to transmit low video frequencies. (3) An isolation trans-

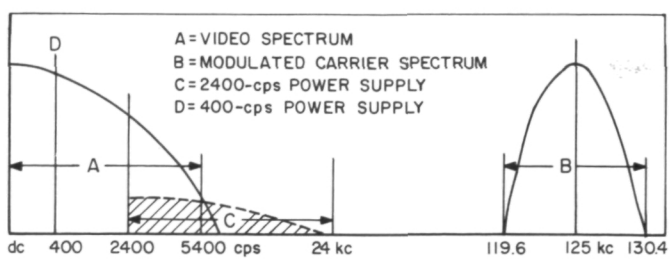

Fig. 6. Signal spectrums for *Mariner* television

former may be used at the preamplifier input. This not only isolates vidicon operating potentials from the amplifier but permits accurate matching to the normally low-impedance input of a transistor preamplifier. RF beam modulation requires adequate shielding between the high-level chopping oscillator and the sensitive preamplifier. However, RF shielding techniques have been well developed for space vehicles and the weight requirements are considerably less than for the equivalent low-frequency shielding.

The usable output signal of the vidicon $I_o = I_s - I_d$, where I_s is the signal current and I_d the dark current. The present trend with the slow-scan mode is to operate with an extremely low I_d so that $I_s - I_d$ will produce the maximum I_o/I_d. While this optimizes I_o/I_d for low values of target illumination, the low values of output current, possibly as low as 5×10^{-9} amp, require an amplifier with a corresponding favorable signal-to-noise ratio. A completely transistorized system is desirable for *Mariner*, particularly to secure the lowest possible primary power consumption. Fortunately the design of low-noise transistor amplifiers has been alleviated by the recent introduction of high-gain, passivated surface, low-noise transistors exemplified by the Fairchild 2N2049.

The vidicon signal output circuit for the 125-kc carrier system is shown in Fig. 7. The photoconductive target corresponds to an extremely high-impedance generator ($>>$ 100 megohm) so that the signal output for usable values of output impedance becomes a direct function of R. As thermal noise varies as $R^{1/2}$, the highest signal-to-noise ratio will be realized by maximizing R. The effective output load $R = Q/\Omega C$. Therefore, R is maximized by minimizing C and operating with the highest possible Q for the tuned transformer. The capacity has been minimized by reducing all capacitances surrounding the target electrode to a minimum. The transformer Q has been optimized by compensating for the loss of response, due to a high Q, in the video amplifier.

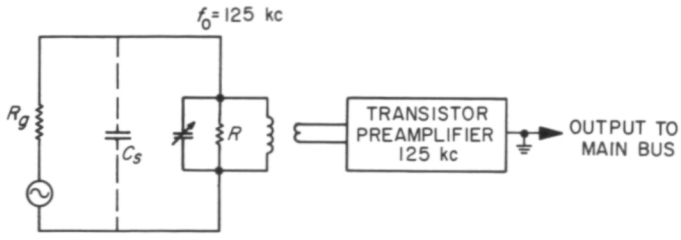

Fig. 7. Vidicon equivalent signal output circuit for *Mariner* television

A resultant input resistance of 0.6 megohm has been achieved for the *Mariner* preamplifier using a powdered-iron toroidal coil. This compares quite favorably with input impedance values obtained with direct-coupled video vacuum tube amplifiers.

Figure 8 shows the noise spectrum for a typical transistor as related to the *Mariner* amplifier. Operation at 125 kc clearly obviates the flicker noise. However, f_{α_b} must be considerably higher than 125 kc because of the term $(1 - \alpha_o)^{1/2}$. The 2N2049 has a specified $f_{\alpha_b} = 800$ kc with I_c at 10 μamp for which $f_{\alpha_b}(1 - \alpha_o)^{1/2} = 112$ kc. However, for lowest noise the recommended collector current is in the 300-μamp region for which f_{α_b} is expected to be much higher than 800 kc. This would place the carrier frequency well within the lowest noise figure region. The optimum required source impedance for the transistor of between 500 to 1500 ohms is readily obtained by adjustment of the transformation ratio of the toroidal transformer.

Figure 9 illustrates a technique for evaluating the video amplifier using an amplitude modulated signal from an RF signal generator to simulate a 5×10^{-9}-amp vidicon high-light signal. Data so obtained is presented in Table 1 where it will be noted that a -40-db signal at the 5×10^{-9}-amp level has a signal-to-noise ratio of 15 db. A measured noise figure for this same amplifier was 3 db, which is close to the best obtainable with vacuum-tube devices. The estimated transfer characteristic data for the vidicon presented previously was based on a 5×10^{-9}-amp maximum high-light signal. Thus, the measured performance data indicates that the present transistorized amplifier system is unlikely to prove a limitation to picture quality with low dark-current operation.

b. Electronic modules and vidicon assembly. The electronic modules for processing the camera output signal

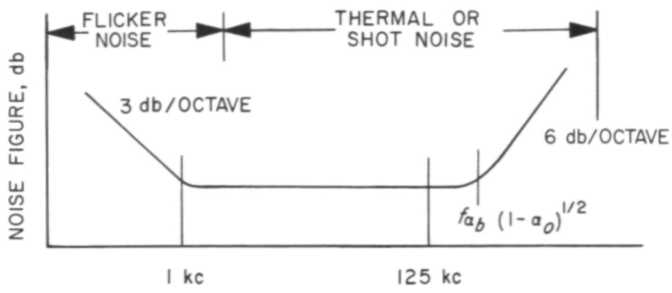

Fig. 8. Transistor noise spectrum related to *Mariner* television amplifier

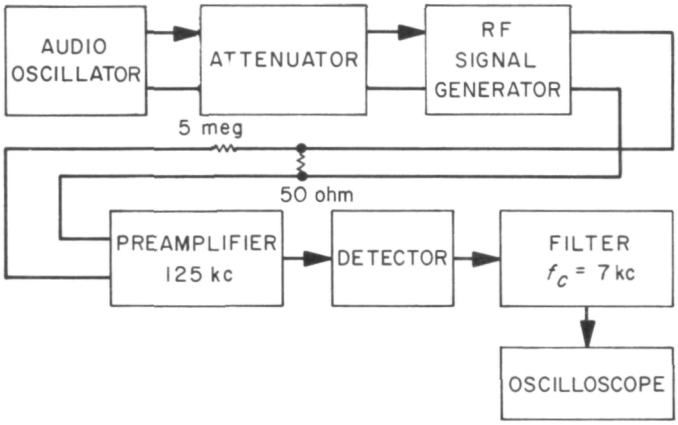

Fig. 9. Measurement of signal-to-noise ratios by simulating vidicon target signal characteristics

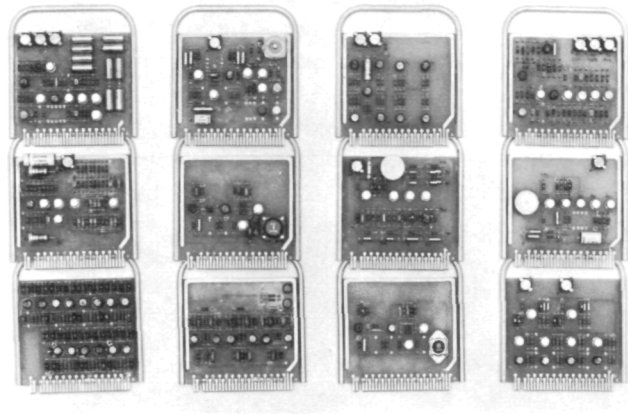

Fig. 10. Electronic modules for *Mariner* television Camera A

and logical controlling of the input signals to the vidicon for slow-scan operation are shown in Fig. 10. The modules are assembled in a container (Fig. 11) that simulates the shielding that would be provided in a payload configuration and yet gives desirable plug-in flexibility during the breadboard phase. Only a line synchronizing signal from the digital encoder is required to provide a continuous succession of pictures from Cameras A and B. Output signals indicating the status of the television scans are available for the data automation system.

All modules have been thermally tested from −40 to +75°C and, with one exception, have operated completely satisfactorily. The performance of one unit, the output video amplifier, was found completely unacceptable. This amplifier is a relatively complex dc amplifier incorporating a dc black-level clamp and a synchronizing dc reference signal. The analog output from this amplifier is fed to the digital encoder, and hence must be highly stable. By changing to a differential amplifier configuration and thermally compensating the dc clamp and the associated impedance transforming circuits, the required stability has been achieved.

Figure 12 shows the breadboard vidicon tube assembly which includes the preamplifier, erase lamps, and shutter. Considerable effort has been taken to ensure adequate shielding of the camera tube to permit low-level I_o operation and to minimize the vidicon output capacitance. The assembly uses a *Ranger* shutter and a Takumar Asahi

Table 1. Measured video amplifier system performance data for a simulated 5×10^{-9} amp vidicon signal

Modulation intensity, db 30% = 0 db	Video output signal, mv peak-to-peak	Noise, mv rms	Signal-to-noise ratio, db
0	1900	3.3	55
−10	600	3.3	45
−20	190	3.3	35
−30	60	3.3	25
−40	19	3.3	15
−50	6	3.3	5

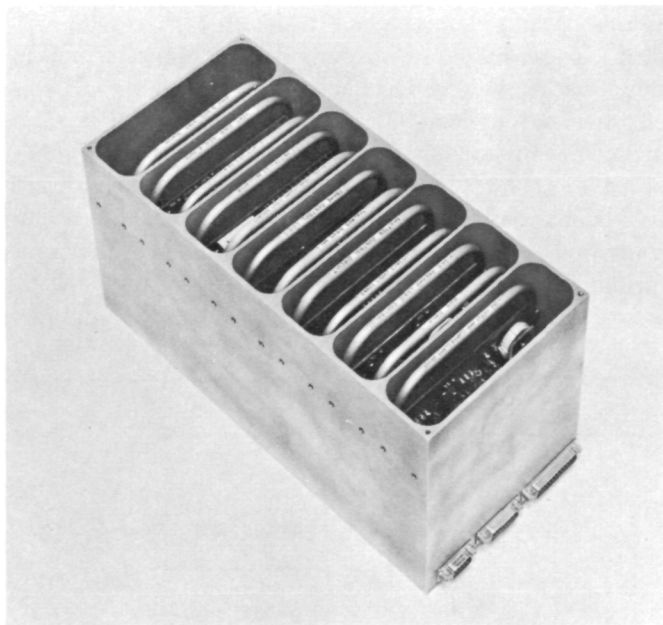

Fig. 11. Simulated payload configurations of *Mariner* Camera A electronic packaging

PAGES MISSING FROM AVAILABLE VERSION

XII. Solar and Interplanetary Studies

A. Sigma Plasma Detector

The *Surveyor* plasma detector, under development at JPL, will examine the solar wind and Moon interaction and is a second generation version of the solar plasma detector flown on *Rangers* 1 and 2. It will be used to measure the charged particle energy spectra as a function of arrival direction. The principal purposes of these measurements are to determine the low energy particle environment of the Moon and to aid in the interpretation of the magnetometer data. The charged particle measurements could be related to the magnetometer measurement as follows:

(1) From the measured magnetic field magnitude and direction, a first iteration field model is constructed. The first iteration field might be a magnetic dipole located at the center of the Moon with the necessary strength and orientation to produce the observed field at the spacecraft. The expected modulation of the motion of interplanetary particles in crossing this model field is then calculated.

(2) A comparison of the calculated and the measured distributions of particles as a function of angle of arrival and energy is made. The general features of any disagreement are then studied qualitatively to aid in the generation of a second iteration model which might be something like a distorted dipole field which is greatly compressed on the Sun side by a solar wind. This process is repeated until one or more models are found for which the calculated and measured particle distributions are in reasonable agreement.

Direction of travel will be determined by five electrostatic analyzers (Fig. 1), each with an acceptance angle of about 18 deg about the normal direction. The analyzers are situated so that one detector analyzes particles incident from the local vertical, while the other four point at 45 deg to the vertical at 90-deg intervals. The package is to be extended from the spacecraft on a 12-ft telescopic boom and gimbaled on two axes to seek the local vertical for proper orientation of the analyzers.

Charged particles entering an electrostatic analyzer are deflected by an electric field which is approximately transverse to the particle velocity. Those particles with a particular charge sign, a certain range of energy per unit charge, and a certain angle of incidence are deflected

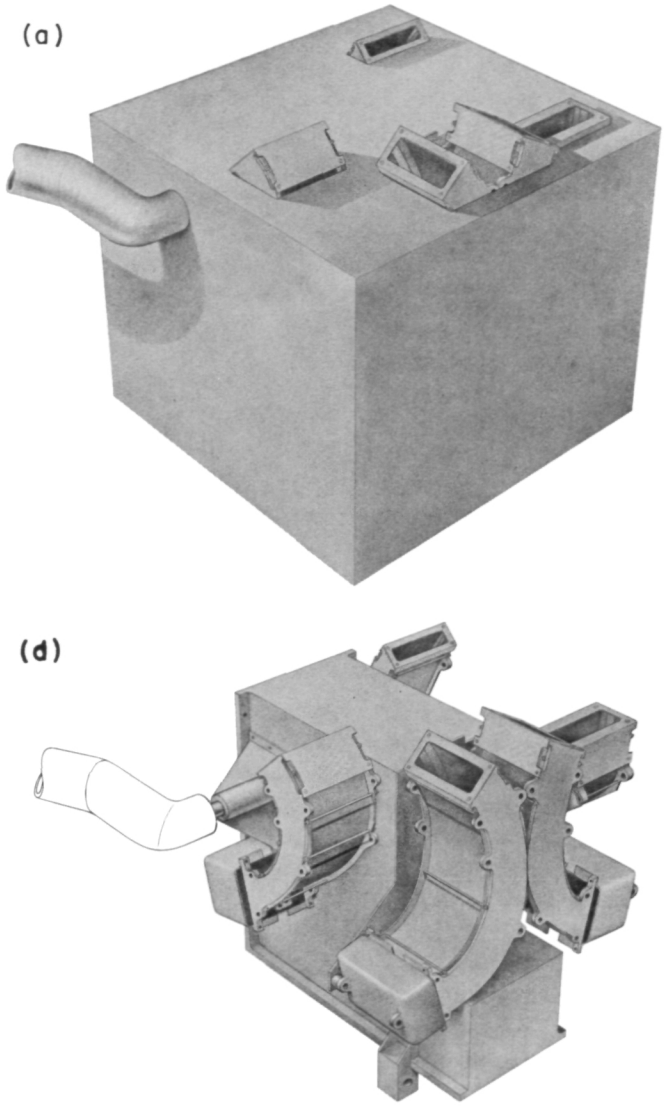

Fig. 1. *Surveyor* sigma plasma detector (a) with and (b) without thermal shield

onto the charge collector cup. Particles which enter the deflection plates with the wrong charge sign, energy per unit charge, or angle of incidence strike the deflection plates and are not recorded. The energy distributions of both positively and negatively charged particles entering the instrument can be determined by varying the sign and magnitude of the deflection voltage. The instrument is capable of analyzing positive ions or electrons with energies between 2 ev and 6 kev.

The five deflection plate systems are grouped around one box and, by means of special high resistance switches (open circuit resistance $> 10^{16}$ ohms), time share a single electrometer amplifier and high-voltage sweep amplifier (Fig. 2). This arrangement results in a significant saving in weight and power over a system in which each set of deflection plates has its own separate electronics. The *Surveyor* detector, with five analyzers, weighs 12 lb and uses 1 w, whereas the six analyzers on *Rangers* 1 and 2 weighed 33 lb and used 2.75 w.

1. Electrometer Amplifier

The electrometer amplifier for the *Surveyor* detector is an improved version of the *Ranger* 1 and 2 models. A development contract was let to the Applied Physics Corporation in April 1961 to devise a piezoelectric pickoff on the vibrating reed dynamic capacitor. This device is used to control a reed resonance tracking oscillator on the *Surveyor* detector. This effort has been successful and the first version of this development will be implemented in the *Mariner* Venus (1962) plasma probe.

Subsequent work on improved sealing methods of the reed capacitor container has led to a marked reduction in contact potential, and a temperature coefficient of contact potential of less than 70 μv/°C. Use of this improved modulator has resulted in an electrometer with increased sensitivity and a greater dynamic range over the temperature span anticipated in the lunar environment (−50 to 100°C). Several prototype reed modulators have been thoroughly evaluated over this range and have successfully passed the sterilization procedure.

Perhaps the most significant improvement in the *Surveyor* probe is the incorporation of an automatic scale factor device (Fig. 3). The feedback element of the *Ranger* electrometer is the bipolar logarithmic compressor which has the approximate transfer function:

$$E_{out} = K \log I_{in}$$

This device, however, requires a well insulated battery to measure electron current; the stability of the electrometer can be no better than the long term stability of the thermionic compressor diodes.

In order to more thoroughly exploit the advantages presented by the electrometer amplifier, an automatic gain system was devised which uses resistors as feedback elements and results in the transfer function:

$$E_{out} = -I_{in} R_f$$

Since the electrometer has a useful dynamic range of ±10 mv to ±10 v, circuits were designed to automatically change the feedback resistors as a function of the output voltage. The feedback resistors selected for

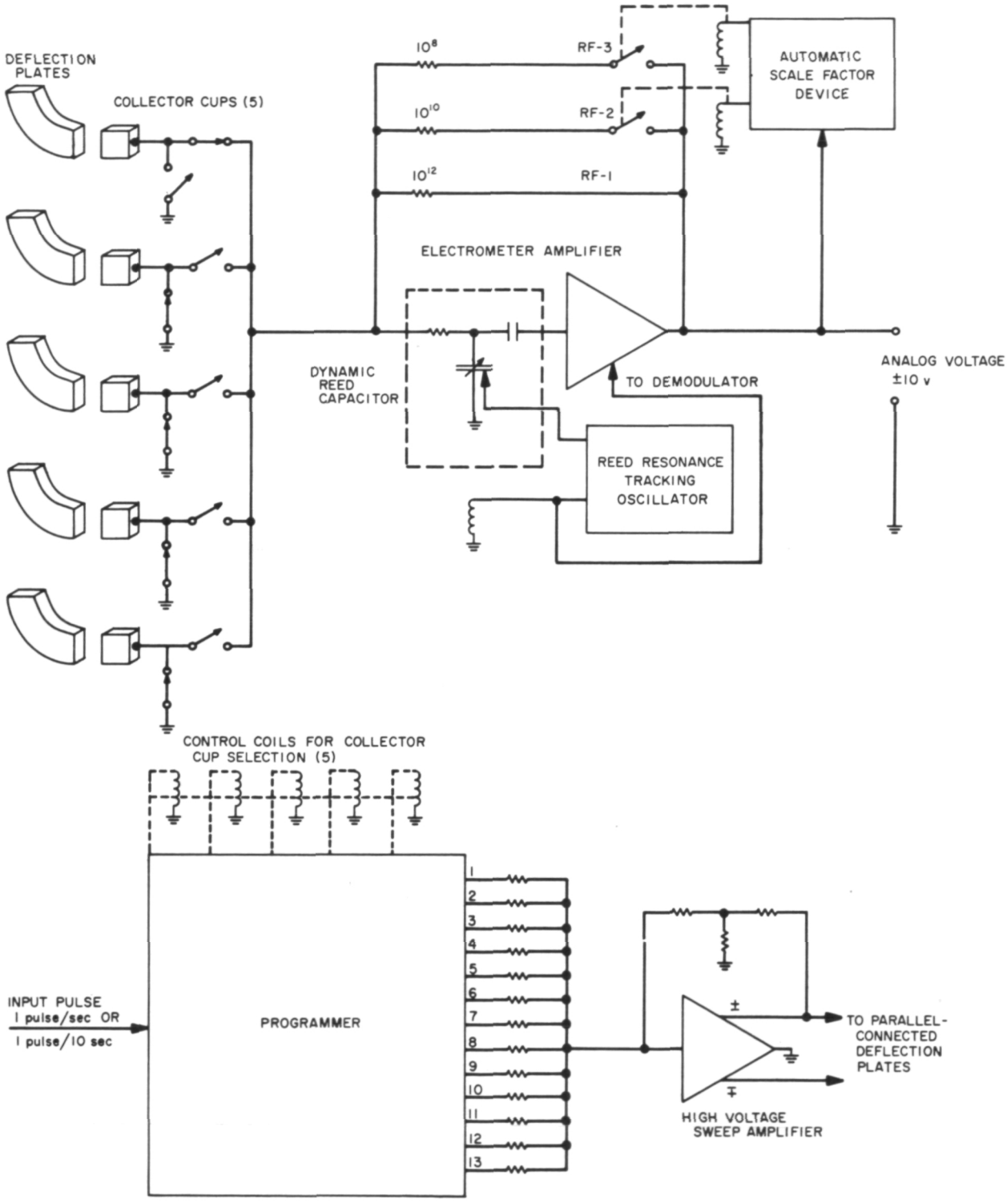

Fig. 2. *Surveyor* sigma plasma detector circuit

the *Surveyor* instrument enable the amplifier to measure currents from $\pm 10^{-7}$ to $\pm 10^{-14}$ amp in three ranges with a decade overlap on each range. For the plate geometry selected this corresponds, respectively, to particle fluxes between 4×10^{10} and 4×10^{3} particles cm^{-2} sec^{-1} for each energy level.

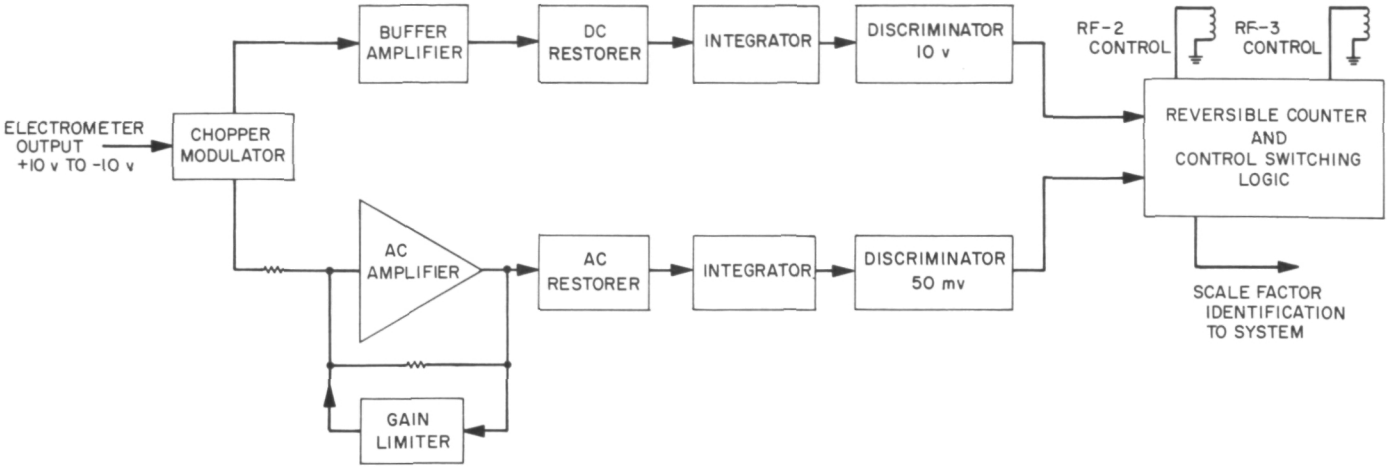

Fig. 3. Automatic scale factor device

The device consists of a chopper input stage (in order to sample both positive and negative voltages) followed by suitably scaled amplifiers. After restoration and integration of the resultant square wave, amplitude discriminators examine the integrator outputs to determine whether the electrometer is within the range of ±50 mv to ±10 v. The discriminator outputs drive a reversible counter up or down, depending upon the appropriate limit crossing, and logic switching on the counter inserts the proper feedback resistor. An analog voltage proportional to the feedback resistor is resistively summed with a voltage proportional to the collector cup number, and this signal is fed to the data system for identification. The overlap between ranges was provided to prevent oscillation between resistors and to take advantage of the fast response of the electrometer with the smaller resistors in place. By increasing the sampling rate at the amplifier output to 10/sec, for example, rapid cyclic variations or waves may be observed in the plasma.

Evaluation is being made of a new low noise silicon input stage for the electrometer to replace the presently used germanium transistor. This will enable the electrometer to more reliably withstand the lunar temperature environment. It is also planned to evaluate field-effect transistors in this application. These units, by virtue of their high power gain, may well result in a significant reduction in circuit components as well as improved performance.

2. Deflection Voltage System

The deflection voltages for the analyzer plates are generated by two fully transistorized assemblies: the programmer and high voltage sweep amplifier (Fig. 2). The programmer consists of a 4 by 13 diode matrix, driven by a four-stage binary scaler, which consecutively gates a reference input voltage to one of the 12 input resistors of the high voltage sweep amplifier. The rate at which the programmer steps is governed by the rate of the input timing pulse from the system. Upon receipt of the 13th pulse, logic steering resets the programmer to the first step, opens all collector cups, and injects a standard current into the electrometer. This self-generated reset pulse is also used to drive a three-stage scaler and a 3 by 6 matrix that controls the collector cup selection switches. The programmer thus sequences the sweep amplifier through 12 energy levels, resets itself, and injects a standard current on the 13th step. It also steps to the next collector cup in the sequence on that step.

In addition, there are three values of standard current which are sampled alternately so that three complete cycles of the programmer and the three scale factor ranges of the electrometer amplifier are tested. This corroborative test procedure seems valid in light of the fact that:

(1) The lunar surface temperature environment is extremely severe by present flight hardware standards and is not fully understood.

(2) Methods of simulating these temperature and vacuum extremes are not fully adequate.

(3) The system must be designed to operate intermittently for a long period (30 days or more).

(4) Since the logic circuitry already exists, only a few components need be added for the task.

The instrument may operate in one of two modes upon ground command. When the largest resistor (10^{12} ohms) is in the feedback loop, the electrometer must settle for a few seconds before a useful reading is obtained. The programmer is, therefore, sequenced only once every 10 sec. If the particle fluxes incident on one of the analyzers are large enough to sequence the electrometer to the 10^8 or 10^{10} ohm resistors, the timing pulse rate may be increased to 1/sec by ground command to take advantage of the rapid amplifier settling time.

The high voltage sweep amplifier is being redesigned as a carrier-type dc operational amplifier in contrast to the direct coupled approach taken on the *Ranger* experiment. Chopper transistors have been made available recently which can ensure the null stability necessary in this application.

c. Temperature evaluation. A temperature control model of the instrument has been constructed. It consists of the outer chassis with the five electrostatic analyzers in place and a covering of insulation material surrounding the whole package. The heat of the electronics is simulated by resistors, and thermocouples are connected at various points around the box.

Table 1. Particle energies corresponding to deflection plate voltages

Programmer step level	Voltage across deflection plates, v	Energy level of particles reaching cup, ev
1	60	240
2	89	356
3	132	528
4	196	784[a]
5	290	1160
6	432[a]	1728
7	642	2568[a]
8	952	3808
9	1412	5648
10	2100	8400
11	−2	–
12	−2	Electrometer calibration

[a]Corrected from those values appearing in Table 1, *SPS 37-13*, Vol. 1, p. 25.

Figure 4 displays the instrumentation in its spacecraft configuration.

The GSE interface checks on the first unit disclosed that the squarewave power on the spacecraft had a faster rise time and higher voltage than the supply used in the laboratory. This manifested itself when the dc voltages generated in the unit were meas-

B. Solar Plasma Analyzer

The solar plasma experiment for the *Mariner* Venus (1962) flyby mission has been designed to measure positive ions in 10 energy levels. The measurement is accomplished by impressing programmed voltages across curved electrostatic deflection plates. The geometry of the plates and voltage across them determines the energy level of the entering particles that reach the collector cup (Table 1). The rate at which these particles are collected is measured as a current by the electrometer amplifier. A feedback diode operated in the retarded field region serves as a logarithmic compressor and permits the electrometer to measure currents from 10^{-6} through 10^{-13} amp.

1. Spacecraft Integration

Two flight units have been assembled, environmentally tested, and delivered to the spacecraft assembly facility. The units were installed in the appropriate hex box and preliminary data conditioning system (DCS) and ground support equipment (GSE) interface checks were made.

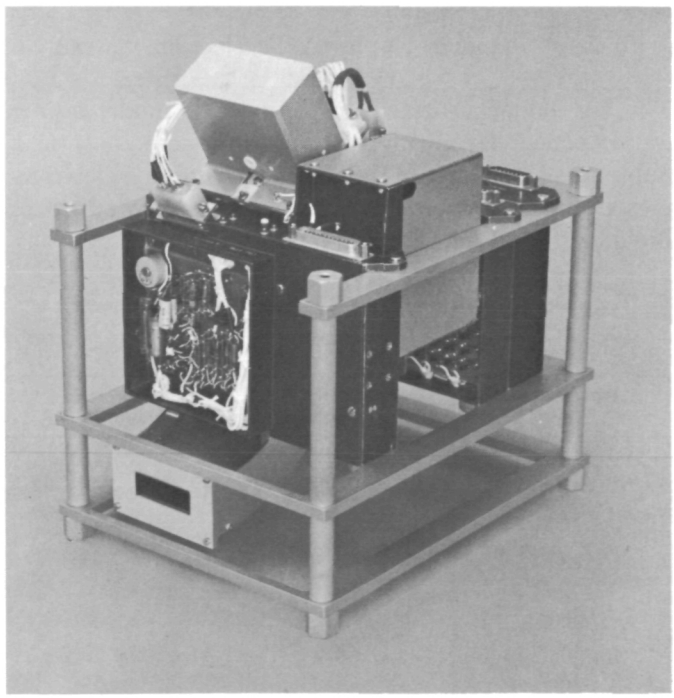

Fig. 4. Solar plasma analyzer

ured. The spacecraft supply was set for 50 v rms while the lab supplies were set to give 50 v peak which is almost, but not quite, the same as 50 v rms for this particular square wave. These larger spacecraft voltages had no effect on the operation of the electrometer (Table 2) but did cause the negative output voltage of the sweep amplifier to be 3 v lower than the positive output. This first unit was returned to the lab to investigate the difference in sweep amplifier output voltages. It was found that the higher voltage and faster rise time of the power supply caused one of the zener diodes used for overload protection in the sweep amplifier output offset supply to fire prematurely due to a poor knee in the zener region. When this diode was replaced, both output voltages were the same.

No problems were encountered during the DCS interface checks. The electrometer output readings that were obtained by the DCS compared closely with those obtained in the lab and by the GSE.

2. Circuits

Problems experienced in the electrometer during assembly were:

(1) Quadrature in the carrier signal as evidenced by a large demodulator waveform.

(2) Low gain in the ac amplifier section.

(3) Low frequency ripple on the electrometer output.

The first unit constituted an engineering model insofar as component layout and wire routing were concerned. Subsequent rerouting of the critical wires in the electrometer compartment either eliminated the quadrature or brought it well within acceptable limits.

Table 2. *Mariner* Unit 23, Serial 1 electrometer calibrations

Input current, amp	Bench calibration, v	Spacecraft GSE calibration, v
10^{-6}	3.077	3.072
10^{-7}	3.348	3.349
10^{-8}	3.589	5.584
10^{-9}	3.803	3.805
10^{-10}	4.024	4.020
10^{-11}	4.237	4.230
10^{-12}	4.450	4.4
10^{-13}	4.643	4.730
zero	4.730	–

The low gain between the modulator and demodulator was investigated thoroughly, although persistent efforts could not restore the gain to the levels obtained with identical circuits on *Ranger*. Drifts occurring in the dc filter–amplifier appear at the electrometer input reduced by the dc gain, G_1, preceding the filter–amplifier (Fig. 5). To preclude input drifts attributable to demodulator and filter–amplifier drifts, a minimum portion of the electrometer loop gain, which may be expressed

$$K_{loop} = G_1 G_2$$

must be incorporated into the carrier section (G_1). The dc carrier gain may be written

$$G_1 = \eta_C G_{ac} \eta_D$$

where

η_C = modulation conversion efficiency

G_{ac} = ac amplifier gain

η_D = demodulation efficiency

The carrier gain and electrometer loop gain were then measured over the instrument's specified temperature range (Table 3). Since the dc filter–amplifier is highly degenerated and as a result produces a gain G_2, that is quite stable, any variations in loop gain, therefore, reflect changes in the carrier gain G_1. The test results, as shown in Table 3, reveal an acceptably stable, though somewhat low, loop gain. While working on the second unit, a minor layout change in the carrier amplifier raised the ac amplifier gain to the desired level. This change was subsequently incorporated into all the units with similar increases in ac gain as a result.

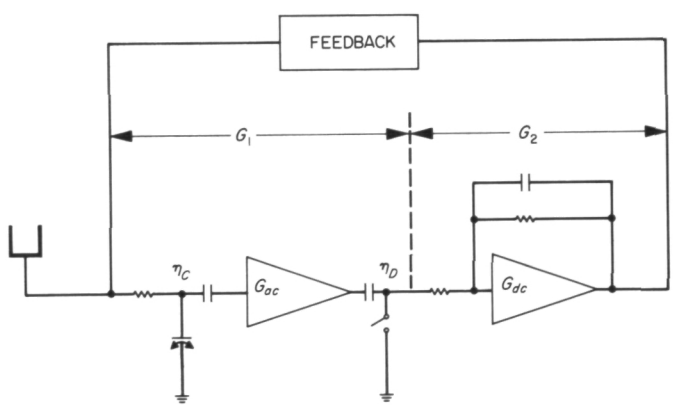

Fig. 5. Electrometer amplifier circuit

Table 3. *Mariner* Unit 23, Serial 1 electrometer gains

Temperature, °C	Loop gain, G_1G_2	Carrier Gain, G_1
−10	470	14.0
25	600	17.7
70	605	17.8

The major problem experienced on the first unit was a low frequency ripple on the electrometer output, the magnitude of which was high enough to give poor output resolution for input currents below 10^{-11} amp. In the worst case, the peak-to-peak magnitude of this signal was large enough to register in any of three adjacent quantization levels of the analog-to-digital converter in the DCS. This ripple was found to be the difference, or beat frequency, produced when the power frequency and the carrier frequency were nearly equal. The 3-db bandwidth of the dc amplifier is 0.5 cps and any beat-frequency signal of a few cps will be amplified and appear at the output.

One solution to this problem was to have the carrier frequency lowered so that the difference frequency would be well out of the pass band of the dc amplifier. Since the carrier frequency is fixed for any modulator by its mechanical resonance, the power frequency was varied and it was found that, when the difference between carrier and power frequency was in excess of 30 cps, no beat frequency ripple was observed at the electrometer output. Modulators with mechanical resonant frequencies of 200 cps lower than that of the power frequency will be used to replace those presently on the instruments.

The second unit also had the problems of quadrature and low ac gain, but the beat frequency ripple did not exist because the carrier frequency was 30 cps lower than the power frequency. Quadrature was eliminated, as in the first unit, by the rerouting of wires in the electrometer compartment. The ac gain was raised to the desired level as mentioned before by a layout change in the ac amplifier.

C. Particle Flux Detector

The ionization chamber, which has already been developed for a radiation monitor (Ref. 1), measures the total ionization rate per unit volume of gas produced by radiation able to reach the sensitive part of the instrument. This ionization is proportional to the rate of energy dissipation per unit volume of gas but does not depend upon the flux of ionizing radiation in a unique way. It is, therefore, useful to measure this flux with an instrument so matched to the ionization chamber that the two instruments respond to particles of the same energies.

The simplest device which can measure the required flux is a Geiger–Müeller (GM) tube with a wall the same as the ionization chamber's. The GM tube puts out a pulse of charge each time an ionizing particle produces one or more ion pairs within its sensitive volume of gas. The pulse rate is therefore proportional, within limits, to the omnidirectional flux of ionizing particles which traverses the sensitive volume. This flux comprises: primary (natural) particles which penetrate the wall of the counter, penetrating secondary particles produced in the spacecraft and surrounding materials, and secondary particles produced in the wall and filling gas of the counter.

In adapting a GM tube to making an actual measurement, two principal problems must be solved. It is first necessary to connect it to a high voltage supply and to an output amplifier which isolates the tube from all following counting equipment. The amplifier should allow the pulse rate to be linear with particle flux up to as high a rate as possible. The associated circuit as a whole must provide a pulse rate which is as independent of temperature and time as possible. Second, the counting rate of the system must be calculated and measured for all possible types of incident radiation.

A GM tube particle flux detector has been developed for use with the ionization chamber on the *Mariner* Venus (1962) spacecraft. Figure 6 shows the complete package, which contains three GM tubes. The thermal shield has

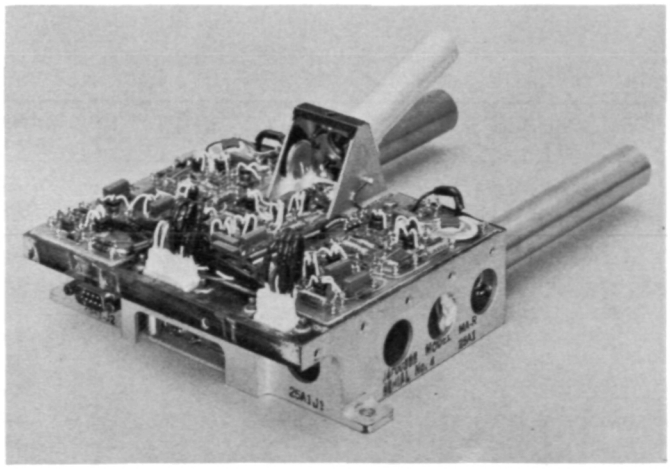

Fig. 6. Geiger-Müeller-tube particle flux detector

been removed. Tubes I and III are mounted in the two large cylindrical shields, while the smaller shield contains GM Tube II. The package also contains the output amplifiers for the three tubes, a pulse shaper for the ionization chamber, and a power supply which converts spacecraft 2400-cps power to the high and low voltages required by both the ionization chamber and the GM tubes.

The Geiger counter detectors use commercial Geiger counters mounted in specially designed shields and coupled to amplifiers designed at JPL to operate at very high counting rates. Tubes I and III are Radiation Counter Laboratories (RCL) No. 10311 Geiger counters that operate at 750 v, and are glass with 0.030-gm/cm^2 thick walls. The sensitive volume is cylindrical (6.6 cm in length and 1.5 cm in diameter) so that the omnidirectional geometric factor is about 8.8 cm^2. Tube I is shielded by 0.160 gm/cm^2 of stainless steel to match (together with the glass of the tube) the 0.2 gm/cm^2 wall of the ion chamber. Tube III is shielded by 0.113 gm/cm^2 of beryllium so that both it and Tube I detect protons with $E > 10$ Mev as does the ion chamber. The tubes will also detect alphas with $E > 40$ Mev, and electrons with $E > 0.5$ Mev by direct penetration. Electrons will also be detected through the bremstrahlung process with the efficiency depending upon their energy; however, the two tubes will respond differently because of the different atomic number of their shields.

The ratio of the counting rates of Tubes I and III will depend upon the number and energy of electrons present. The ratio of the rate of ionization (measured by the ion chamber) and the counting rate of GM Tube I will be proportional to the average specific ionization of the detected particles.

Tubes I and III will count approximately 15/sec due to galactic cosmic rays. Their maximum apparent rate with the present amplifiers is about 45,000 counts/sec. Due to the finite dead time of the counters, the corresponding true rate is considerably higher.

Tube II is an Anton 213 end window Geiger counter which measures the flux of particles unable to penetrate the other detectors. The window is covered by approximately 1.2 mg/cm^2 of mica, and admits electrons with $E > 40$ kev and protons with $E > 0.5$ Mev. A small shield defines the solid angle through which particles can enter the window. The solid angle has the shape of a cone with an opening angle of 90 deg.

The unidirectional geometric factor for the window is 0.1 cm^2 sterad. The remainder of the tube is shielded by approximately 0.55 gm/cm^2 of matter, which permits the passage of electrons with $E > 1$ Mev and protons with $E > 20$ Mev. The tube has an omnidirectional geometric factor of 0.2 cm^2 Galactic cosmic rays will produce about 0.2 counts/sec in this tube. The maximum apparent counting rate is 20,000 counts/sec, which corresponds to a maximum resolvable rate of about 10^7 true counts/sec. (Tube II in its shield is being supplied to JPL by Dr. J. A. Van Allen of the State University of Iowa, Physics Department; the tubes are calibrated at Iowa.)

Table 4 summarizes the characteristics of the GM tubes and of the accompanying ion chamber

Each GM tube is associated with a separate pulse amplifier. The amplifiers contain three stages and are similar in design. The first two stages contain minor loop feedback, while the output stage stability is enhanced by a large ratio of base bias to minimum holding current.

Table 4. Characteristics of *Mariner* Venus (1962) radiation detectors

Detector	Shielding, gm/cm^2	Corresponding energy for penetration, $E >$ Mev	Geometric factors	Dynamic range and counting rates[a]
Integrating ion chamber	0.2 gm/cm^2 stainless steel	Protons: 10 Electrons: 0.5	1 liter argon at 4 atm, 10^{-10} coulombs per count	10^{-3} to 10^2/sec, 300 to 3×10^7 ion pairs per cm^3-sec-atm-of-air
GM Tube I (RCL 10311)	0.030 glass plus 0.160 stainless steel	Protons: 10 Electrons: 0.5	8.8 cm^2, omnidirectional	15 to 45,000/sec
GM Tube II (Anton 213)	0.0012 mica window	Protons: 0.5 Electrons: 0.040	0.1 cm^2 sterad, unidirectional	0.1 to 30,000/sec
	0.55 stainless steel and magnesium	Protons: 20 Electrons: 1	0.2 cm^2, omnidirectional	
GM Tube III (RCL 10311)	0.030 glass plus 0.113 beryllium	Protons: 10 Electrons: 0.5	8.8 cm^2, omnidirectional	15 to 45,000/sec

[a]Minimum rates are those to be expected from galactic cosmic rays, detectors can count slower by a factor 10^{-2}, and maximum rates are determined by the instrument responses.

Stability and fast time resolution are especially important in the electronics for Tubes I and III, since at high counting rates average dead times and charge amplitudes decrease in excess of an order of magnitude.

The first stage of each amplifier consists of a two-transistor charge-sensitive preamplifier. The current integration time constant is set to 2.2 μsec for Tubes I and III and 130 nsec for Tube II. The integration capacitor in each case is 10 pf. The preamplifier is long-time-constant coupled to a one-transistor inverting stage with emitter current feedback. The output stage is a three-transistor one-shot multivibrator with a complementary output to provide both a low and symmetric drive impedance. The multivibrator has a current sensitivity of 200 μamp; is coupled with a short time constant to the inverting amplifier; and has a minimum output pulse width of 3 μsec.

At counting rates of the order of 100/sec, the rate remains stable within $\pm 1\%$ at room temperature. The tubes and amplifiers will be more sensitive to temperature at higher counting rates. However, at a nominal rate of 12,000/sec, the rate does not vary more than $\pm 8\%$ over the temperature range -30 to 75°C.

The detectors respond to particles moving in all directions. Therefore, to minimize the number of secondaries from the spacecraft which can be detected, the particle flux package must be placed as far as possible from the main mass of the spacecraft. It is also necessary to place the ionization chamber close to the particle flux detectors in order that both shall see the same flux of radiation. The window of GM Tube II must be shielded from the Sun.

The effective volumes of Tubes I and III are measured by JPL using a collimated beam of beta rays and by calipering the bare tubes. Their efficiency for detecting penetrating charged particles will be measured with a coincidence technique using sea level cosmic rays as the source of radiation. The response to gamma rays is measured using radioisotopes, while the effect of the shields upon protons and heavier particles can be calculated using range–energy tables.

The response to electron bremstrahlung must be measured using electrons incident upon shields having the same atomic number as the tube shields. This calibration will be accomplished at the State University of Iowa (SUI) over the range 0 to 140 kev electron energy. In order to extend this measurement to higher energy, it is planned to place GM tubes having both beryllium and stainless steel shields in the beam from an electron accelerator capable of producing energies from 0.150 to 1 or 2 Mev.

The relationship between apparent counting rate and true counting rate (i.e., that which would be observed by a GM counter with zero dead time) must be measured with tubes and amplifiers connected in the final flight configuration using a source of very high radiation flux. Each unit must be calibrated individually. This is being accomplished at SUI by using an X-ray machine which has been previously calibrated with a Victoreen R meter. Tube II and the ion chamber are being calibrated at the same time.

It is anticipated that a similar set of detectors will be used with the ionization chamber as a monitor of radiation on future spacecraft. In some cases the Anton 213 tube may not be carried. The coincidence rate between the RCL 10311 tubes will be measured as well as individual counting rates to provide better discrimination between electrons and heavier particles.

D. Plasma Probe

A development program has been initiated to perfect an advanced design plasma probe (Fig. 7) for use on the advanced *Mariner* spacecraft. Although the eventual goals of the experiment are much the same as those intended for the *Ranger* 1 and 2 instruments, utilization of techniques achieved in the development of the *Surveyor* plasma probe will afford higher resolution measurements of a broader particle energy spectrum than obtainable with the *Ranger* instrument.

The instrument will contain seven sets of electrostatic analyzers with Faraday charge collector cups whose look angles are arranged to cover small segments of a solid angle of about 2π sterad centered on the Sun. Because of the increased sensitivity and improved response time of the electrometer amplifier, the deflection plates will be substantially smaller than those used in the *Ranger* and early *Mariner* probes; this will result in a more narrow angle of acceptance. The spread in particle energy for a given electric field between the plates will also be reduced; both the directional sensitivity and the differential particle energy selectivity will be increased. At present, the absolute values of the particle energy spec-

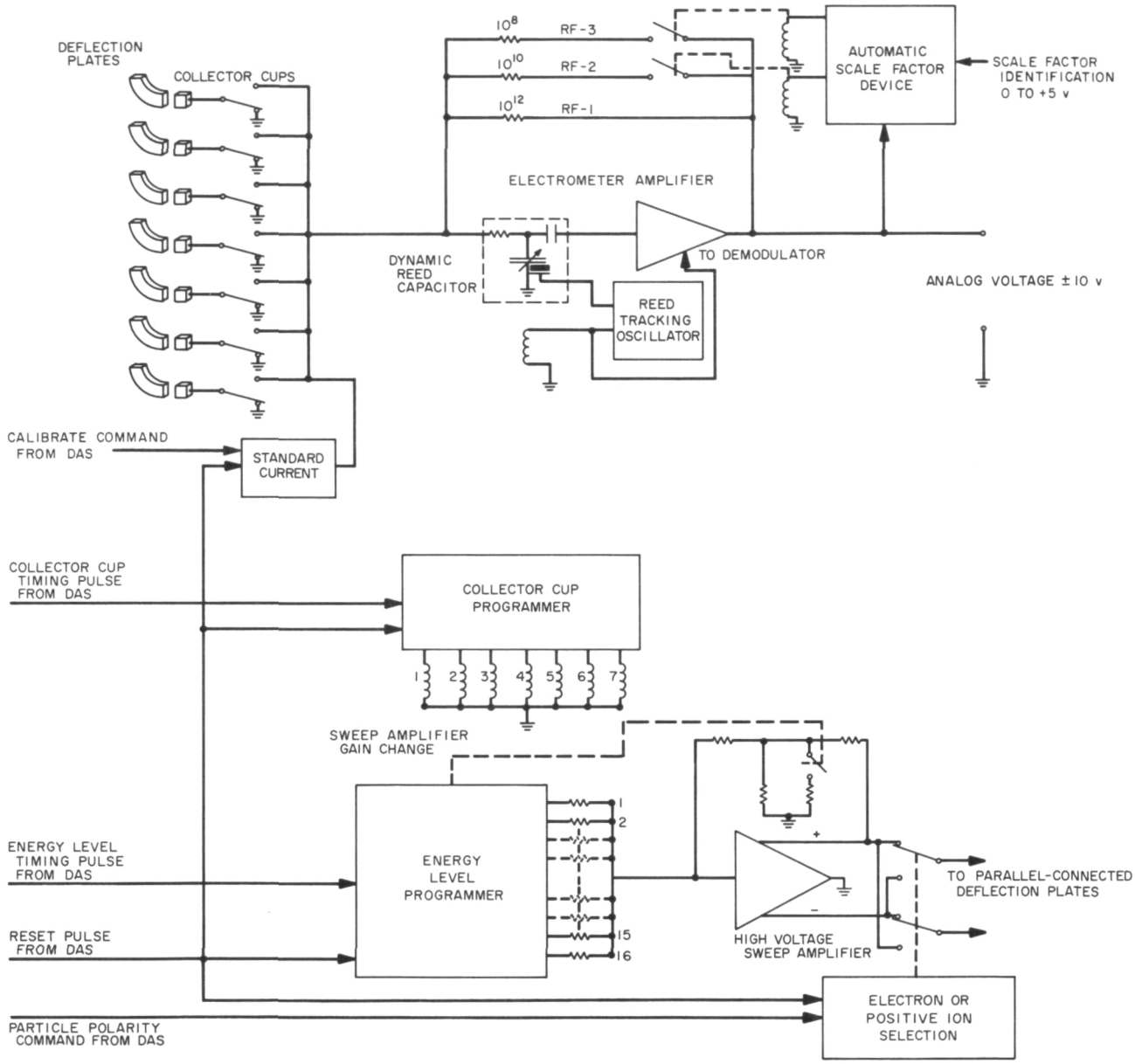

Fig. 7. Logical diagram of plasma probe for the advanced *Mariner*

trum to be examined have not been determined, but there will be provisions for monitoring 32 electron and 32 positive ion energy levels. According to the proposed deflection plate geometry, the energy levels will lie between 20 ev and 20 kev.

As in previous versions of JPL plasma probes, the advanced instrument will consist of the deflection plate-collector cup assemblies with an electrometer amplifier, and a deflection voltage and cup selection programmer system.

1. Electrometer Amplifier

The probe will use the electrometer with the linear range compression that was developed for the *Surveyor* plasma probe. (See previous section: *A. Sigma Plasma Detector.*) The collector cups are consecutively gated into the electrometer by a 3 by 7 diode matrix driven by a three-stage binary counter which receives a timing pulse from the data automation system (DAS). The idle collector cups are grounded when not in use to prevent a high voltage buildup across the collector cup capacitance due to continuously incident charged particles.

2. Deflection Voltage System

The deflection voltages for the electrostatic deflection plates are generated by a carrier-type high voltage operational amplifier driven by a digital programmer. The digital programmer consists of a 4 by 16 diode matrix driven by a four-stage circulating binary counter. While the counter circulates through one cycle, it injects 16 different signal currents into the sweep amplifier; upon completion of one cycle it changes the feedback resistance of the sweep amplifier and circulates once more. Thus, by changing the gain of the sweep amplifier in this manner and cycling through the matrix a second time, 32 discrete output voltages are obtained for 16 discrete inputs. The rate at which the deflection voltages are changed is governed by a timing pulse from the DAS. A programmable polarity pulse from the DAS changes the connection of the high voltage sweep amplifier to the deflection plates and, thereby, permits measurement of 32 energy levels of electron current.

A programmable reset pulse from the DAS resets both the cup selection and energy level programmers to the zero state. It also drives a standard current device which injects a known current into the electrometer amplifier. The current device cycles through three different current levels (one for each reset pulse) so that all ranges of the automatic scale factor device, controlling the feedback loop of the electrometer, are checked.

E. Meteorite Research

About 90% of all meteorites that have been observed to fall are stones which consist primarily of silicate minerals. Genetic interpretation of the textures, mineral associations, and chemical compositions is of importance because these rocks are samples from extraterrestrial bodies and should provide information concerning the early development of the solar system.

1. Relationships Among Chondrites

Prior (Ref. 2) first stated that the several chondrite meteorite types could be produced from one another by addition or subtraction of oxygen. He observed that bulk iron in chondrites is reasonably constant and that "the less the amount of nickel-iron in chondritic stones, the richer it is in nickel and the richer in iron are the magnesium silicates" (Ref. 2, p. 26). Urey and Craig (Ref. 3, p. 57) found a bimodal distribution with respect to total iron and did not see any clear evidence that bulk iron should be regarded as constant. Mason (Refs. 4, 5) and Ringwood (Ref. 6) both pointed out that Prior's rule was qualitatively correct; both measured some compositions of the olivine $[(Mg, Fe)_2 SiO_4]$ and orthopyroxene $[(Mg, Fe) SiO_3]$ phases which did become more magnesian within rocks with higher free metal contents. The most striking examples of this general relationship are the extremes—the carbonaceous chondrites with variable but iron-rich silicates and no metallic iron, and the enstatite chondrites with nearly pure $MgSiO_3$ and the highest free iron contents among the chondrites. Mason also made the point that in any given meteorite the olivine and pyroxene seemed to be of constant composition—that is, the rocks were in or near chemical equilibrium. Both Mason and Ringwood suggested that carbonaceous chondrites are the primary chondrite type and that carbon has reduced the iron in the other chondrite groups now seen, with the enstatite chondrites being the final result. Wiik (Ref. 7) gave analyses for 16 carbonaceous chondrites. They fell into three natural groups with differing amounts of carbonaceous compounds and water. Mason maintained that those groups were the first three steps in a genetic sequence embracing all chondrites, and he wrote the reaction

$$\underset{\text{olivine}}{(Mg,Fe)_2SiO_4} + \underset{\text{orthopyroxene}}{(Mg,Fe)SiO_3} + C \rightarrow \underset{\text{enstatite}}{2MgSiO_3} + 2Fe + CO_2\uparrow$$

Here, iron-bearing olivine and pyroxene react to magnesian orthopyroxene plus free metal and CO_2. Ringwood (Ref. 6) envisioned the same process as having occurred at the surface of the primitive Earth to produce both a gigantic atmosphere which has since been lost and the metal we now see in the core. The main point to understand in a reaction of this type is that as Fe is extracted from a silicate phase, the remaining silicate phases must have a lower cation/Si ratio. Thus olivine, with a cation/Si ratio of 2:1, could react to give more magnesian pyroxene (ratio = 1:1) plus free metal.

Several tests may be made of a hypothesized genetic sequence that depends upon progressive reduction (or oxidation). Normative mineral compositions for 147 reliable chondrite analyses were computed in order to:

(1) Compare the normative (calculated) mineral composition with the modal (measured) compositions where reliable data exist.

(2) Ascertain trends in mineral compositions when plotted against free iron percentages.

(3) Compare the orthopyroxene/olivine ratios with free iron percentages.

It must be emphasized that these studies are to test hypotheses that chondrites as now seen form a kind of continuum from their original state as unrecrystallized chondrules, rock fragments, matrix, and carbon to an assemblage which has recrystallized in the solid state and which approaches chemical equilibrium.

Figure 8 is a graph of the normative percentages opx/(opx + ol) plotted against normative En and Fo in the pyroxene and olivine for 147 reliable chondrite analyses. The trend in Fig. 8 has the slope expected if oxidation-reduction equilibria are obtained in a general way during their formation. The series is quite discontinuous in the regions opx/(opx + ol) = 10 to 15% and 70 to 75%, however.

Figure 9 is a plot of analyzed atomic percent free iron vs normative En and Fo molecular percentages for the same 147 meteorites as in Fig. 8. Again, the general trend

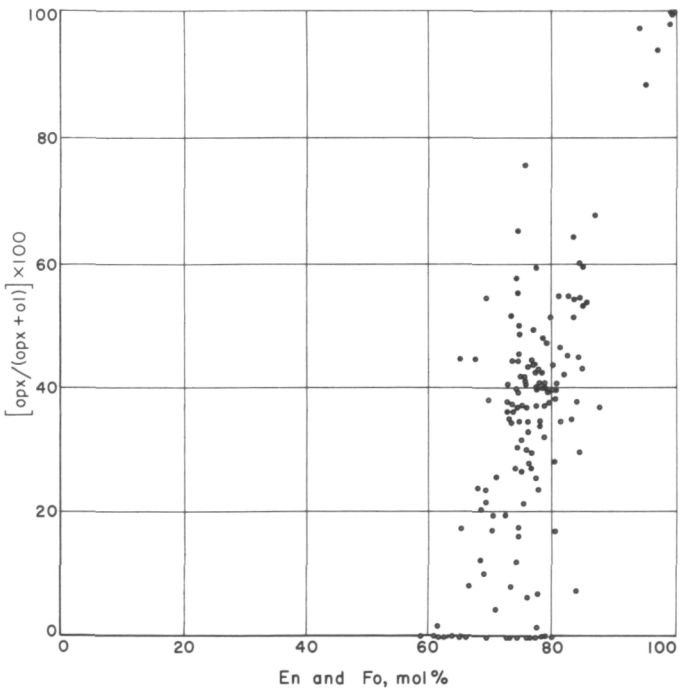

Fig. 8. Percentage of normative orthopyroxene in the total of orthopyroxene plus olivine vs their normative compositions for 147 reliable chondrite analyses

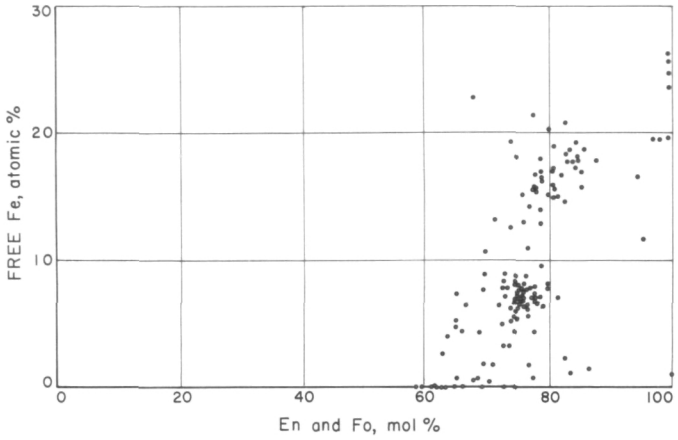

Fig. 9. Free iron atomic percentage calculated volatile-free vs normative enstatite and forsterite molecular percentage in orthopyroxene and olivine

indicates that a relation between silicate mineral composition and free iron concentration exists—the more free iron the less iron and more magnesium in the silicates. But the trend is not continuous to those stones with En and Fo over 90% (the enstatite chondrites). The bimodal distribution of total iron is mainly expressed by the free iron atomic percentage because there is not much difference in bulk iron in the silicates between En and Fo 65 and 70% . If the groups are separated at 10 to 12% free iron, and each group taken individually, there is very little obvious trend for each. The significant feature is the fact that the groups themselves define the trend, not the individuals within the groups. Figures 10 and 11 are histograms showing oxidized iron and total iron abundances, respectively. The bimodal distribution of iron is reflected only in the free iron percentage. In Fig. 10, the small maximum centered at 19 to 20% is the car-

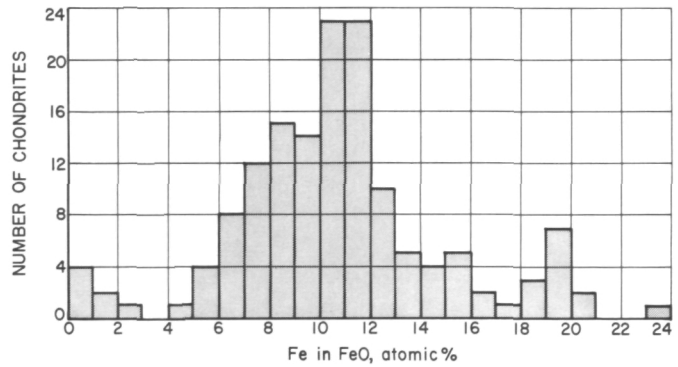

Fig. 10. Histogram of iron held as FeO in silicates or oxides for 147 chondrites in atomic percent

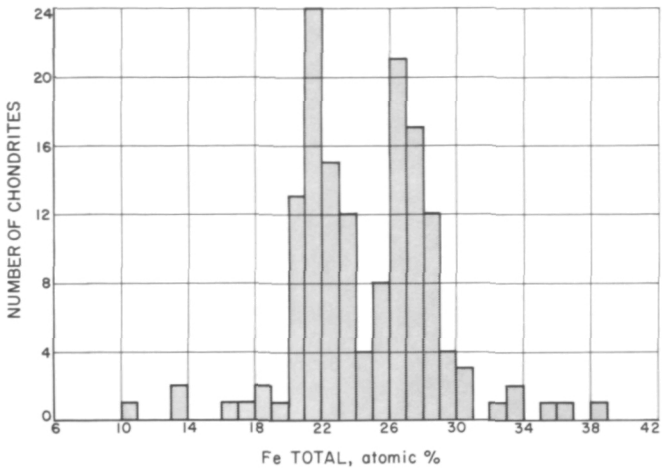

Fig. 11. Histogram of atomic percent total iron for 147 chondrites calculated volatile-free

bonaceous chondrite group. The distribution is not strongly bimodal. Comparison of Fig. 11 with Fig. 10 shows that the bimodal distribution of iron in chondrites is due to the amount of free iron, since Fe as FeS is quite constant.

It is not clear why the group with the highest total iron should have the highest free iron content, and the cause of the bimodal distribution is itself a problem. Figure 9 shows that the high-iron group contains the most magnesian silicates, but the extra free iron should not be taken to mean that these stones were buried more deeply, and hence have iron added from rocks above undergoing recrystallization. Textural evidence on relative amounts of recrystallization (*RS 36-12*) and the occurrence of both high and low iron rocks in most chondrite categories indicates that the chondrites have a more complex parentage than only one or two bodies. The problem of free iron as well as total iron partition among the terrestrial planets and the Moon extends to the stony meteorites as well.

If Mason's general equation of olivine + carbon → orthopyroxene + metal + CO_2 is correct, free iron and opx/(opx + ol) should show a postive correlation. Figure 12 indicates that the trend is really very slight if it does exist at all, and indicates the reaction as written is not correct. The small cluster of points at zero on both the ordinate and abscissa is distorted; all should read 0 for both. They are the bulk of the carbonaceous chondrites. No real continuum can be said to exist from those meteorites with little free iron and pyroxene to the bulk of the meteorites. It will be shown that the amount of carbon at the end of the hypothesized carbonaceous chondrite genetic series is incapable of producing the other meteorites plotted in Fig. 10, even though the postulated reaction is thermodynamically feasible.

Figures 8 and 9 showed the lack of continuity of enstatite chondrites with other chondrites. Figure 12 and Table 5 will show the carbonaceous chondrites are not continuous with other types. Figure 13 is a histogram for 147 chondrites showing the distribution of normative En and Fo. Enstatite chondrites definitely are separated from the main group. Figure 14 is a histogram of the normative orthopyroxene/(orthopyroxene+olivine percentage). Carbonaceous chondrites fall below 5%, enstatite chondrites above 85%.

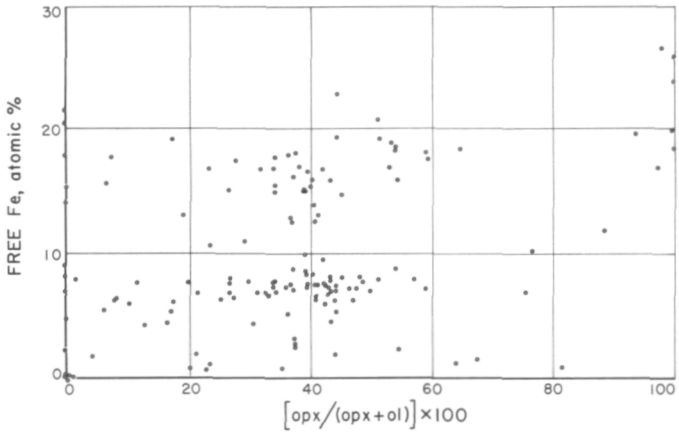

Fig. 12. Free iron vs normative orthopyroxene percentage of the total orthopyroxene plus olivine for 147 chondrites

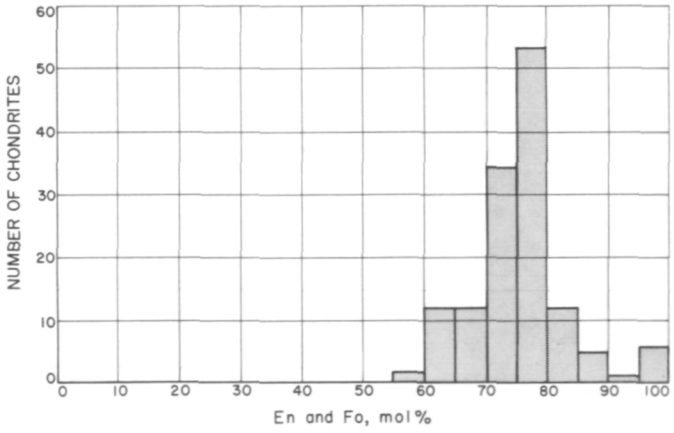

Fig. 13. Histogram of distribution of normative enstatite and forsterite molecular percentages in orthopyroxene and olivine for 147 chondrites

Table 5. Average analyses for Wiik's (Ref. 7) three groups of carbonaceous chondrites

	Group 1			Group 2			Group 3		
	Wt %	Metal atoms	C, H, S	Wt %	Metal atoms	C, H, S	Wt %	Metal atoms	C, H, S
SiO_2	22.65	0.3769		27.69	0.4608		33.78	0.5622	
Al_2O_3	1.65	0.0330		2.22	0.0436		2.63	0.0516	
TiO_2	0.07	0.0009		0.09	0.0011		0.12	0.0015	
FeO	10.42	0.1450		19.84	0.2761		24.35	0.3389	
MnO	0.20	0.0028		0.18	0.0025		0.20	0.0028	
MgO	15.90	0.3943		19.16	0.4752		23.74	0.5888	
CaO	1.55	0.0276		2.02	0.0360		2.31	0.0412	
Na_2O	0.75	0.0242		0.48	0.0154		0.48	0.0077	
K_2O	0.07	0.0014		0.08	0.0016		0.13	0.0014	
H_2O+	16.0(?)	1.7758		11.4(?)	1.2652		0.6(?)	0.0333	
P_2O_5	0.35	0.0050		0.29	0.0040		0.32	0.0046	
Cr_2O_3	0.35	0.0046		0.40	0.0052		0.51	0.0068	
NiO	1.28	0.0171		1.57	0.0210		0.31	0.0042	
CoO	0.76	0.0008		0.08	0.0011		0.00		
FeS	16.72	0.1902	0.1902S	9.50	0.1081	0.1081S	6.05	0.0688	0.0688S
Fe	0.00			0.00			2.31		
Ni	0.00	Total oxygens 0.00 = 2.5506		0.00	Total oxygens 0.00 = 2.4722		0.92	Total oxygens 0.59 = 2.3136	
Co									
Organic	5.53		0.0238S 0.5172H 0.2586C	1.41		0.0061S 0.1464H 0.0732C	0.00		
C	3.96		0.3300C	2.46		0.2050C	0.39		0.0325C
Total	97.51			98.97			99.74		

Oxidizable atoms	Reducible atoms	Oxidizable atoms	Reducible atoms	Oxidizable atoms	Reducible atoms
0.0238S 0.5172H 0.5886C	0.0008 (CoO) 0.0171 (NiO) 0.1450 (FeO) 0.1476 (FeS)	0.0061S 0.1464H 0.2782C	0.0011 (CoO) 0.0210 (NiO) 0.2761 (FeO) 0.0562 (FeS)	0.0325C	0.0042 (NiO) 0.3389 (FeO) 0.0088 (FeS)
Total 1.1296	0.3105	0.4307	0.3544	0.0325	
Potential reduction to:					
En and Fo_{100}		En and Fo_{100}		En and Fo_{65}	

Group 1: Orgueil, Ivuna.
Group 2: Nogoya, Cold Bokkeveld, Mighei, Nawapali, Haripura, Boriskino, Santa Cruz, Murray.
Group 3: Warrenton, Lance, Felix, Mokoia.

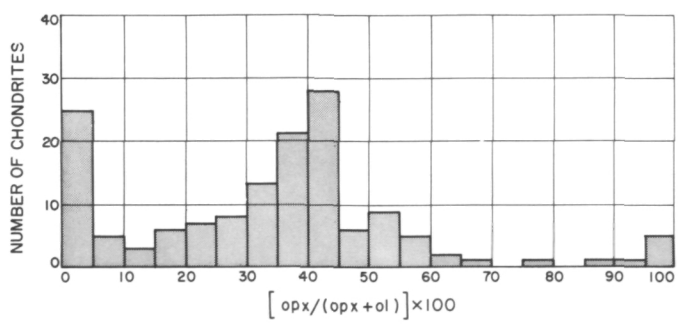

Fig. 14. Histogram of the distribution of the percentage of normative orthopyroxene in the total orthopyroxene, plus olivine. Carbonaceous chondrites (0 to 5%) and enstatite chondrites (90 to 100%) which are separate from the main group

The average analyses of Wiik's (Ref. 7) three groups of carbonaceous chondrites can be recomputed into atoms and check the ability of the potential reducing agents, C, H, and S, to reduce the required number of metal atoms from an oxidized state to free metal. Table 5 gives the average of the complete analyses for Wiik's Groups 1, 2, and 3, and the analyses recomputed into atoms. The atomic ratios for the organic material are only approximate; the ratios of $C_{12}M_{24}SO_2$ were derived from Müeller's (Ref. 8, p. 2) data on Cold Bokkeveld. The totals under *oxidizable atoms* do not include the sulfur from FeS. The totals under *reducible atoms* include enough Fe from FeS to bring the final total FeS to 5.7 weight percent after all water and other volatiles have been driven off. The number of oxidizable atoms is far more than enough to reduce CoO, NiO, FeO, and the

Table 6. Presence or absence of subsilicic normative minerals in Wiik's (Ref. 7) carbonaceous chondrite analyses, based on final 5.7% FeS[a]

	Nepheline for Albite	Leucite for Orthoclase	Larnite for Diopside	Kaliophilite for Leucite	Subsilicic beyond Kaliophilite	En and Fo when enough SiO_2 for Albite	
Group 1							
Tonk	X	X	X	X	X	75.2	75.2
Orgueil	X	X	X	X	X	71.4	
Ivuna	X	X	X	X	X	79.0	
Group 2							
Nogoya	X	X	X	X	X	62.4	68.3
Cold Bokkeveld	X					63.6	
Mighei	X					65.6	
Nawapali	X	X	X			73.0	
Haripura	X	X	X	X	X	70.1	
Boriskino	X	X	X	X	X	83.0	
Santa Cruz	X	X	X	X	X	68.1	
Murray	X					60.6	
Group 3							
Warrenton	X					65.0	67.7
Lance	X	X	X			71.2	
Felix	X					65.7	
Mokoia	X					69.0	

[a]See text for explanation.

necessary amount of FeS in Group 1, and somewhat more than enough in Group 2. However, these cannot be part of an evolutionary sequence as suggested by Mason and by Ringwood (Ref. 6, p. 172) because the oxidizable atoms in Group 3 are not plentiful enough even to produce bronzite.

Table 6 indicates the presence or absence of subsilicic normative minerals in Wiik's (Ref. 7) carbonaceous chondrite analyses, based on final 5.7% FeS. Cations would have to be removed (for example, by reduction of iron to the metal) from the potential silicate phases to produce the standard chondrite assemblage upon recrystallization. Normative En and Fo percentages when just enough iron has been reduced to produce enough SiO_2 for albite from nepheline are given. Partial normative silicate compositions are given in Table 6 for the carbonaceous chondrites. They appear to be subsilicic, in that the standard norms contain not only nepheline but many have Ca-orthosilicate, kaliophilite, and even free MgO and FeO. The significance is that much free iron must be formed in order for the cations to form common silicates. Nepheline has never been reported from meteorites, and we must assume that albite is the only sodic mineral. If so, the amount of iron can be calculated that would be left in the silicates after enough had been reduced to leave enough silica to form albite from nepheline. The resulting En and Fo percentages are tabulated in Table 6. If the carbonaceous chondrites were to recrystallize, the silicates would have to be at least that magnesian for the assemblage not to contain nepheline. The oxidizable atoms for Group 3 are not plentiful enough to produce albite and no nepheline upon recrystallization. The potential normative values for Groups 1 and 2 were calculated on the basis of a final 5.7% FeS, the chondrite average. Note that the number of oxidizable atoms in Group 3 (from Table 5) is only sufficient to produce En and Fe 65; thus the average Group 3 rock could not recrystallize to form a normal chondrite without loss of oxidized cations or gain of more reducing agents. These considerations, along with the chemical discontinuities between carbonaceous chondrites and other chondrite types discussed previously, suggest that carbonaceous chondrites may be a small genetic series among themselves, but that they are not the forerunners of other meteorite types through recrystallization.

2. Achondrites

Achondrites may be divided into calcium-rich and calcium-poor types. Each main group contains several subtypes; a discussion and presentation of most available chemical analyses is given by Urey and Craig (Ref. 3). The Ca-poor types are largely composed of bronzite or enstatite, with only minor amounts of olivine, clinopyroxene, oligoclase, and pyrrhotite. The Ca-rich types average about 40 to 50% hypersthene or ferrohypersthene, 30 to 40% calcic bytownite, and 20% ferroaugite. The two types have previously been interpreted (e.g., Ref. 9) as differentiated layers in a planetary body. Average normative compositions for pyroxene and plagioclase compositions and the average weight percentages of orthopyroxene plus olivine, plagioclase, and diopside are given in Table 7. The occurrence of the lower temperature iron-rich members of the mafic phases with the high-temperature calcic plagioclase is not easily explained by either fractional melting or by fractional crystallization of a single original liquid. Even though feldspars only occur in very small amounts in the Ca-poor achondrites, it would be expected to have been a calcic phase unless some high-pressure or solid solution effect played a part. The Ca-poor achondrites contain less than 5% normative diopside, most of which is probably in solid solution in the orthopyroxene.

Descriptions of Ca-rich achondrites commonly show less than 1% oligoclase although there is 2 to 3% in the norms. Much of this normative excess may be due to solid solution of (Na + Al) for two divalent cations in the pyroxene structures. Existing petrographic descriptions are not complete enough to decide whether or not the modal plagioclase is an exolved phase. Further investigation will be carried out here because this is a key point in petrologic interpretation of these rocks.

If the oligoclase present is exolved from the high-temperature pyroxene phases, it is reasonable to postulate that the Ca-poor rocks are accumulations of early-crystallized minerals and the Ca-rich types are the late differentiates. The latter would be analogous to common terrestrial ferrogabbros, the main difference being that the original liquids were much more mafic than basalts so that the feldspars and diopside did not crystallize at all until about half the liquid had solidified and separated. Table 8 lists average analyses for the two achondrite types (Ref. 3) and their normative compositions. Column (3) is an average of the two groups and is a rough approximation to a liquid that could differentiate to produce both achondrite types by fractional crystallization.

The significance of such a liquid lies in whatever chemical relationship to the chondrites and to the bulk composition of the terrestrial planets it may have. Chondritic material is nearly always equated with the bulk composition of the Earth and Moon although the iron partition problem remains unsolved. The use of a chondrite model for the Earth and Moon has been made mostly because chondrites constitute three-fourths of all meteorite falls. The abundances of radioactive elements in chondrites are used to compute thermal models for the Moon, even

Table 7. Normative compositions and weight percentages of olivine + orthopyroxene and plagioclase for achondrite analyses of Urey and Craig (Ref. 3)

	En and Fo	Weight percent of total rock	An	Weight percent of total rock	Diopside weight percent of total rock
Ca-poor achondrites	83	90 to 95	24	2 to 3	3 to 4
Ca-rich achondrites	51	45	79	35	20

Table 8. Approximation to liquid which could fractionally crystallize to give both Ca-rich and Ca-poor achondrites

	Analyses		
	(1) Average Ca-rich achondrite (Ref. 3)	(2) Average Ca-poor achondrite (Ref. 3)	(3) Composite average of (1) and (2)
SiO_2	48.6	51.4	50.0
Al_2O_3	11.7	1.1	6.4
TiO_2	0.5	0.1	0.3
FeO	16.3	11.2	13.8
MnO	0.5	0.4	0.4
MgO	9.9	29.8	19.9
CaO	10.4	1.2	5.8
Na_2O	0.8	0.4	0.6
K_2O	0.3	0.1	0.2
P_2O_5	0.1	0.1	0.1
Cr_2O_3	0.4	0.8	0.6
Fe	0.0	2.6	1.3
FeS	0.6	0.9	0.7
Total	100.1	100.1	100.1
Partial mineral norms			
Orthoclase	1.6	0.6	1.1
Plagioclase	34.9	3.6	19.3
Diopside	20.0	3.3	11.6
Orthopyroxene	35.6	76.5	56.1
Olivine	6.3	14.6	10.4
An	79	24	52
En, Fo	51	83	67

though such a high rate of heat production suggests considerable melting at the present time.

Chondrites contain plagioclase which is more sodic than that of the average of the achondrites, and, considering free iron as FeO originally, contain more iron-rich normative ferro-magnesian minerals. They also contain a higher percentage of alkalies and, therefore, probably radioactive elements as well. Chondrites could well be truly volcanic rocks (as has been suggested from textural evidence since the 19th century) formed by partial melting of material with the composition of the achondrite average [Table 7, column (3)].

If most meteorites as we see them (compact rocks commonly of the size of a foot or so in diameter) were thrown from the surfaces of bodies during impact of smaller bodies, it is expected that many more pieces of near-surface rocks (volcanic chondrites?) and progressively fewer Ca-rich and Ca-poor achondrites, would be found, which is the observed relation.

If chondrites can be shown not to represent primordial material, present thermal and compositional models for the Earth and Moon will have to be revised. Experimental melting work is underway.

References

1. Jet Propulsion Laboratory, *Scientific Experiments for Rangers 1 and 2*, Technical Report No. 32-55, Jet Propulsion Laboratory, Pasadena, California, January 3, 1961.
2. Prior, G. T., "On the Genetic Relationship and Classification of Meteorites," *Mineralogical Magazine*, Vol. 18, pp. 26–44, 1916.
3. Urey, H. C., and H. Craig, "The Composition of the Stone Meteorites and the Origin of the Meteorites," *Geochimica et Cosmochimica Acta*, Vol. 4, pp. 36–82, 1953.
4. Mason, B., "Origin of Chondrules and Chondritic Meteorites," *Nature*, Vol. 186, pp. 230–231, 1960.
5. ——————, "The Origin of Meteorites," *Journal of Geophysical Research*, Vol. 65, No. 9, pp. 2965–2970, 1960.
6. Ringwood, A. E., "Chemical and Genetic Relationship Among Meteorites, *Geochimica et Cosmochimica Acta*, Vol. 24, pp. 159–197, 1961.
7. Wiik, H. B., "The Chemical Composition of Some Stony Meteorites," *Geochimica et Cosmochimica Acta*, Vol. 9, pp. 279–289, 1956.
8. Müeller, G., "The Properties and Theory of Genesis of the Carbonaceous Complex Within the Cold Bokevelt Meteorites," *Geochimica et Cosmochimica Acta*, Vol. 4, pp. 1–10, 1953.
9. Wood, J. A., *Silicate Meteorite Structures and the Origin of the Meteorites*, Technical Report 10, A. F. Office of Scientific Research, p. 165, 1958.
10. Mason, B., and Wiik, H. B., *Geochimica et Cosmochimica Acta*, Vol. 21, pp. 266–271, 1961.

Page intentionally left blank

Page intentionally left blank

XIII. Exobiology

A. Soil Studies–Microflora of Desert Regions

1. Introduction

Knowledge and understanding of the interrelationships occurring between micro-organisms and their terrestrial micro-environments is of primary importance in any program for extra-terrestrial life detection. A sound background of information pertinent to these interrelationships is likewise important for sensible design and instrumentation of a life detection system. This system can be based upon microbial ecology in that micro-organisms are ubiquitous in terrestrial habitats in soil, water, and air, and not only survive, but reproduce at the extreme limits of the natural environment. Furthermore, terrestrial micro-organisms are considered to be protobionta, and have successfully adapted to a wide range of environmental conditions. Some of these very severe terrestrial habitats (which could approach the more austere macro- and micro-environment expected on other planets) are restricted to microbial inhabitants. Even our own planet, which has a relatively favorable environment, has huge expanses devoid of structurally complex macroplants and animals.

While it would definitely be easier to interpret a complex macro structure found in an extraterrestrial environment as one similar to a terrestrial macro life-form, it should not be assumed that such life-forms exist outside of our own planetary environment. It also should not be assumed that where there are no macro inhabitants, there are no micro-organisms. Micro-organisms are essential to macro life and to biogenic cyclic processes, but the converse is not true, and as indicated by the fossil record, did not occur in the early evolution of our own planet. All organisms and their habitats, therefore, need not be studied since preliminary knowledge of extraterrestrial environments, if correct, limits speculation as to the kinds of organisms that might be encountered. Any investigation for extraterrestrial biota can then be based on microbial ecology in severe terrestrial environments.

Micro-organisms are found primarily in three naturally occurring terrestrial habitats: water, air, and soil. Water, although found in wide expanses on this planet, may be much less abundant on other planets. Air, although it frequently contains micro-organisms, is essentially a "sterile" environment for microbial activities. The micro-organisms found in aerial situations are essentially transients from the soil, scattered throughout a large volume

by various dispersal mechanisms. The soil, in contrast to the air, is the natural substratum for numerous micro-organisms and serves as a reservoir for many others which become active only under certain conditions; e.g., upon addition of moisture or increase in food supply. In general, there is no soil lacking in micro-organisms, whether they are indigenous to the soil or temporary contaminants, even under the severest environmental conditions.

Deserts provide one of the most austere environments for life. Water is frequently lacking, irregularly distributed, rapidly lost through evaporation or runoff, and if present in quantity, is commonly of an adverse quality due to dissolved salts. Surface irradiation is intense and there is less cloud cover to intercept ultraviolet and infra-red rays. Temperature, also a limiting factor, may have a relatively high mean value and contribute to a high rate of evaporation. The food supply in the desert ecosystem is frequently low, limited by the paucity of organic matter, or is unavailable through lack of adequate moisture. The soils of the desert, while fertile, are unproductive due to the lack of water. The biotic populations and communities that exist in desert areas are therefore ecotypes especially adapted to the rigorous arid environment characteristic of desert regions.

2. *Studies of the Soil and Microbial Environment*

Few soil surveys have been made of desert areas, and very little is known of the desert microflora. Soil studies should then be directed toward the measurement of those properties which are relevant to the nature and behavior of the soil and its dependent biota, especially the microflora.

General information of value includes that which characterizes the physical and chemical systems of the soil, and its solid, liquid, and gaseous phases. Specific analyses should be primarily those concerned with measurement of limiting factors. These include environmental factors related to the following characteristics:

(1) Water: total percent, forms, quality, and suctions.

(2) Temperature and humidity: actual, effective minimum, maximum, mean, and seasonal.

(3) Aeration (gases): total percent, composition, pressures, distribution, and interchange.

(4) Surface irradiation: quality and quantity of visible light, ultraviolet and infra-red rays.

(5) Biogenic salts: composition and concentration, especially those salts which are available (not "bound"), including carbonates, bicarbonates, sulfates, nitrates, and phosphates.

(6) *p*H: soil reaction in the range of effective acidity or alkalinity.

(7) Eh: oxidation-reduction power of the soil.

(8) Organic matter: total percent, organic carbon, organic nitrogen, and C:N ratio.

(9) Mechanical analysis: soil grain size distribution.

(10) Porosity: percentages of soil volume exclusive of solid particles.

(11) Density: soil weight relationships.

A general study of any microbial ecology in the soil should then consider measurement of the above characteristics in order to determine certain pertinent environmental parameters.

Specific biological problems of microbial ecology include the study of soil bacteria, actinomycetes, fungi, algae, and lichens as they behave in their natural environment, or as they respond to an induced environment. This study can be subdivided into an examination of populations and communities of micro-organisms in natural and simulated environments as follows:

(1) Development of sampling, isolation, and culturing methods and techniques.

(2) Determination of organisms present, their associations, enumeration, occurrence, distribution, and form.

(3) Metabolic and physiological characteristics including microbial modification of the environment.

(4) Response and adaptation to a change in environment.

(5) Consideration of environmental parameters which cause death, limit life to survival, retard metabolism, limit growth, or restrict reproduction.

(6) Differential and comparative studies with microflora of similar groups in different soils and correspondingly different environments.

(7) Adaptivity, survival, growth, and reproduction of nondesert microflora when inoculated into a desert micro-environment.

Not all of the soil parameters can be investigated any more than all of the induced and natural microbial ecologies can be studied. The main problem is, therefore, to

select the soil factors considered to be most important to microbial ecology, and to measure each factor by a desirable method.

3. Methods and Measurements

For a preliminary study of soil and microbial ecology, soil samples were examined and collected from desert areas in Southern California. Descriptions of the collection areas are given in Table 1. Soil samples were taken from five levels:

(1) The surface, from 0 to ½ in.

(2) Below the surface to 6 in.

(3) At 1-ft level.

(4) At 2-ft level.

(5) At 3-ft level.

Table 1. Area descriptions

Area No.	Soil No.	Description
I	1, 2, 51, 65, 53, 54	Colorado Desert, Riverside County, 2.8 mi east of Thermal, California, below Coachella Canal. Elevation: 10 ft. Land gently sloping, moderate erosion, good drainage, no visible alkali. Ancient beach sand containing shells and shell fragments. Parent material: granitic sands. Soil: Entisol, Ustent; Coachella sand. Vegetation: scattered desert shrubs.
II	6, 68, 69, 63, 61	Colorado Desert, Riverside County, 5 mi east of Thermal, California. Elevation: 45 ft. Land with 45-deg slope in narrow canyon, severe erosion, drainage fair, calcareous patches. Recently extruded clay along San Andreas Fault. Parent material: calcareous clay. Soil: Entisol, former Haplaquent; red clay in an area of rough, stony land. Vegetation: none.
III	4, 62, 66, 64, 67	Colorado Desert, Riverside County, 15 ft from above location. Elevation: 45 ft. Land precipitous with 90-deg slope. Severe erosion, drainage fair, some cementation, especially at 2½ to 3 ft. Recently extruded loamy soil along San Andreas Fault. Soil: Entisol, Psammustent; isolated hummock of loamy soil in an area of rough, stony land. Vegetation: none.
IV	74, 70, 71, 72, 73	Mojave Desert, Los Angeles County, 21 mi east of Lancaster, California, in Joshua Tree State Park. Elevation: 2,910 ft. Land gently sloping, slight to moderate erosion, no alkali. Abrupt change in color, texture, moisture content, and unconfined strength at 20 in. Parent material: granitic rock alluvium. Soil: Aridisol, Argid; Adelanto sand. Vegetation: desert shrubs including Joshua trees and common yucca.
V	75, 76, 77, 78, 79, 81	Mojave Desert, Kern County, 0.5 mi northwest of Mojave, California. Elevation: 2,760 ft. Relatively flat land, minor erosion, no alkali. Parent material: granitic rock alluvium. Soil: Aridisol, Orthid; Hesperia sand; gravel surface with scattered rabbit fecal pellets. Vegetation: scattered desert shrubs, predominantly creosote bush, some dried grasses.

In some cases, caliche, (hardpan, or claypan) horizons were encountered and the depth sampled did not proceed beyond 2½ ft; e.g., Area IV. For one profile, Area V, a sample was taken at 4 ft. During collecting and processing, precautionary techniques were used insofar as possible to avoid contamination of samples from various horizons.

Measurements were made in both the field and the laboratory. Field measurements included those for *p*H, Eh, maximum temperature for the air and soil, air humidity, unconfined compressive strength, infiltration rate, and soil color. A separate sample was obtained for soil moisture, porosity, and bulk density; these values were determined in the laboratory. Physical analyses performed in the laboratory included mechanical analysis for grain size distribution, and measurement of certain soil–water relationships as indicated by moisture present in soil during storage, when saturated, at the field capacity, and at the wilting coefficient. Other physical measurements included the percent of reflectivity, absorptivity, soil color, and Munsell notation when the soil was air dry and at the field capacity. The latter measurements were made in the field and repeated in the laboratory. Chemical analyses performed in the laboratory included *p*H, Eh, resistivity, specific conductance, osmotic pressure, total soluble salts, organic carbon, organic matter, organic nitrogen, protein, and N value. Only a few preliminary biological tests were performed. These included determinations of the number of aerobes, anaerobes, fungi, and coliforms with soil depth.

Soil analyses were made by standard methods in most cases. A brief résumé of methods is given below. Only the physical methods and measurements are reported.

(1) Air temperature: by a shielded thermometer at 3 ft above the ground surface.

(2) Air humidity: by means of a sling psychrometer.

(3) Soil temperature: (a) surface temperature, by a shielded thermometer; (b) subsurface temperature, by a brass soil thermometer.

(4) Infiltration rate: the time required for 2 in. of water to completely enter the soil.

(5) Unconfined compressive strength: soil hardness as measured by a pocket penetrometer.

(6) Mechanical analysis: time–density measurements of grain size distribution by the hydrometer method.

(7) Material >2.0 mm: the percent of gravel, stones, and organic matter retained by a 10 mesh sieve.

(8) Texture: by vector intersection plotted on a soil texture triangle.

(9) Percent of water in field soil and during storage: standard gravimetric analysis by weight loss after heating soil to 105°C.

(10) Percent water of saturation: gravimetric, as above, after soil was saturated with water.

(11) Percent of water at field capacity (moisture equivalent): gravimetric, as above, after soil was saturated and centrifugally subjected to 1000 *g* for 30 min.

(12) Percent of water at wilting coefficient: calculated from the field capacity (moisture equivalent/1.84).

(13) Percent of pore space: calculated from the bulk density.

(14) Bulk density: the weight of soil/unit volume.

(15) Soil color and Munsell notation: by reference to soil color charts and notations for hue, value and chroma.

(16) Percent reflectivity: determined by photoelectric reflection meter using zero suppression and a tristimulus green filter.

(17) Percent of absorptivity: calculated from the reflectivity (100 − reflectivity).

4. Results and Discussion, Physical Measurements

The physical data obtained for each of the five soil profiles is given in Tables 2, 3, and 4. No statistical correlations were prepared for this report, but on the basis of preliminary measurements, the following information was obtained. The maximum air temperature during the time of collection was in all cases less than the soil surface temperature, ranging from 62 to 82°F. The maximum relative humidity of the air at these temperatures ranged from a high of 42 to a low of 14%. The lowest relative humidity was 8%. The maximum soil surface temperature was in all cases higher than the maximum air temperature, ranging from 84 to 114°F. This was 18 to 32°F more than the maximum air temperature. The maximum soil temperature at 2 in. below the surface was in all cases also higher than the corresponding air temperature, but lower than the surface temperature, ranging from 73 to 102°F. A few measurements were made at 6 in. below the surface. There was a definite lag period in soil temperature equilibration at this level, and during the measurement period of a few hours, it was observed that the subsoil temperature could approach the surface temperature.

Certain physical measurements of the soil are greatly dependent upon soil texture and structure. The infiltration rate, for example, usually varied from a few seconds to a few minutes and was most rapid through the clay soil only because it was cracked at the surface. For 2 in. of water, the infiltration depth for all soils varied from 4 to 5 in. Soil hardness was also dependent upon soil texture and structure. A loose sand, e.g., Soil 1, had a compressive strength of <0.25 kg/cm^2 in some places, but where it was united by microbial organic matter, it was 0.75 kg/cm^2. Duripans or cemented layers were indicated by readings of >4.5 kg/cm^2, e.g., Soils 67, 72, 73, and 78.

Mechanical analyses for grain size distribution in the five profiles gave values for sand of 35.6 to 93.6%; silt, from 2.0 to 23.8%; and clay, 2.9 to 48.8%. For desert soils a dispersion medium such as calcium hexametaphosphate, instead of a sodium salt, must be used in the mechanical analysis, otherwise the soil flocculates and lower values are obtained. Material >2.0 mm was removed from the soil since it has very few soil properties. Quantities of coarse material can be expected at any horizon in the profile, e.g., Soils 75, 77, and 81. Soil 67 had a significant amount of coarse cemented material approaching that of consolidated rock. The textural classes of the desert soils ranged from that of sand to clay, with two intermediate textures of sandy loam and loamy sand. Soils 72 and 73 showed distinct changes in texture and other features from the overlying horizons. Cementation was so strong at the subsurface depths that the profile could not be investigated further with hand-operated equipment.

Soil moisture relationships were considered to a limited extent. Soil moisture retention depends considerably on soil temperature, texture, structure, porosity, and amounts of organic matter, and salt, as well as other factors. The percent of moisture for the *in situ* soil was quite low for most horizons. Below the surface 2 in. was the driest part of the profile, except for Soil 6. The sandy soils were drier than the clay soils, although all of the field soils had a soil moisture content beyond the calculated wilting coefficient. After the soils were brought to the laboratory it was noted that when the samples were stored aerobically they could have moisture values different from those in the field. These new values were soil moisture contents in equilibrium with the laboratory environment. Soils 72 and 73, for example, lost moisture

Table 2. Physical measurements (No. 1)

Soil No.	Depth	Maximum air temperature, °F (at 3 ft)	Relative humidity	Maximum soil temperature, °F		Infiltration time (2 in. of H_2O)	Unconfined compressive strength, kg/cm^2	Mechanical analysis, %			Percent material > 2.0 mm	Textural class
				Surface	2 in. below			Sand 2.0 to 0.02 mm	Silt 0.02 to 0.002 mm	Clay 0.002 mm or less		
1	Surface 1/16 in.	79	34	109	88	15 to 45 sec	<0.25 to 0.75	91.7	5.4	2.9	7.8	Sand
2	1/16 to 1 in.							90.7	5.3	4.0	4.3	Sand
51	1/16 to 6 in.							93.3	2.0	4.7	3.1	Sand
65	1 ft							93.6	2.8	3.6	> 2.0	Sand
53	2 ft						2.5 to 3.0	87.2	8.8	4.0	2.3	Sand
54	3 ft							91.4	4.9	3.7	4.0	Sand
6	Surface 1/2 in.	82	42	100	96	(soil cracked) 5 sec	0.5 to 1.0	36.2	18.0	45.8	0.6	Clay
68	1/2 to 6 in.							35.6	15.6	48.8	0.1	Clay
69	1 ft							37.6	16.6	45.8	0.6	Clay
63	2 ft							38.0	14.6	47.4	0.1	Clay
61	3 ft							36.6	15.8	47.6	1.0	Clay
4	Surface 1/8 in.	82	42	114	102	1 to 4 min	1.0 to 1.75	61.8	21.8	16.4	0.5	Sandy loam
62	1/8 to 6 in.							62.6	21.0	16.4	1.7	Sandy loam
66	1 ft							67.6	19.0	13.4	0.2	Sandy loam
64	2 ft							67.2	19.0	13.8	2.1	Sandy loam
67	3 ft						> 4.5	61.6	23.8	14.6	37.3	Sandy loam
74	Surface 1/4 in.	62	14	84	73	30 sec	0.25	91.4	4.5	4.1	3.8	Sand
70	1/4 to 6 in.							91.4	3.1	5.5	0.4	Sand
71	1 ft							86.6	8.8	4.6	0.4	Sand
72	2 ft						> 4.5	74.1	6.3	19.6	2.4	Loamy sand
73	2 1/2 ft						> 4.5	77.3	7.0	15.7	7.3	Loamy sand
75	Surface 1/4 in.	72	14	93	80	1 1/2 to 9 min	0.75 to 1.75	89.9	5.3	4.8	34.6	Sand
76	1/4 to 6 in.							88.4	11.6	6.3	12.4	Sand
77	1 ft							89.7	10.3	8.1	23.3	Sand
78	2 ft						> 4.5	83.4	7.0	9.6	16.6	Sand
79	3 ft							84.0	7.0	8.1	22.0	Sand
81	4 ft							88.1	5.5	6.4	45.5	Sand

when stored. Clay Soils 6 through 61 were equilibrated to within 0.2% moisture under storage conditions.

The percent moisture of saturation, field capacity, and wilting coefficient are soil moisture constants that further characterize a soil and greatly influence biotic activities. The percent moisture of saturation is the smallest amount of moisture at which the soil can be saturated when the soil grains are worked into the position of closest packing. There is no capillary potential at this moisture content and very little air. Sandy soils hold considerably less moisture of saturation than clay soils, or soils with large amounts of organic matter and/or hydrated salts. Anaerobic conditions prevail at this moisture content. By contrast with the saturation percentage, the field capacity represents the amount of moisture retained by the *in situ* soil after water has been removed from it under the influence of gravity. This value is approximated centrifugally

Table 3. Physical measurements (No. 2)

Soil No.	Depth	H_2O field, %	H_2O air-dry storage, %	H_2O saturation, %	H_2O, field capacity (moisture equivalent), %	H_2O, wilting coefficient (moisture equivalent/1.84), %	Pore space, %	Bulk density, gm/cc
1	Surface 1/16 in.	0.28 (2 in.)	0.51	29.50	7.58	4.12	44.16 (2 in.)	1.48 (2 in.)
2	1/16 to 1 in.		0.27	22.50	3.07	1.67		
51	1/16 to 6 in.	0.29 (6 in.)	0.23	24.58	3.51	1.91	43.40 (6 in.)	1.50 (6 in.)
65	1 ft	0.31	0.18	26.06	3.05	1.66	47.17	1.40
53	2 ft	0.35	0.34	21.18	2.98	1.62	41.89	1.54
54	3 ft	0.46	0.29	22.77	3.13	1.70	40.38	1.58
6	Surface 1/2 in.	3.29 (2 in.)	3.75	73.88	36.92	20.07	64.53 (2 in.)	0.94 (2 in.)
68	1/2 to 6 in.	2.54	3.84	74.40	35.22	19.14	62.27 (6 in.)	1.00 (6 in.)
69	1 ft	2.61	3.82	64.01	33.40	18.15	55.85	1.17
63	2 ft	4.54	3.98	72.84	38.59	20.97	53.59	1.23
61	3 ft	2.63	3.78	54.95	35.69	19.39	64.91	0.93
4	Surface 1/8 in.	0.59 (2 in.)	0.56	34.00	15.14	8.23	65.85 (2 in.)	1.17 (2 in.)
62	1/8 to 6 in.	0.62 (6 in.)	1.23	32.27	11.36	6.17	56.61 (6 in.)	1.15 (6 in.)
66	1 ft	0.68	0.69	31.67	7.76	4.22	57.36	1.13
64	2 ft	0.69	0.75	31.28	10.30	5.60	52.08	1.27
67	3 ft	0.71	0.87	31.68	15.97	8.69	41.89	1.54
74	Surface 1/4 in.	0.37 (2 in.)	0.41	20.82	3.72	2.02	39.62 (2 in.)	1.60 (2 in.)
70	1/4 to 6 in.	0.67 (6 in.)	0.40	24.74	4.69	2.54	44.91 (6 in.)	1.46 (6 in.)
71	1 ft	0.91	0.36	24.01	3.60	1.96	43.77	1.49
72	2 ft	6.86	2.60	37.39	14.79	8.04	25.66	1.97
73	2 1/2 ft	5.69	2.30	34.57	23.28	12.65	40.38	1.58
75	Surface 1/4 in.	0.60 (2 in.)	0.54	22.40	4.93	2.68	44.53 (2 in.)	1.47 (2 in.)
76	1/4 to 6 in.	1.44 (6 in.)	0.93	24.57	7.10	3.86	41.13 (6 in.)	1.56 (6 in.)
77	1 ft	1.76	1.15	21.86	5.91	3.21	42.64	1.52
78	2 ft	2.43	1.21	22.58	7.82	4.25	46.04	1.43
79	3 ft	2.57	0.53	20.94	5.88	3.20	43.77	1.49
81	4 ft	1.62	0.43	20.25	4.11	2.23	41.89	1.54

in the laboratory as the moisture equivalent, and also represents an inherent characteristic of the soil. The value obtained can be plotted on a soil-moisture scale and is always found to be some proportion of the saturation percentage. As shown here, sandy soils very low in organic matter had field capacity values of about one-half to one-quarter of the saturation percentage, whereas the clay soils had higher values of about one-half the saturation percentage. All of this moisture is available for microbial activities. The wilting coefficient is a lower moisture value obtained for the soil, usually through the use of plants or soil suction apparatus. The calculated wilting coefficient is not as reliable as the direct determination of this value. It is a critical moisture value for "higher" plants. Death of plants results in many cases if the wilting coefficient is prolonged over a certain time period.

The percent of pore space and bulk density are determined largely by structural conditions and texture and by the sum of the relative percentages of soil, air, and water. The porosity was somewhat greater in clay Soils 6 through 61 than in sandy soils. Soil 72 was quite dense and possessed a limited amount of pore space. This would restrict the growth of aerobic micro-organisms and macro plants. The bulk density, which indicates the degree of compactness of the soil, ranged from 0.94 to 1.97. Clay soils, as well as those high in organic matter, tend to have a low bulk density. In more typical soils the bulk density tends to increase with depth.

Soil color is usually determined on *in situ* soil and at two moisture contents: the air dry state and the field capacity. Upon addition of moisture, soil colors com-

Table 4. Physical measurements (No. 3)

Soil No.	Depth	Soil color and Munsell notation				Reflectivity in lab, %		Absorptivity (100–reflectivity) in lab, %	
		In field		In lab					
		Dry	Wet (field capacity)	Dry	Wet (field capacity)	Dry	Wet (field capacity)	Dry	Wet (field capacity)
1	Surface 1/16 in.	Light gray 2.5 Y 7/2	Grayish brown 2.5 Y 5/2	Light gray 2.5 Y 7/2	Light grayish brown 2.5 Y 6/2	34.0	14.0	66.0	86.0
2	1/16 to 1 in.				↓	38.0	16.5	62.0	83.5
51	1/16 to 6 in.					41.5	20.0	58.5	80.0
65	1 ft				Grayish brown 2.5 Y 5/2	45.0	25.0	55.0	75.0
53	2 ft				Gray 2.5 Y 5/0	36.5	18.0	63.5	82.0
54	3 ft			↓	Grayish brown 2.5 Y 5/2	37.5	17.5	62.5	82.5
6	Surface 1/2 in.	Pink 5 YR 7/4	Reddish brown 5 YR 5/4	Light reddish brown 5 YR 6/3	Reddish brown 5 YR 5/4	24.5	11.5	75.5	88.5
68	1/2 to 6 in.				Reddish brown 5 YR 4/3	24.5	12.0	75.5	88.0
69	1 ft				↓	25.5	11.5	74.5	88.5
63	2 ft					24.5	11.5	75.5	88.5
61	3 ft			↓	↓	26.5	13.5	73.5	86.5
4	Surface 1/8 in.	Light olive gray 5 Y 6/2	Olive gray 5 Y 5/2	Light olive gray 5 Y 6/2	Olive gray 5 Y 4/2	30.5	8.5	69.5	91.5
62	1/8 to 6 in.					25.0	8.0	75.0	92.0
66	1 ft					27.5	8.0	72.5	92.0
64	2 ft					27.0	7.0	73.0	93.0
67	3 ft			↓	↓	31.0	8.5	69.0	91.5
74	Surface 1/4 in.	Light yellow brown 10 YR 6/4	Brown 10 YR 5/3	Pale brown 10 YR 6/3	Brown 10 YR 5/3	30.0	13.5	70.0	86.5
70	1/4 to 6 in.					25.5	11.0	74.5	89.0
71	1 ft					25.5	10.5	74.5	89.5
72	2 ft	Red 2.5 YR 4/6	Dark red 2.5 YR 3/6	Yellowish red 5 YR 5/6	Reddish brown 5 YR 5/4	13.5	8.5	86.5	91.5
73	2 1/2 in.	↓	↓	↓	Reddish brown 5 YR 4/6	16.5	10.0	83.5	90.0
75	Surface 1/4 in.	Pinkish gray 7.5 YR 6/2	Brown 7.5 YR 4/2	Pinkish gray 7.5 YR 6/2	Brown 7.5 YR 5/4	31.0	16.5	69.0	83.5
76	1/4 to 6 in.		Dark reddish brown 5-YR 3/3	Brown 10 YR 5/3	Brown 10 YR 4/3	18.5	7.5	81.5	92.5
77	1 ft		Reddish brown 5 YR 4/4	Light yellowish brown 10 YR 6/4	Yellowish brown 10 YR 5/4	20.5	12.0	79.5	88.0
78	2 ft		Yellowish red 5 YR 5/6	↓	Yellowish brown 10 YR 5/6	26.5	15.5	73.5	84.5
79	3 ft		Reddish brown 5 YR 5/4	Light yellowish brown 10 YR 6/4	Yellowish brown 10 YR 5/6	33.5	18.5	66.5	81.5
81	4 ft			Very pale brown 10 YR 7/4	Light yellowish brown 10 YR 6/4	34.5	19.5	65.5	80.5

monly are darker by ½ to 3 steps in value and may likewise change in chroma but not usually in hue. As shown here, the soil colors varied from gray to brown and pink to red. According to Munsell notation, hues varied from 2.5Y to 10YR, the value from 3/ to 7/ and the chroma from /2 to /6. Soil color is considerably influenced by

moisture content, aeration, organic matter, mineralogical composition, weathering, and oxidation state. Values obtained in the field may or may not be repeatable on processed samples in the laboratory. Reflectivity and absorptivity measurements are not commonly performed on soils but they are inherent characteristics of the soil that can be used in conjunction with soil color determinations. Reflectivity on air dry soils ranged from 13.5 to 45.0% and from 7.0 to 25.0% on the soil at the field capacity. An air dry soil reflects about twice as much light as a soil at the field capacity. Absorptivity is therefore somewhat higher for a correspondingly wet soil than a dry soil.

5. Concluding Remarks

Soil physical properties as measured in the field and laboratory are reported. These characteristics are inherent soil properties which can be used in characterizing the micro environment of soil microflora. Chemical and biological measurements will be summarized in the next report, and an attempt will be made to establish significant correlations between the physical and chemical properties of desert soils in regard to the distribution and abundance of various groups of micro-organisms.

Primary emphasis will be given to the influence of two limiting factors (soil moisture, and organic matter) on the development of the indigenous microflora. Soil algae, an important photosynthetic component of the desert microflora, have not been enumerated by a satisfactory method. These organisms will be investigated by means of fluorescence microscopy in order to determine their abundance and distribution.